JAERI-M
91-120

CONCEPTUAL DESIGN OF SC MAGNET SYSTEM FOR ITER (I)

— OVERVIEW —

August 1991

Kiyoshi YOSHIDA, Mitsuru HASEGAWA, Kiyoshi OKUNO, Masataka NISHI
Yoshikazu TAKAHASHI, Hideo NAKAJIMA and Hiroshi TSUJI

日本原子力研究所
Japan Atomic Energy Research Institute

JAERI-Mレポートは，日本原子力研究所が不定期に公刊している研究報告書です。
入手の問合わせは，日本原子力研究所技術情報部情報資料課（〒319-11茨城県那珂郡東海村）あて，お申しこしください。なお，このほかに財団法人原子力弘済会資料センター（〒319-11茨城県那珂郡東海村日本原子力研究所内）で複写による実費頒布をおこなっております。

JAERI-M reports are issued irregularly.
Inquiries about availability of the reports should be addressed to Information Division, Department of Technical Information, Japan Atomic Energy Research Institute, Tokai-mura, Naka-gun, Ibaraki-ken 319-11, Japan.

編集兼発行　日本原子力研究所
印　　刷　㈱原子力資料サービス

JAERI-M 91-120

Conceptual Design of SC Magnet System for ITER (I)
- Overview -

Kiyoshi YOSHIDA, Mitsuru HASEGAWA+, Kiyoshi OKUNO
Masataka NISHI, Yoshikazu TAKAHASHI, Hideo NAKAJIMA
and Hiroshi TSUJI

Department of Fusion Engineering Research
Naka Fusion Research Establishment
Japan Atomic Energy Research Institute
Naka-machi, Naka-gun, Ibaraki-ken

(Received July 8, 1991)

The International Thermonuclear Experimental Reactor (ITER) is an experimental thermonuclear tokamak reactor that will test basic technologies of physics. The conceptual design activity of ITER required joint international work at the Max Plank Institute for Plasma Physics in the Garching Germany from 1988 to 1990. The proposals from Japan were summarized by the Fusion Experimental Reactor (FER) Team and the Superconducting Magnet Laboratory, both of the Japan Atomic Energy Research Institute (JAERI).

This paper describes the Japanese contributions to the design concepts of the magnet system for ITER. The concepts of a magnet system design originated from the test data from the Large Coil Task and the Demo Poloidal Coil programs at JAERI. Most of design concepts are adapted for an option of the ITER Magnet design. The differences between Japanese design and the other designs will be analyzed using experimental results.

Keywords: Super Conducting, Magnet, Fusion, ITER

+ Fusion Experimental Reactor Team

JAERI－M 91－129

ITER用超電導マグネット・システム概念設計（I）
－概　要－

日本原子力研究所那珂研究所核融合工学部
吉田　清・長谷川　満＋・奥野　清・西　正孝
高橋　良和・中嶋　秀夫・辻　博史

（1991年7月8日受理）

21世紀初頭に完成が予定されている国際熱核融合実験炉（ITER）の概念設計活動の超電導マグネット・システムに対する日本の提案を示す。1988年から90年まで西ドイツのミュンヘン郊外のガルヒンにあるマックスプランク・プラズマ物理学研究所で，このITER概念設計活動は行われた。原研那珂研究所の核融合実験炉特別チームが中心になり，超電導磁石研究室が日本の設計案のまとめを日本で行った。

この設計は原研独自に行ったものである。LCT計画や実証ポロイダル・コイルの開発結果を取り入れることで技術的妥当性を高め，これまでの開発経験から達成可能な目標に従って設計を進めた。ITERの共通設計書とは一部食い違いはあるが，基本的な概念はITER設計案に採用されていた。今後の詳細設計活動に行う長期R&D計画において，ハードウェアーによる実験によってこれらの食い違いは確定されるだろう。

本誌は①応力解析②交流損失③コイル設備④材料データのテーマを基にした日本の設計案の基本概念を示したものである。詳細な解析については別冊を参考にしていただきたい。

那珂研究所：〒311－01　茨城県那珂郡那珂町大字向山801－1
＋　核融合実験炉特別チーム

Contents

目　　次

PREFACE

All of technical design reports from Japanese contributors to ITER magnet design are listed below:

JAERI-M 91-120
CONCEPTUAL DESIGN OF SC MAGNET SYSTEM FOR ITER (I)
- OVERVIEW -

(1) Design Basis
(2) Toroidal Field Coils
(3) Central Solenoid Coils
(4) Outer Ring Coils
(5) Mechanical Design Guideline

JAERI-M 91-121
CONCEPTUAL DESIGN OF SC MAGNET SYSTEM FOR ITER (II)
- STRESS ANALYSIS -

(1) Toroidal Field Coils at End of Burn
(2) Toroidal Field Coils at Fault Conditions
(3) Center Solenoid Coils
(4) PF Coil Support Structure and Outer Ring Coil
(5) Winding Rigidity Analysis

JAERI-M 91-122
CONCEPTUAL DESIGN OF SC MAGNET SYSTEM FOR ITER (III)
- AC LOSS -

(1) Analysis and Measurement of AC Losses in Large Superconducting Coil
(2) AC Loss Analysis
(3) AC Loss in Cryogenic Structure

JAERI-M 91-123
CONCEPTUAL DESIGN OF SC MAGNET SYSTEM FOR ITER (IV)
- POWER SUPPLY AND CRYOGENIC SYSTEM -

(1) Power Supply System for Magnet System
(2) Fault Analysis of TF Power Supply System
(3) Cryogenic System

JAERI-M 91-124

CONCEPTUAL DESIGN OF SC MAGNET SYSTEM FOR ITER (V)

- MATERIAL -

(1) Superconducting Material

(2) Steels

(3) Insulator

JAERI-M 91-125

CONCEPTUAL DESIGN OF SC MAGNET SYSTEM FOR ITER (VI)

- R&D PROPOSALS -

(1) Requirements of Scalable Model Coil Test

(2) TF Scalable Model Coil

1. INTRODUCTION

The Internal Thermonuclear Experimental Reactor (ITER) is an experimental thermonuclear tokamak reactor testing the basic physics performance and technologies. The conceptual design activity of ITER required the joint work at a technical site at the Max Plank Institute for Plasma Physics in the Garching Germany from 1988 to 1990. The proposals from Japan were summarized by the Fusion Experimental Reactor (FER) Team and the Superconducting Magnet Laboratory of the Japan Atomic Energy Research Institute (JAERI).

The toroidal and poloidal field coils must operate reliably in the tokamak machine because of their difficulty of replacement in the fusion reactor. It is essential that the coils be superconducting, because of the need to achieve high field and current densities during long pulse operation and to minimize power consumption.

The ITER magnet system consists of 16 superconducting Toroidal Field (TF) coils and 14 Poloidal Field (PF) coils. The cold mass of the ITER magnet system is nearly 12,000 tons. The TF coil system was designed to produce the required field on its axis while keeping field ripple at the plasma edges. The PF coil system was designed for ramp-up control of a 22 MA plasma while allowing variations over a range of plasma parameters.

The design of ITER superconducting coils are based on existing and on-going technology. However, materials and components development are required to improve its performance during the next R&D phase.

This paper describes the Japanese contributions to the design concepts of the magnet system for ITER. The concepts of a magnet system design were derived from the test data of the Large Coil Task and the Demo Poloidal Coil programs at JAERI.

2. DESIGN BASIS

2.1 Introduction

This session describes the design basis (specifications) for the superconducting magnet of the ITER. Overview of the superconducting magnet system is shown in Fig. 2.1.

2.2 TF Design Condition

The main design parameters of the TF coils are shown in Table 2.1.

2.2.1 Magnetic Field

(1) Magnetic field at plasma center is 4.85 T
(2) Total current of each coil is 9.1 MA
(3) Maximum field in winding is 11.1 T
(4) Field change during plasma disruption
- parallel : 40 T/s, 2.0 T / 50 ms
- perpendicular : 10 T/s, 0.5 T / 50 ms

2.2.2 Loads

(1) Normal operation

The TF coil system shall be designed for the design load cycle.

(a) Central force
(b) Out-of-plane force by poloidal coil operation
(c) Gravity force
(d) Thermal stress during cool-down and warm-up

(2) Upset loads

The TF coil system shall be recovered within one or two days.

(a) Quench
(b) Trouble of sub-system (cryogenic and power supply)

(3) Faulted Load

The TF coil system shall not destroy the Tritium container (vacuum vessel).

(a) Unbalanced current during dumping

(b) Ground fault
(c) Internal short
(d) Meltdown

2.2.3 Electrical Condition

(1) Maximum operational voltage
(a) Terminal : DC 20 kV
(b) Ground : DC 20 kV

(2) Test voltage before installation[1]
(a) Terminal : DC 50 kV
(b) Ground : DC 50 kV

2.2.4 Nuclear Heating and Radiation

(1) Nuclear heating loads
TF case : 42 kW
TF winding : 23 kW

(2) Radiation
Insulation dose : 20 MGy
Neutron fluence : 6×10^{21} n/m^2
Copper dose : 7×10^{-4} dpa

(3) Room temperature annealing
The warm-up and cool-down will be done every 2 or 3 years for inspections and for maintenance.

(4) Resistivity of copper
The maximum resistivity of copper is 9×10^{-10} Ohm-m was selected for the analysis.

2.2.5 Maintenance

(1) Cold Operation Phase : Full maintenance
(2) Hot Operation Phase : Limited maintenance

2.3 PF Design Condition

The main Parameters of the PF coil system are listed in Table 2.2. The current variations of the PF coils are shown in Fig. 2.2. The detailed current pattern is listed in "Volume III. AC LOSS".

2.3.1 Magnetic Field

(1) Maximum supplying magnetic flux is 315 Vs

(2) Maximum field and total current of each coil are shown in Table 2.3 and Table 2.4.

(3) Maximum field in the PF-1 winding is 13.5 T.

(4) Field change during plasma disruption

- parallel : 40 T/s, 2.0 T / 50 ms

2.3.2 Magnetic Loads

(1) Normal operation

The PF coil system shall design up to the design load cycle.

(a) Compression force

(b) Out-of-plane force by toroidal ripple field

(c) Gravity force

(d) Thermal stress during cool-down and warm-up

(2) Upset loads

The PF coil system shall be recovered within one or two hours.

(a) Quench

(b) Trouble of sub-system (cryogenic and power supply)

(3) Faulted Load

The PF coil system shall not destroy the Tritium container (vacuum vessel).

(a) Unbalanced current during dumping

(b) Ground fault

(c) Internal short

(d) Meltdown

2.3.3 Electrical Condition

(1) Maximum operational voltage

- Terminal : DC 20 kV
- Ground : DC 20 kV

(2) Test voltage before installation

- Terminal : DC 50 kV
- Ground : DC 50 kV

2.3.4. Maintenance of PF coils

(1) Central Solenoid Coils (PF-1,4) : One or more maintenance checkups is scheduled during their life time

(2) Diverter Coils (PF-5) : Only at trouble

(3) Outer Ring Coils (PF-6,7): Maintenance only in the Cold Phase, no maintenance after D-T burning.

2.4 Design Criteria

2.4.1. SC Cable Design

(1) Limiting Current

(a) Limiting current of the PF conductors shall be higher than the operating current. The current is calculated by the equation E.1.

(2) Stability Margin

(a) Stability margin of the poloidal conductors shall be more than 200 mJ/cc-metal.

(b) This 200 mJ/cc-metal is come from 100 mJ/cc of AC loss and 100 mJ/cc of mechanical disturbance.

(c) Stability margin versus temperature margin of Cr plating strand is shown in Fig. 2.2 [3].

(d) Stability margin of a monolithic conductor will have others losses besides more than AC loss input from plasma disruption.

(3) Hot Spot Temperature

(a) Hot spot temperature [4] of each conductor, calculated with only heat capacity of strands, shall be less than 150 K.

(b) Hot spot temperature is some margin with in the hot spot temperature region with consideration given to the heat capacity of helium and conduit material[5].

(c) The temperature is calculated by the equation E.2.

(4) AC Loss

AC loss analysis method is described in "Report III. AC LOSS".

(5) Hydraulic Parameter

(a) Pressure drop is calculated by the equation of E.3.

(b) In case of cable-in-conduit conductor,on experimental factor is multiplied with the friction fraction of a smooth pipe[6].

2.4.2. Mechanical Design

(1) Maximum Design stress intensities of each material are shown in Table 2.5.

(2) Design stress are described in the session 6.

2.4.3. Electrical Insulation Design

(1) The safety margins of the design thickness of insulators.

- 6 times for normal voltage
- 3 times for test voltage

2.5. Material Data

2.5.1. SC Cable

(1) Critical current for $(NbTi)_3Sn$ at zero external strain is 800 A/mm2, as shown in Fig. 2.3.

(2) Resistivity of copper as function of magnetic field is shown in Fig. 2.4.

2.5.2. Cryogenic Materials

The mechanical properties of the materials are summarized in Volume V (Material).

2.6. Interpolation of Summary

The completion of the conceptual design was productive in revealing technically previously unknown problems especially stability and stress problems. However, experimental data is minimal because basic research of high field and large conductors have not been extensively performed. Instead,most of the current research is starting to be directed to high temperature superconductivity.

The requirements for a tokamak fusion machine were understood during the conceptual design activities. The long term R&D program will solve our assumptions and the manufacturing problems. And research activities of high field, large size SC magnet shall be promoted by ITER activities.

References

[1] Japanese Electrotechnicl Committee, JEC-204-1978
[2] T. Ando,et. al.,"Measurement of the Stability of Nb_3Sn Cable-in-Conduit Conductors", IEEE Transactions on Magnetics, Vol.25, No.2 (1989) 2386
[3] T. Ando, et.al.,"DPC-EX Test results", to be presented at SOFT 90
[4] Y. Iwasa, et.al.,"Normal zone propagation in adiabatic superconducting magnets over range 4.2 - 80 K", Cryogenics, Vol. 30 (1990) 37
[5] J. Yoshida, et.al., "Hot Spot Temperature of a Cable-in-conduit Conductor", JAERI-M 90, to be published
[6] E. Tada, et.al., "Thermal Performance of the Nb-Ti Demo Poloidal Coils (DPC-U1,U2)", Proc. of MT-11 (1990)

Equations

E.1. Limiting Current

$$Ilim^2 * Rou = H * (Tc - Top) * Scu * P$$

$$Tc = 16.3 - 0.33\ B(T) \quad (K)$$

Ilim	:	Limiting current	(A)
Rou	:	Resistivity at operation field	(Ohm-m)
H	:	Heat flux	($W/m^2/K$)
Tc	:	Critical temperature	(K)
Top	:	Operation temperature	(K)
Scu	:	Area of copper	(m^2)
P	:	Cooling Perimeter	(m)
B	:	Magnetic Field	(T)

Reference: T. Ando,et. al.,"Measurement of the Stability of Nb_3Sn Cable-in-Conduit Conductors", IEEE Transactions on Magnetics, Vol.25, No.2 (1989) 2386

E.2. Hot spot temperature

$$Jcu^2 * (tau / 2 + td) = \int_{Top}^{Ths} Cstr / Rcu \, dT$$

Jcu	:	Current density of copper	(A/mm^2
tau	:	Time constant of dumping	(K)
td	:	Dead time before protection	: 1 sec
Cstr	:	Specific Heat of strand	(J/kg/K)
Rcu	:	Resistivity of copper	(Ohm-m)
Ths	:	Hot spot temperature	(K)
Top	:	Operational temperature	(K)

E.3 Pressure Drop for bundle conductor

$$dP = 2 * f * Denh * V^2 / Dhyd$$

$$f = a * 0.076 * Re^{-0.25}$$

$$Re = V * Dhyd * Denh / Visc$$

dP	:	Pressure drop	(Pa/m)
f	:	Friction factor	
a	:	experimental factor:	bundle : 1.8 - 2.0
			smooth pipe : 1.0
Re	:	Reinold's number	
Denh	:	Density of Helium	(Kg/m^3)
V	:	Velocity	(m/s)
Dhyd	:	Hydraulic Diameter	(m)
Visc	:	Viscosity	(Pa*s)

Reference : D. E. Daney, et.al., "Friction factors for flow of near-critical helium in curved tube", CRYOGENICS 18 (1978) 345

Table 2.1 Main Parameters of the TF Coils

Number of Coils	16	
Total current per coil	9.09	MA
Coil dimensions:		
Virtual clear bore	14.7	m
Horizontal bore	7.1	m
Radius of clear bore for CS	2.130	m
Field on axis at 6.0 m	4.85	T
Maximum field in the winding	11.1	T

Table 2.2 Main Parameter of the PF system

Number of PF coils	14
Central Solenoid Coils	8
Diverter coils	2
Outer Ring Coils	4

Location, Area and turns

Coil No	R	Z	dR	dZ	N
PF-1	1.73	0.95	0.60	1.90	550
PF-2	1.73	2.85	0.60	1.90	550
Pf-3	1.73	4.75	0.60	1.90	550
PF-4	1.73	6.65	0.60	1.90	550
PF-5	3.90	9.00	0.872	0.970	400
PF-6	11.50	6.00	0.586	1.642	320
PF-7	11.50	3.00	0.586	1.070	200

Table 2.3 Central Solenoid Coils (PF-1 to PF-4)

	INIT	EOB	
Total current	20.6	22.4	MA
Maximum field	13.6	12.5	T

Table 2.4 Diverter Coils and Outer Ring Coils

Total current		
PF-5	18.5	MA
PF-6	14.01	MA
PF-7	8.82	MA
Maximum field		
PF-5	9.5	T
PF-6	5.2	T
PF-7	4.6	T

Table 2.5 Mechanical Property of Materials

Superconductor		
Critical current of non-Cu Nb_3Sn at 12 T and 4.2 K	800	A/mm^2
Copper Stabilizer		
Resistivity of Cu at 12T and 4.2 K	7.1 E-10	Ohm-m
Conduit Steel		
Yield strength	1,000	MPa
Case Steel		
Yield strength	1,200	MPa
Young's modulus	200	GPa
Insulator in winding		
Ultimate strength	1,000	MPa
Young's modulus	20	GPa
Insulation of coil case		
Ultimate strength	1,800	MPa

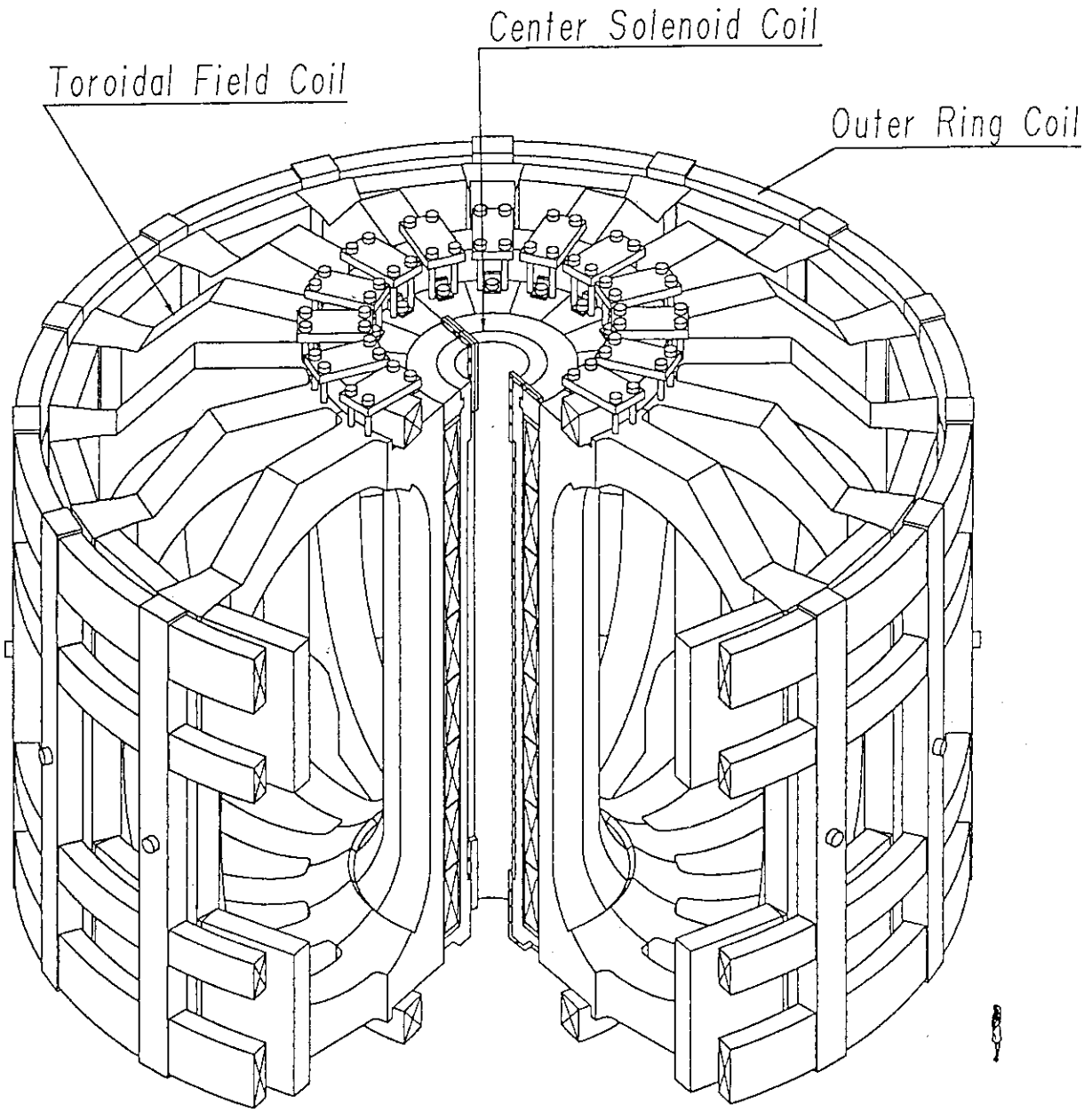

Fig. 2.1 Overview of the Superconducting Magnet System

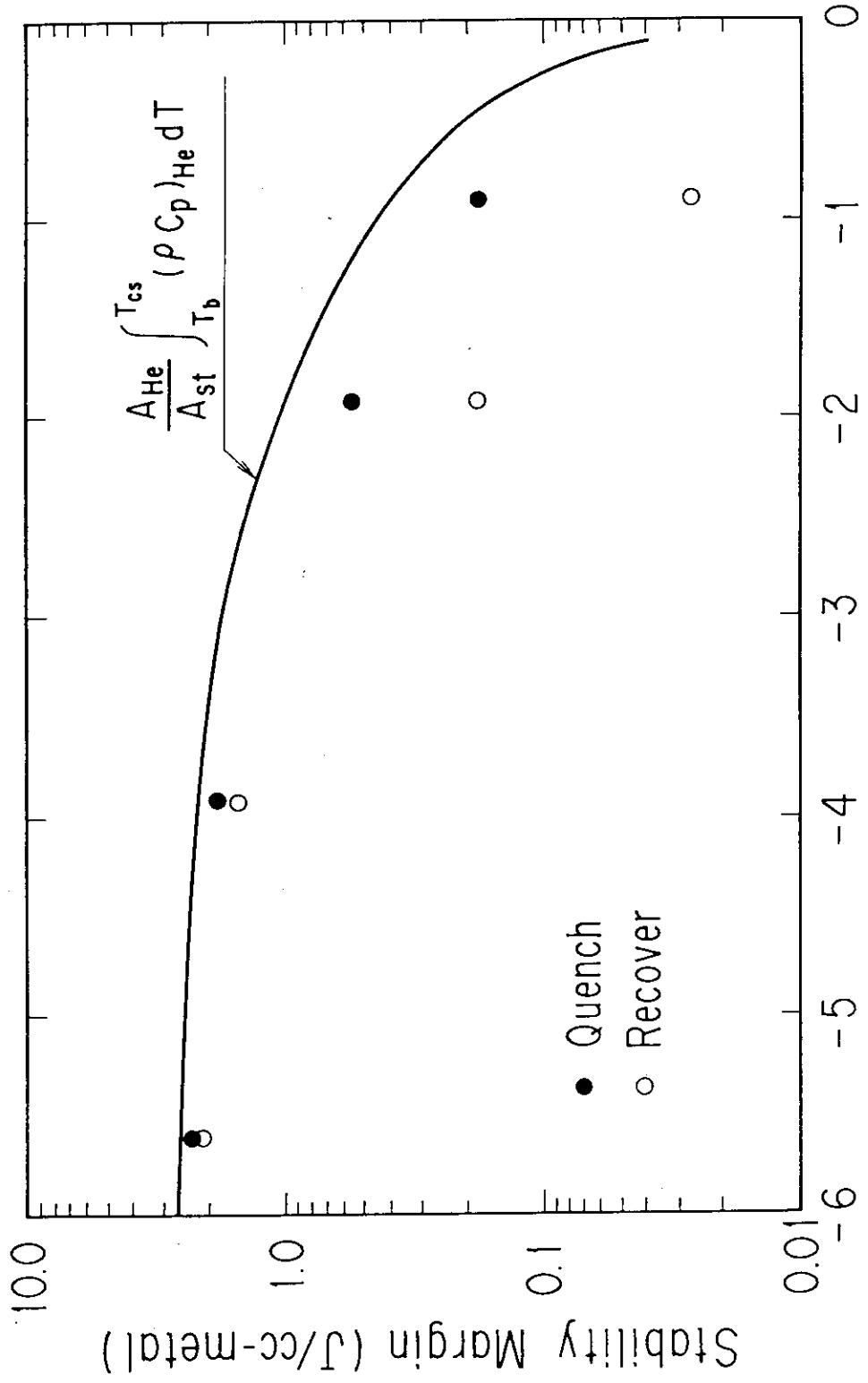

Fig. 2.2 Current variations of the PF coils during standard operation

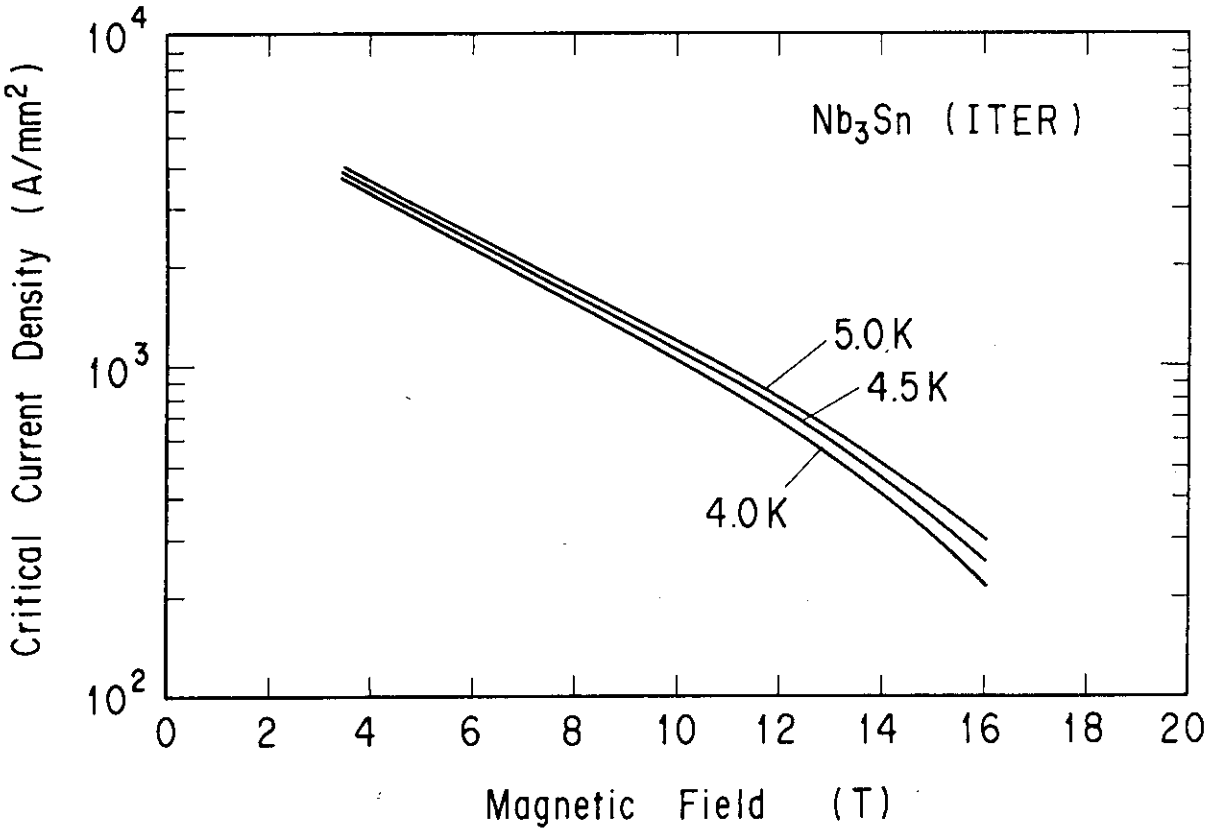

Fig. 2.3 Stability Margin of DPC-EX

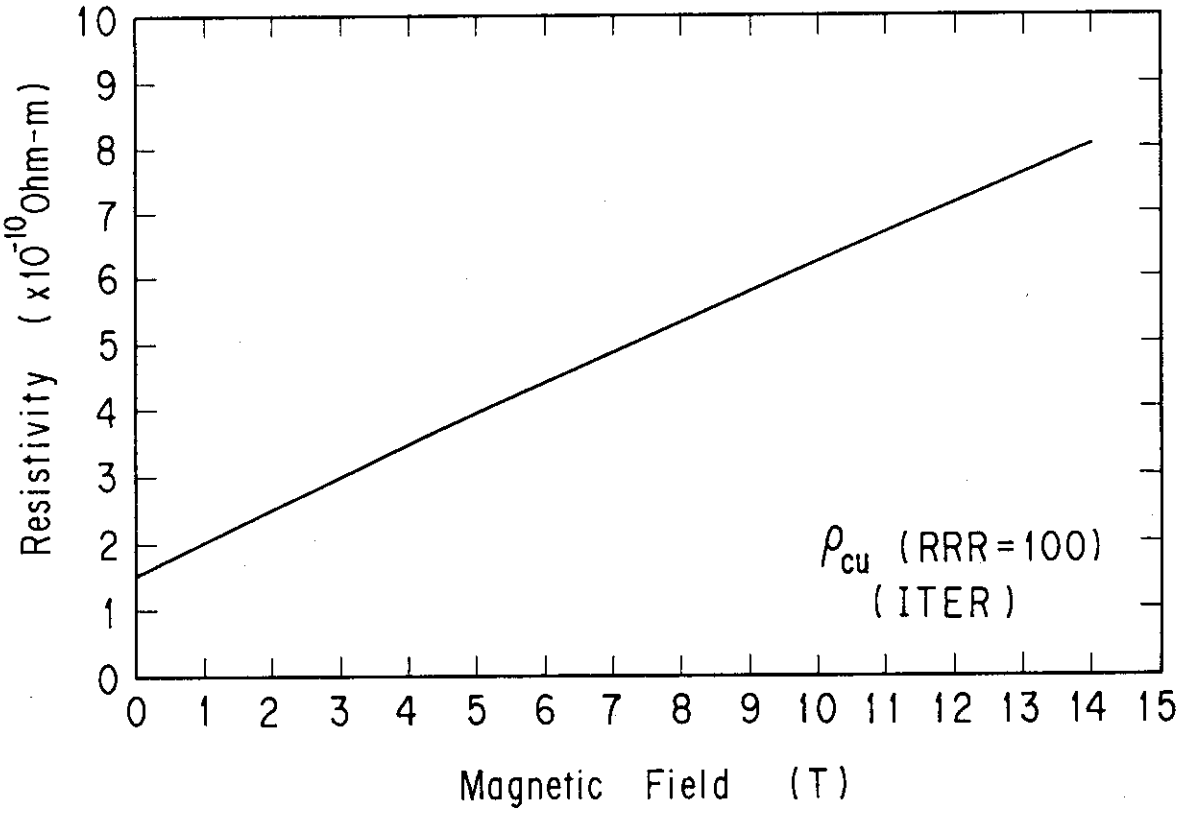

Fig. 2.4 Critical Current for $(NbTi)_3Sn$ at zero external strain

3. TOROIDAL FIELD COILS

3.1 Introduction

This section describes the conceptual design of the toroidal coil system for ITER[1]. The general requirements are as follows:

(1) Function

The Toroidal Field (TF) coil's function is to generate a 4.88 T magnetic field at plasma center (r = 6.0m).

(2) Size

Bore size of the TF coil is 3.1 to 4.4 times larger than that of the LCT coil [2]. Horizontal and vertical bore size of the TF coil for the ITER are 7.38 m and 14.83 m, respectively. On the other hand those of the LCT are 2.35 m and 3.35 m, respectively. Comparison of the coil sizes among ITER, FER[3,4] and LCT coil are shown in Fig. 3.1.

(3) Conductor

The monolithic hollow cooling conductor is selected for the TF coil because of its requirements on the mechanical properties and electrical insulation. The cable-in-conduit (CIC) conductor is mainly studied in the poloidal field coil. Good comparisons are also made between the hollow conductor and CIC conductor.

(4) Maintenance

Because it takes long term to replace the toroidal field coils,they are one of the most important components in the tokamak fusion reactor.

(5)Neutron damage

The neutron irradiation is a serious problem for on the TF coils. The calculated insulation dose is 20 MGy, and the nuclear heating is 1 kW/m^3 in the winding pack. The DPA of copper will be reduced by room temperature annealing[5]. The nuclear heating can be removed by increasing of the mass flow rate.

3.2 Design Concept

(1) Main parameter

The design parameters of the Toroidal Field Coil System are also listed in Table 3.1.

(2) Conductor [6,7]

(a) Monolithic conductor : TMC coil

(b) Hollow conductor : LCT-EU coil[2]

(c) $(NbTi)_3Sn$ for high field, Nb-Ti for low field

(d) Low AC loss : no copper in strand, insulated copper

(3) Winding

(a) React and winding technique : TMC coil

(b) Rigid winding : cured by semi-cured tape

(4) Case

(a) Thick plate

(b) Insulated to reduce AC loss

(c) broader : LCT-EU coil

(5) Intercoil support

(a) Wedge support for central force

(b) Insulated support

3.3 Basic Analysis

3.3.1 Magnetic Field

(1) Condition

Operating current in PF coils at "end of burn" (EOB) is selected from PF scenario as shown in Table 3.2. EOB1 is a standard scenario, and EOB2 is selected by plasma parameters, l_i=0.55 b_p=0.0.

(2) Maximum magnetic field

Maximum magnetic field is 10.8 T when the TF coil is operating alone. Maximum magnetic field is 11.1 T at EOB2 condition.

(3) Distribution of magnetic field

Magnetic field distribution in in-bore and out-bore winding pack at TF coils solo operation are shown in Fig. 3.2. Magnetic field distribution along inner bore at only TF coils operation and EOB are shown in Fig. 3.3.

(4) Ripple of magnetic field

Ripple of magnetic field in the plasma is shown in Fig. 3.4

3.3.2 Magnetic Loads

The TF coil is loaded by the magnetic centering force, hoop force, and over-turning force as a result of the poloidal field.

(1) Hoop force

The hoop force is relatively large and supported by the coil case. This is done because the side shape is relatively long in the vertical direction. Hoop force of TF coil along winding are shown in Fig. 3.5.

(2) Central force

The centering force of 475 MN per coil is supported by coil wedging between the TF coil. Central force of TF coil along winding is shown in Fig. 3.6.

(3) Out-of-plane Load

The over-turning moment is supported by both the shear panel and the wedging. Out-of-plane Force along the windings at EOB1 and EOB2 are shown in Fig. 3.7.

3.3.3 Inductance

(1) Self and mutual inductance and stored energy of TF coils are listed in Table 3.3.

(2) Stored energy is 43 GJ. The TF coil system will have the largest magnetic energy.

3.4 **Cable**

3.4.1 Configuration

(1) Hollow conductor

There are of the bundle-type and of the hollow type forced-flow conductors. In the case of LCT, the WH coil uses the bundle-type conductor. The EU coil and the CH coil use the hollow-type conductor.

(2) Plasma disruption

The TF coil generates the steady magnetic field. During plasma disruption, however, a pulsed field of 2.0 T/s - 50 ms is applied to the TF coil. Classic hollow-type conductor with a large-area copper stabilizer of low resistivity between strands will quench. This quench is due to eddy currents in the

copper and the strands.

(3) TMC-FF type conductor

The low AC loss in the conductor is realized by the TMC-FF conductor[6], as shown in Fig. 3.8 for the TF coil. The characteristics of the TMC-FF conductor are as follow:

(a) All-bronze strands to reduce the strand coupling loss,

(b) Insulation of the copper stabilizer, and

(c) Thick conduit (3 mm) to prevent damage of the Nb_3Sn strands. Main parameters of the monolithic conductor (TMC-FF) are listed in Table 3.4.

3.4.2 Hot Spot Temperature

(1) High current density

The current density of the cable space which is composed of the superconductor, the copper stabilizer, the helium coolant without the structural material, and the insulator are the key points of the design study.

(2) Current density

In the case of the LCT coil, the cable space current density of the WH coil and the EU coil are 64.6 and 43.5 A/mm^2, respectively. The cable space current density of the conductor for the ITER is 80 A/mm^2, corresponding to the difference of magnetic field between 12 T and 8 T. The real current density of the TF is 67.8 A/mm^2. This is due to the increase in magnetic resistivity and the displacement per atom (DPA) of the copper from the neutron irradiation.

(3) Dump time constant

If the coil current is dumped 1 to 2 sec after the magnet quench, there will be no damage in the coil. However, this TF coil system has 44.3 GJ magnetic energy. The dump time constant is limited by the coil terminal voltage. The maximum insulation voltage is designed for 20 kV. There fore, the dump time constant is about 10 sec from the coil terminal voltage of 10.9 kV. It is, therefore, important to solve the coil protection problem.

(4) Hot spot temperature

This point relates to current density because the area of the copper stabilizer and the helium coolant controls the tem-

perature rise after the magnet quench. Calculated temperature during dumping are shown Fig. 3.9.

(5) Experimental data

There are no design criteria for the protection problem. The DPC program [8] has the DPC-TJ coil [9] and the US-DPC[10], which are both high current density coils. These experimental results from these DPC coils will solve the coil protection problem.

3.4.3 AC Loss

(1) Conductor:

AC Loss and magnetic diffusion time constant of the monolithic conductor (TMC-FF) are shown in Table 3.5. Main improvements of conductor are as follows:

(a) Add CuNi to the copper stabilizer (between 1 mm 170 of conductor thickness

(b) Ceramic insulation for the core plate

(2) Cycle loss

Retter to Technical design report of Volume III. AC Loss

(3) Disruption loss

Retter to Technical design report of Volume III. AC Loss

3.4.4 Stability

(1) Design

Stability margin of monolithic conductor shall be greater than the energy released from AC loss input from plasma disruption.

(2) AC loss at plasma disruption

AC loss of cable space are 16.4 and 18.5 mJ / cc-metal at strait leg, horizontal leg and respectively.

(3) Stability margin

The current sharing temperature of conductor is 9 K. The heat capacity of strand and copper from 4 K to 9 K is 24 mJ/cc. Heat flux to helium is 39 mJ/cc during 50 ms. Total heat capacity of cable space is 63 mJ/cc. Therefore, stability margin is 3.4 times larger than the heat input from AC loss. The mechanical heat input is negligibly small for a monolithic conductor.

3.4.5 Hydraulic Parameter

(1) Equation

The experimental data of normal smooth pipe is selected.

(2) Pressure drop

Pressure drop of conductor is 2.1 mbar/m. Total pressure drop is 0.58 bar with 276 m of cooling path.

3.5 **Winding Pack**

3.5.1 Layout

(1) Side

The layout of the TF coil winding is shown in Fig. 3.10.

(2) Cross sectional

Cross sectional view of the TF coil is shown in Fig. 3.11.

(3) Details

Details of the TF coil winding is shown in Fig. 3.12. Four turns need to be removed in order to fit in the coil case. Thickness of ground insulation is 10 mm. 10 mm thickness of void filling is also use for adjustments to install the winding into the case.

3.5.2 Pancake Connection

The Nb-Ti are selected for low field applications(< 5 T). Conversional technology is selected for pancake joints.

3.5.3 Stress Analysis

The peak compressive stress component is highly localized due to the simple modeling of the insulation (ROD elements) between the winding and coil case. The maximum compressive stress of the insulator between the winding and coil case is 127 MPa.

The load transmission between windings and case are difficult to solve by stress analysis.

3.6 **Case and Filling**

3.6.1 Layout

(1) Case of the TF coil is shown in Fig. 3.13.

(2) Interface' for the structural supports of the TF coil is

shown in Fig. 3.14.
(3) Virtual cross sectional view of the TF coil winding and case are shown in Fig. 3.15.
(4) Insulation

Coil case is insulated at the mid-plane of winding as shown in Fig. 3.12.

3.6.2 Void filling

(1) Metallic bladders are used for void filling as shown in Fig. 3.12.
(2) The epoxy resin and chopped fibers are impregnated into the metallic bladder developed for the LCT-EU coil.

3.6.3 Stress Analysis

The stress analysis of ITER TF coil under normal loading condition at the "end of burn" was performed by using idealized boundary conditions specified by cyclic symmetry. The displacements and the stress level in the TF coil are almost acceptable. But in some regions, a high stress of more than 650 MPa occurs in the inner leg of outer ring. Also, high stress peaking in the winding, stress over the allowable level of 600 MPa, are calculated.

3.6.4 Cooling Pipe

Cooling pipes are located at surface of the coil case's winding side, and bore side as shown in Fig. 3.12.

3.7. **Coil Support Structures**

3.7.1 Inter-coil Structures

(1) Outer inter-coil (Shear panel)

The electrical insulation for the shear panel is separated from mechanical connection. The insulation joint is manufactured and then machined such that the surface is free of mechanical interface. The outer inter-coil structure is shown in Fig. 3.16.

(2) Inner inter-coil

The same idea is applied (key of wedge) The key structure is shown Fig. 3.17. This key carries shear forces of 60 MN.

3.7.2 Gravity Support

The gravity support of all of coils is located at their legs, as shown in Fig. 3.14.

3.8. Others

(1) Piping

The cooling passages of the TF winding and case are shown in Fig. 3.18.

(2) Voltage monitor

The winding by two cable in hand has good results to detect quench in case of the LCT-EU.

(3) Fluid monitor

The fluid monitor are selected for quench monitoring as detailed described in Volume IV (P.S. and Cryogenic System).

3.9. Summary

The stress at the strait legs are serious. Especially, stress of the insulator between wedge is critical. The monolithic conductor can be operated during the plasma disruption. The monolithic conductor shall be studied to backup the data or the CIC conductor. The manufacturing of non circular winding and thick coil case is impossible to solve by the design study. The uncertainties of load transmission between windings and case are difficult to solve using software. The Scalable Model Test of the TF coil is indispensable to realize the largest superconducting magnet system.

References

[1] M. Hasegawa, K. Yoshida, K. Koizumi, et al., "JAPANESE DESIGN OF ITER SUPERCONDUCTING MAGNET SYSTEM", Proc, of MT-11 (1990) 902.

[2] D. S. Beard, W. Klose, S. Shimamoto and G. Vecsey, "THE IEA LARGE COIL TASK", Fusion Engineering and Design, 7 (1988)

[3] E. Tada, et al.,"THE FUSION EXPERIMENTAL REACTOR - DESIGN CONCEPT", Proc, of 13th Symposium on Fusion Engineering, (1989)

239
[4] K. Yoshida, K. Koizumi, M. Sugimoto, et al., "DESIGN STUDY OF FER SUPERCONDUCTING MAGNET SYSTEM", Proc, of MT-11 (1990) 908.
[5] K. Nakata, S. Takamura, N. Tada and I. Massaka, "Electrical Resistivity Change in Cu and Al Stabilizer", JAERI-M 83-230 (1983)
[6] K. Yoshida, M. F. Nishi, Y Takahashi, et al.," DESIGN OF THE PROTO-TYPE CONDUCTORS FOR THE FUSION EXPERIMENTAL REACTOR", IEEE Transactions on Magnetics 25-2 (1989) 1488
[7] K. Yoshida, M. F. Nishi, Y. Takahashi, et al., "DEVELOPMENT OF PROTOTYPE CONDUCTORS AND DESIGN OF THE TEST COIL FOR THE FUSION EXPERIMENTAL REACTOR", Proc, of MT-11 (1990) 890
[8] T. Ando, et al., "Development of high field superconducting coil for the Tokamak fusion machine in Japan", Proceeding of 11th Symposium of Fusion Engineering (1986) 991
[9] T. Hamajima, A. Tanaka, H. Shiraki, et al., "DEVELOPMENT OF A FORCED-COOLED SUPERCONDUCTING COIL WITH HIGH AVERAGE CURRENT DENSITY (DPC-TJ)", IEEE Transactions on Magnetics 25-2 (1989) 1721
[10] M. M. Styeeves, M. O. Hoenig, M. Takayasu, et al., "PROGRESS IN THE MANUFACTURE OF THE US-DPC COIL", IEEE Transactions on Magnetics 25-2 (1989) 1738

Table 3.1 Design Parameter of the Toroidal Field Coil System

Max. Field	11.2	T
Rated Current	30.3	kA
Margin of Ic	1.9	
Current Density of		
Coil Space	14.7	A/mm^2
Winding	33.9	A/mm^2
Ampere-turn / Coil	9.09	MAT
/ Total	145.5	MAT
Bore Height	14.83	m
Width	7.379	m
Width of Coil	1.30	m
Number of		
Coil	16	
Total Turn	292 (7*2*11*2)	
Double Pancake	11	
Cooling Pass	44	
Stored Energy	44.5	GJ
Inductance	95.9	H
Dump Time	10	s
Pulse Field at disluption	2 T / 50	ms
Length of Cooling Pass	276	m (39.98m)
Inlet Temperature	4.2	K
Pressure	6.0	bar
Pressure Drop	0.58	bar
Nuclear Heating /coil		
Winding	1.44	kW (23kW)
Case	2.63	kw (42kW)
Insulation Dose	4-16	MGy
Cu DPA	1.8×10^{-4}	
Poloidal Cycle	< 10,000	
Charge Cycle	< 100	
Cool-down Cycle	< 20	

Table 3.2 Current in PF coils at EOB

	EOB1	EOB2 (MA)
Plazma	22.0	22.00
PF-1	-23.30	-22.42
PF-2	-22.30	-22.42
PF-3	-9.14	-11.45
PF-4	0.00	2.61
PF-5	6.25	11.71
PF-6	-6.49	-13.61
PF-7	-5.25	0.36

EOB1 : standard scenario
EOB2 : li=0.55, bp=0.00

Table 3.3 Inductance and stored energy of TF coils

Self Inductance		2.6	H
Mutual inductance			
	L01vsL02	0.76	H
	L01vsL03	0.37	H
	L01vsL04	0.21	H
	L01vsL05	0.13	H
	L01vsL06	0.087	H
	L01vsL07	0.065	H
	L01vsL08	0.054	H
	L01vsL09	0.051	H
Rated Current		30.3	kA
Stored Energy		44.5	GJ

Table 3.4 Monolithc Conductor Parameter Program for ITER

[Condition]			
Bop	:	11	T
Iop	:	30300	A
Top	:	4.2	K
Jc	:	922	A/mm^2
[Design Parameter]			
Damage of Cabling	:	0.1	
Number of Strand	:	23	
Diam of strand	:	2.6	mm
S core	:	87.39	mm^2
Diam of core	:	2.20	mm
Awire	:	111.01	mm^2
Ahe	:	99.0	mm^2
Acu	:	232.5	mm^2
Ass	:	344.5	mm^2
Ains	:	60.8	mm^2
[Analysis Results]			
Tc	:	12.57	K
Tcs	:	9.07	K
Temperature Margin	:	4.87	K
Ic/Iop	:	2.39	
JcSC	:	829.8	A/mm^2
JCableSpace	:	66.29	A/mm^2
Jcu	:	130.30	A/mm^2
Jwinding	:	35.13	A/mm^2
Acable space	:	457.05	mm^2
Aconductor	:	862.49	mm^2
[Pressure Drop]			
Hydroric Diameter	:	3.09	mm
Mass Flow	:	10	g/s
Density He	:	0.143	g/cc
Viscosity	:	4.247E-05	g/cm/s
He Velocity	:	70.636	cm/s
Reynold's Number	:	73496.77	
Friction Factor	:	4.615E-03	
Press. Drop	:	2.10E-03	bar/m
[Limiting Current]			
Cool Perimeter	:	142.84	mm
Rou of Cu at 11 T	:	6.78E-10	Ohm-m
Heat Flux	:	1000	$W/m^2/K$
I-limit	:	20249.	A
Jcs-limit	:	44.30	A/mm^2
Area of metal	:	364.	mm^2
Area of eff. helium	:	4.28	mm^2
Stability Margin	:	63.6	mJ/cc-metal

Table 3.5 Tau Calculation for TMC-FF Conductor

	parallel	perpendicular	
Strand Eddy Tau	8.522E-06		(sec)
Filament Coupling	9.922E-07	1.342E-04	(sec)
Strand Coupling	3.932E-05	0.01331	(sec)
Copper Eddy	2.112E-04	1.312E-03	(sec)
Conduit Eddy	4.520E-05	6.126E-05	(sec)
Ave. Tau/conductor	8.361E-05	2.474E-03	(sec)
Eddy Loss in Wire	0.4099	5.210	(J/m)
Eddy Loss in Cu	3.107	1.180	(J/m)
Eddy Loss in SS	0.9890	8.374E-02	(J/m)
Hysteresis Loss	1.460	0.2731	(J/m)
Magnetic Energy	1591.5	99.47185	(mJ/cc)
Total AC loss	5.967	6.747	(J/m)
Total AC loss (SC+Cu)	16.39	18.53	(mJ/cc-metal)

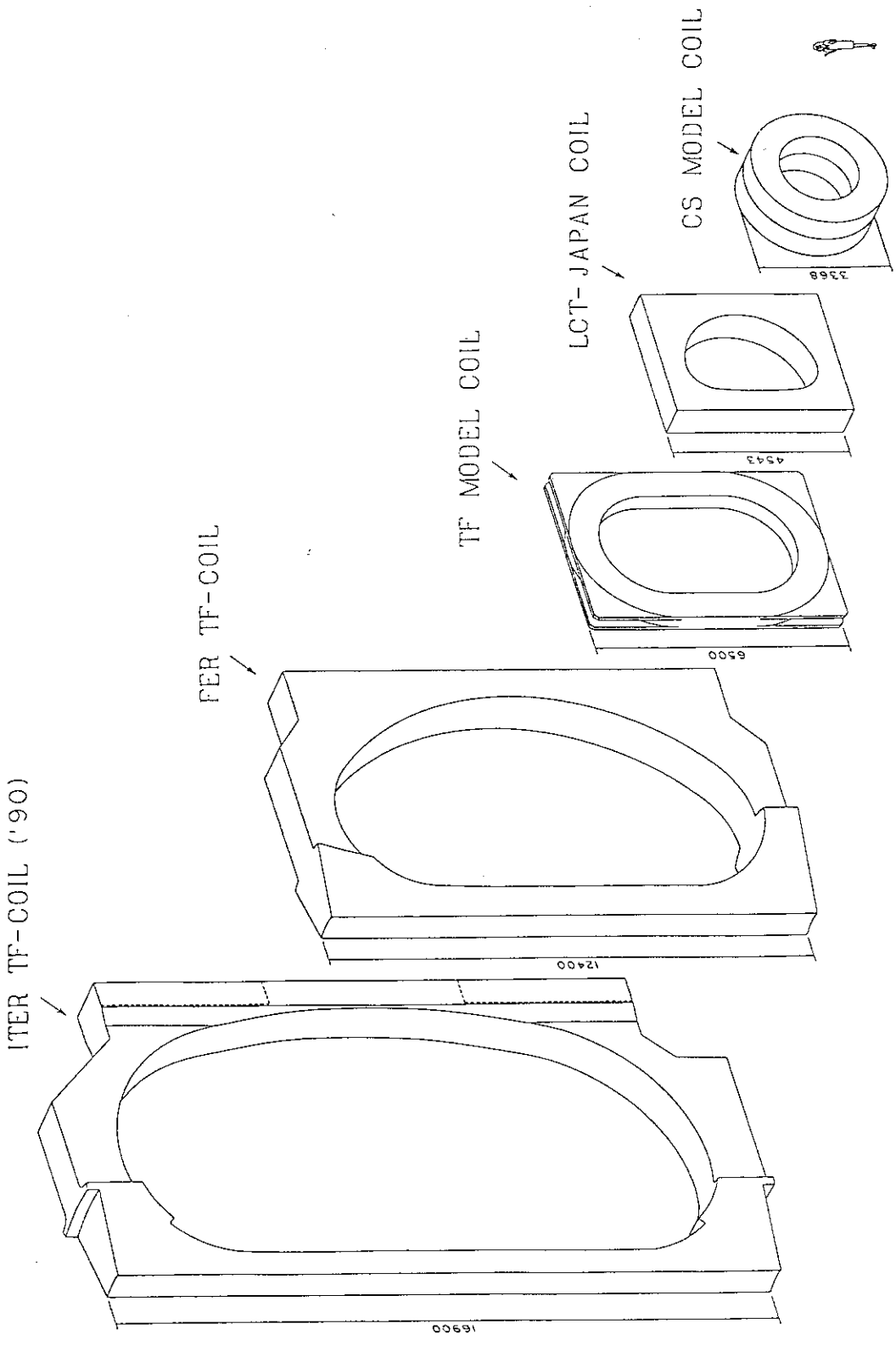

Fig. 3.1 Comparison between coil sizes of ITER, FER and LCT toroidal field coil

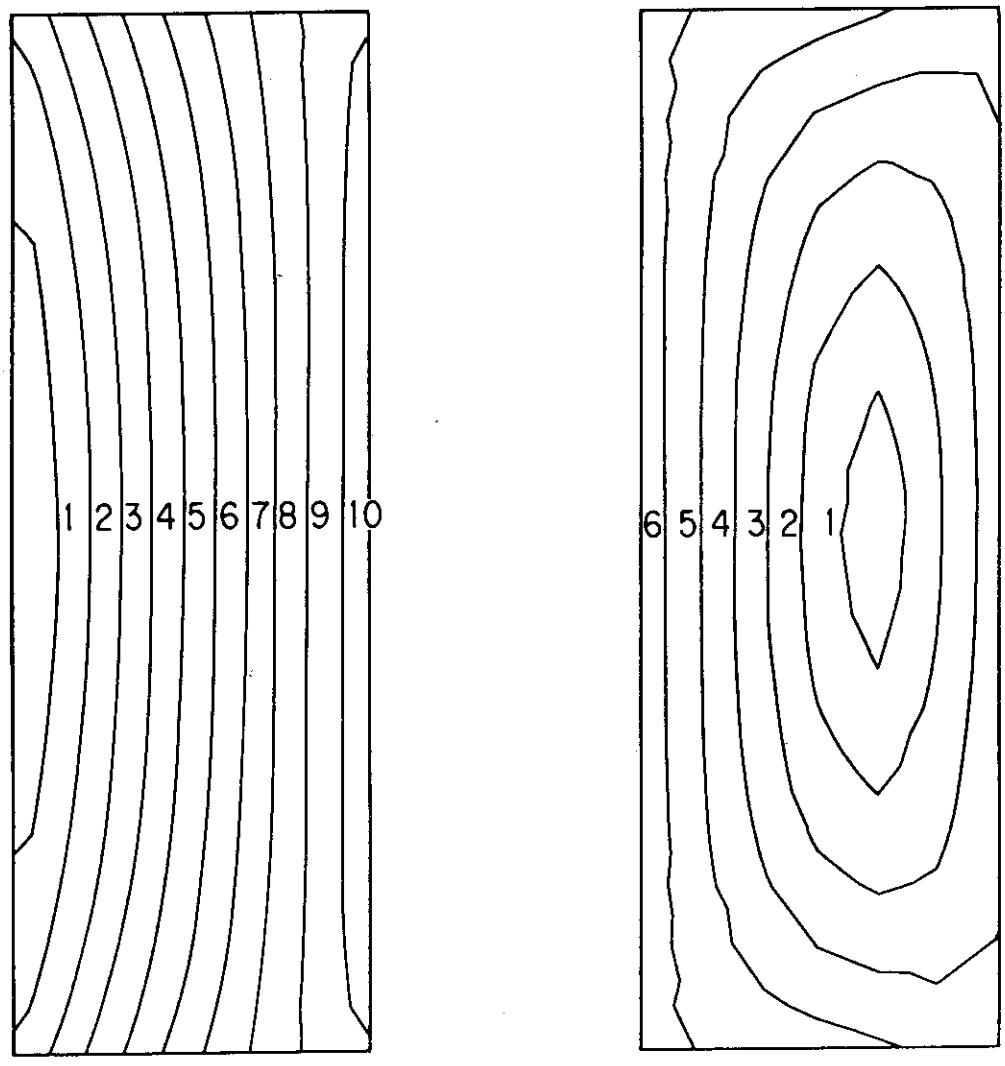

Fig. 3.2 Magnetic field distribution in in-bore and out-bore winding pack at TF coils solo operation

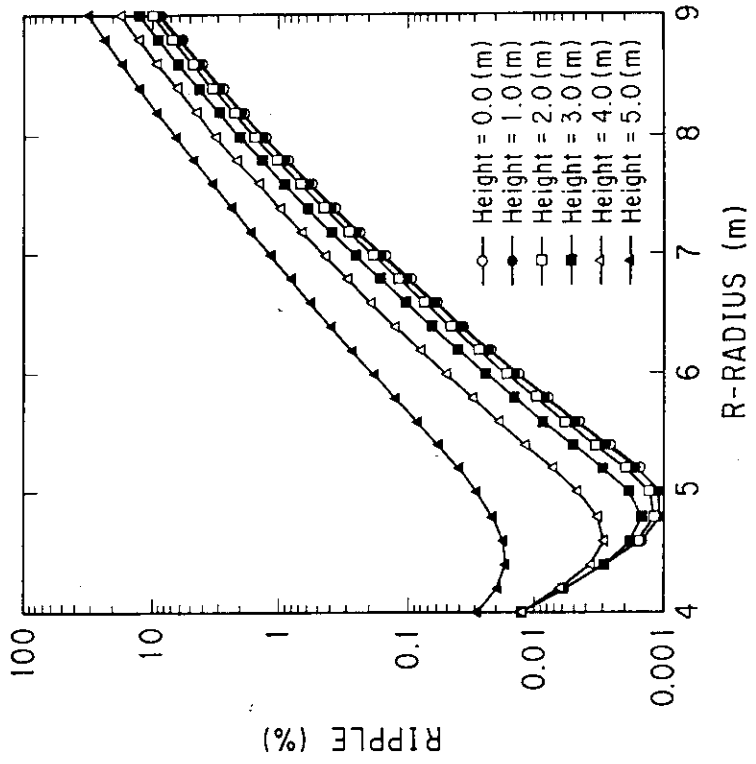

Fig. 3.4 Field ripple in plasma by the TF coil system

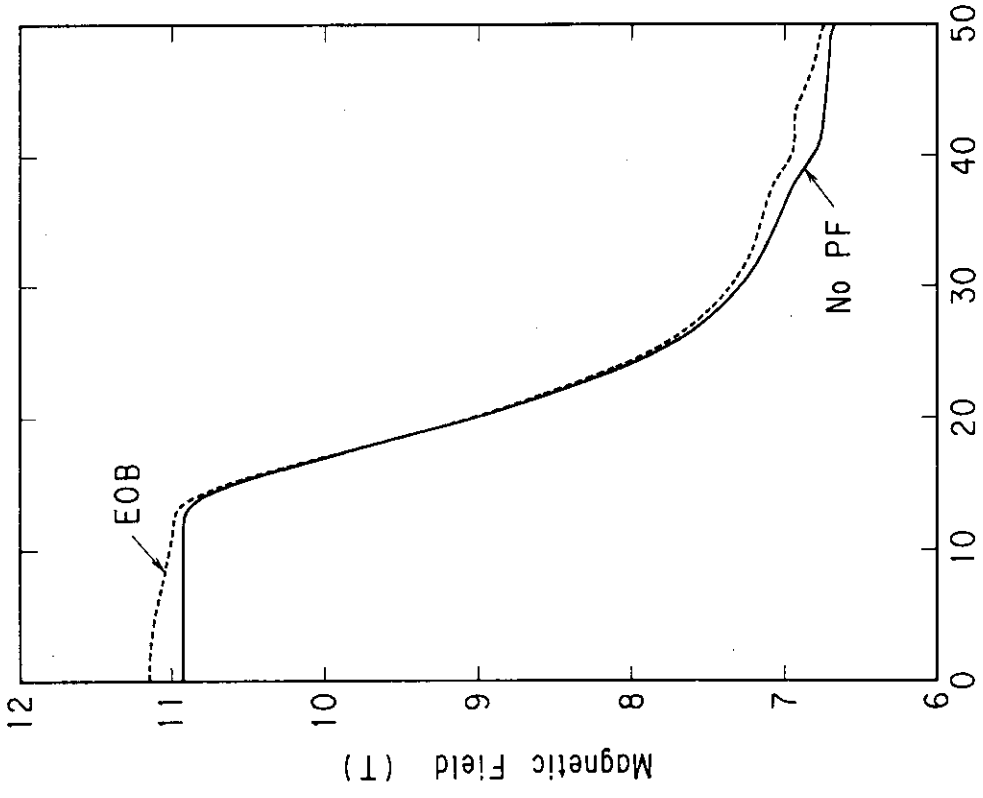

Fig. 3.3 Magnetic field distribution along inner bore at TF coils solo operation and EOB1

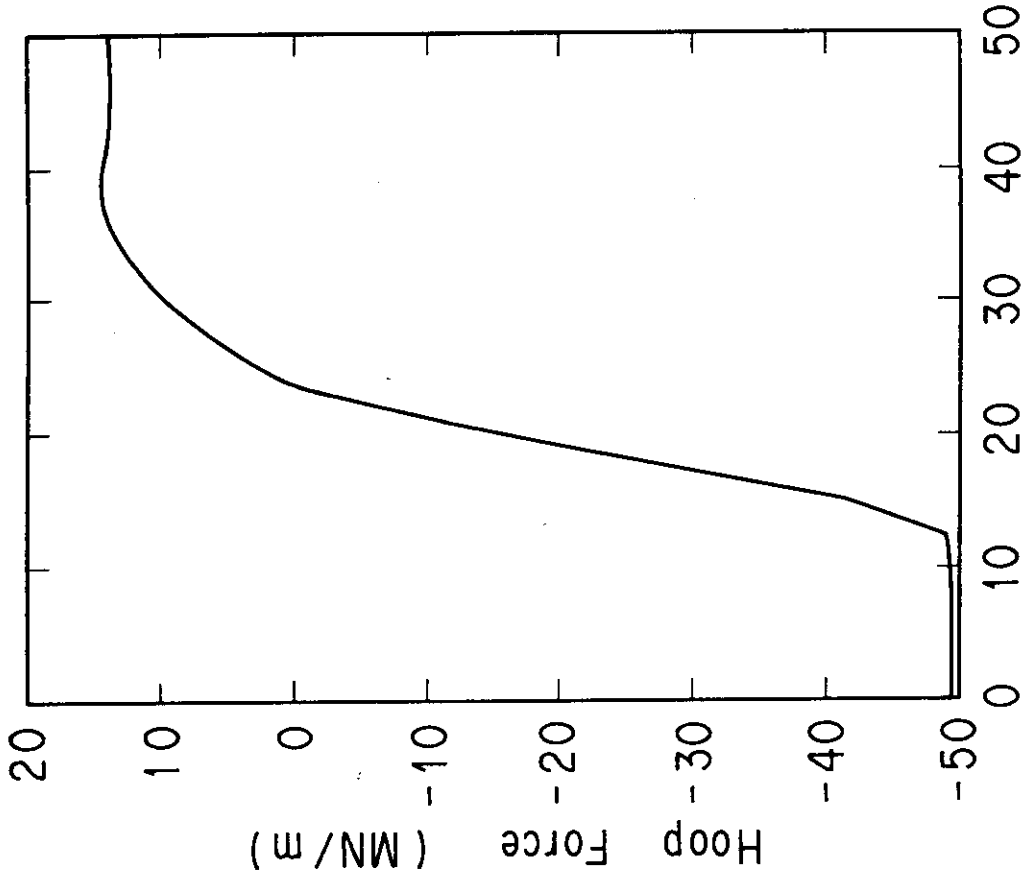

Fig. 3.6 Central force of the TF coil along winding

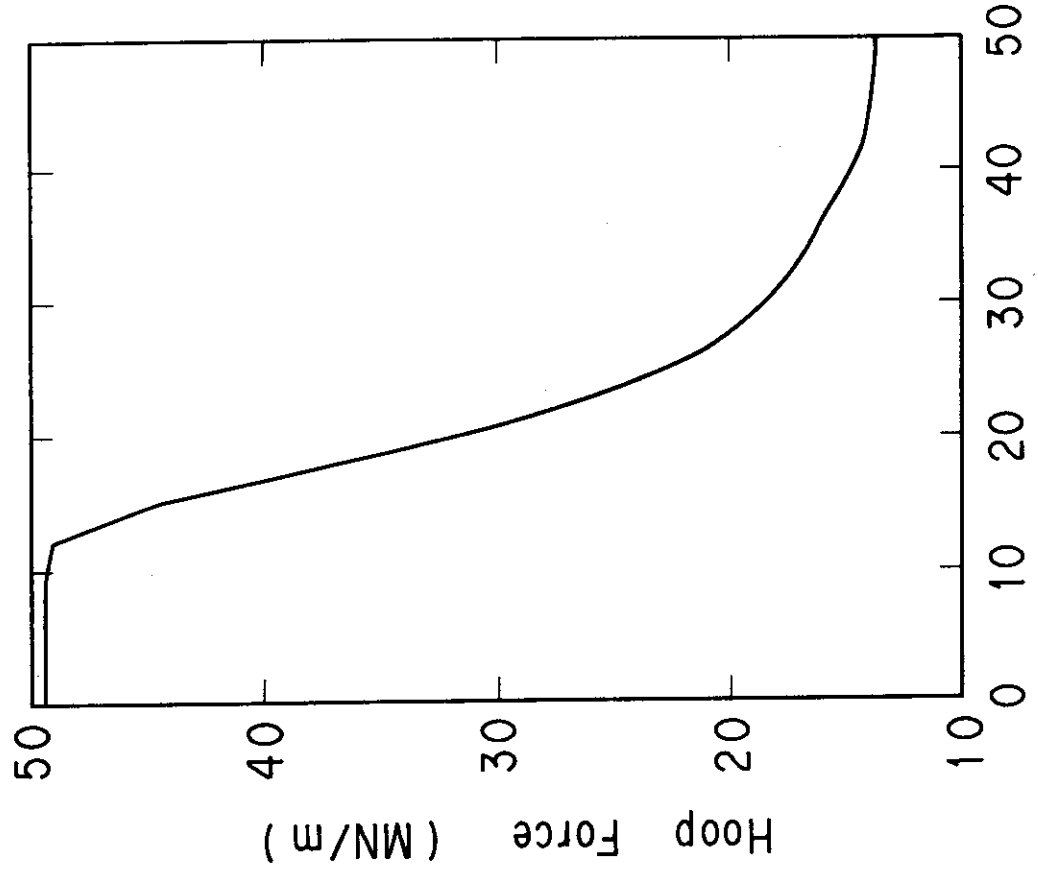

Fig. 3.5 Hoop force of the TF coil along winding

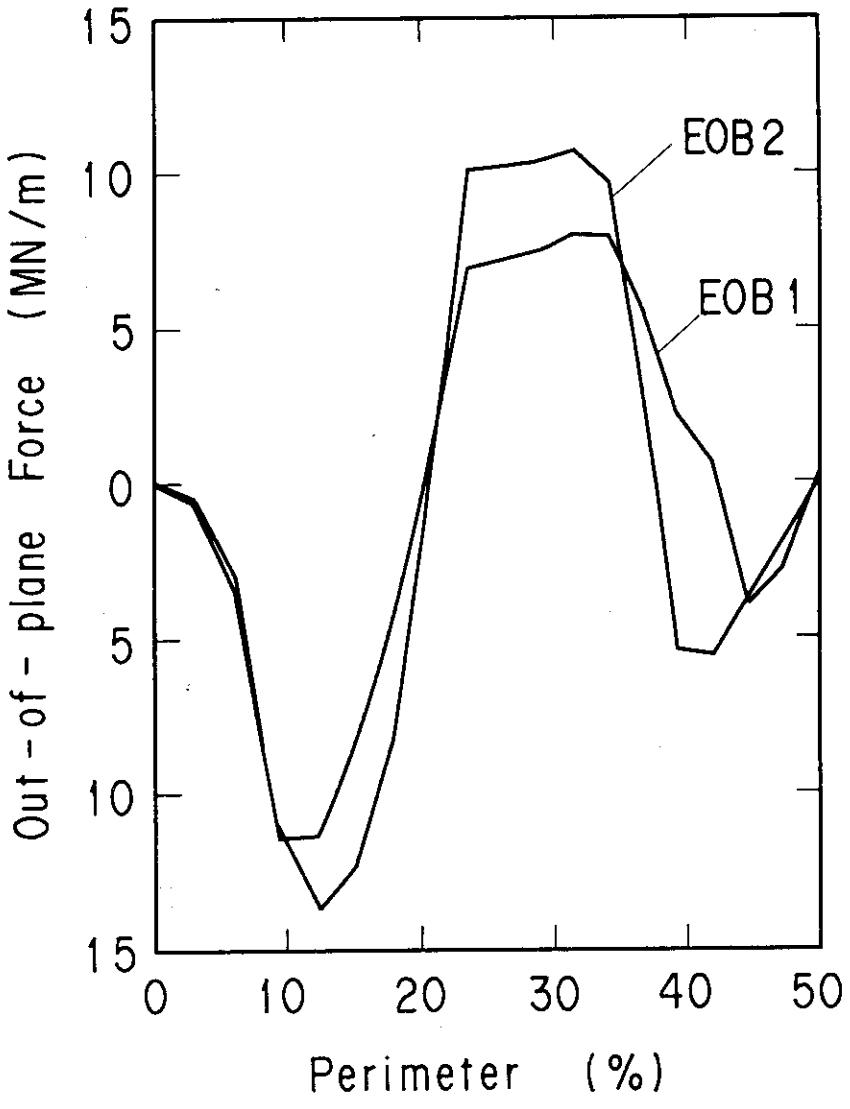

Fig. 3.7 Out-of-plane forces along winding at EOB1 and EOB2.

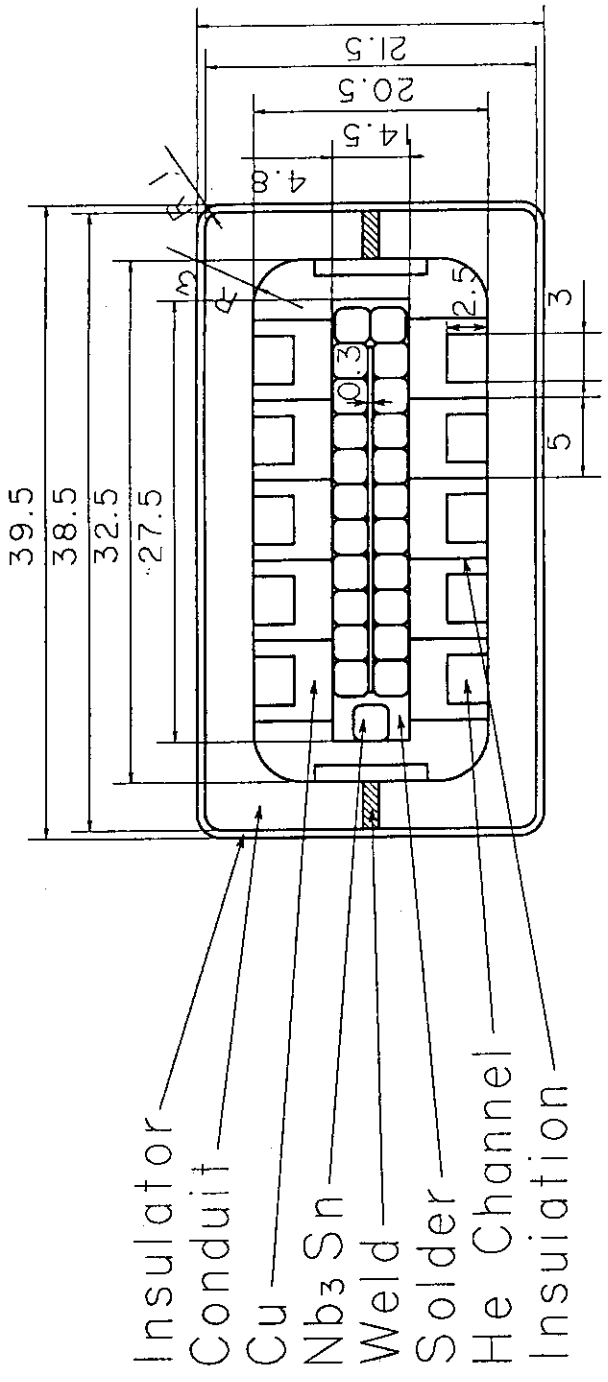

Fig. 3.8 Cross sectional view of the monolithic conductor for the TF conductor

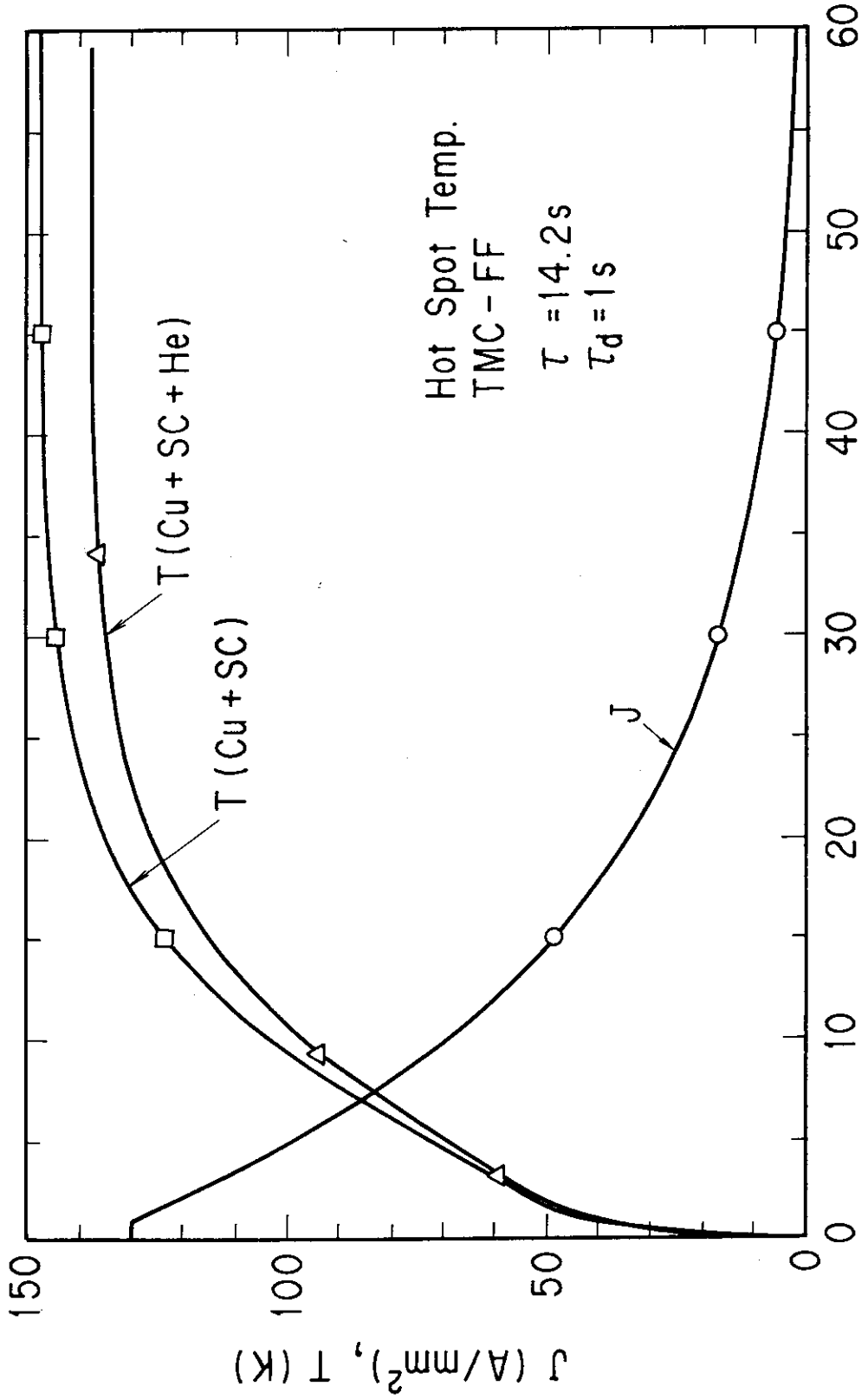

Fig. 3.9 Hot spot temperature of the TF conductor

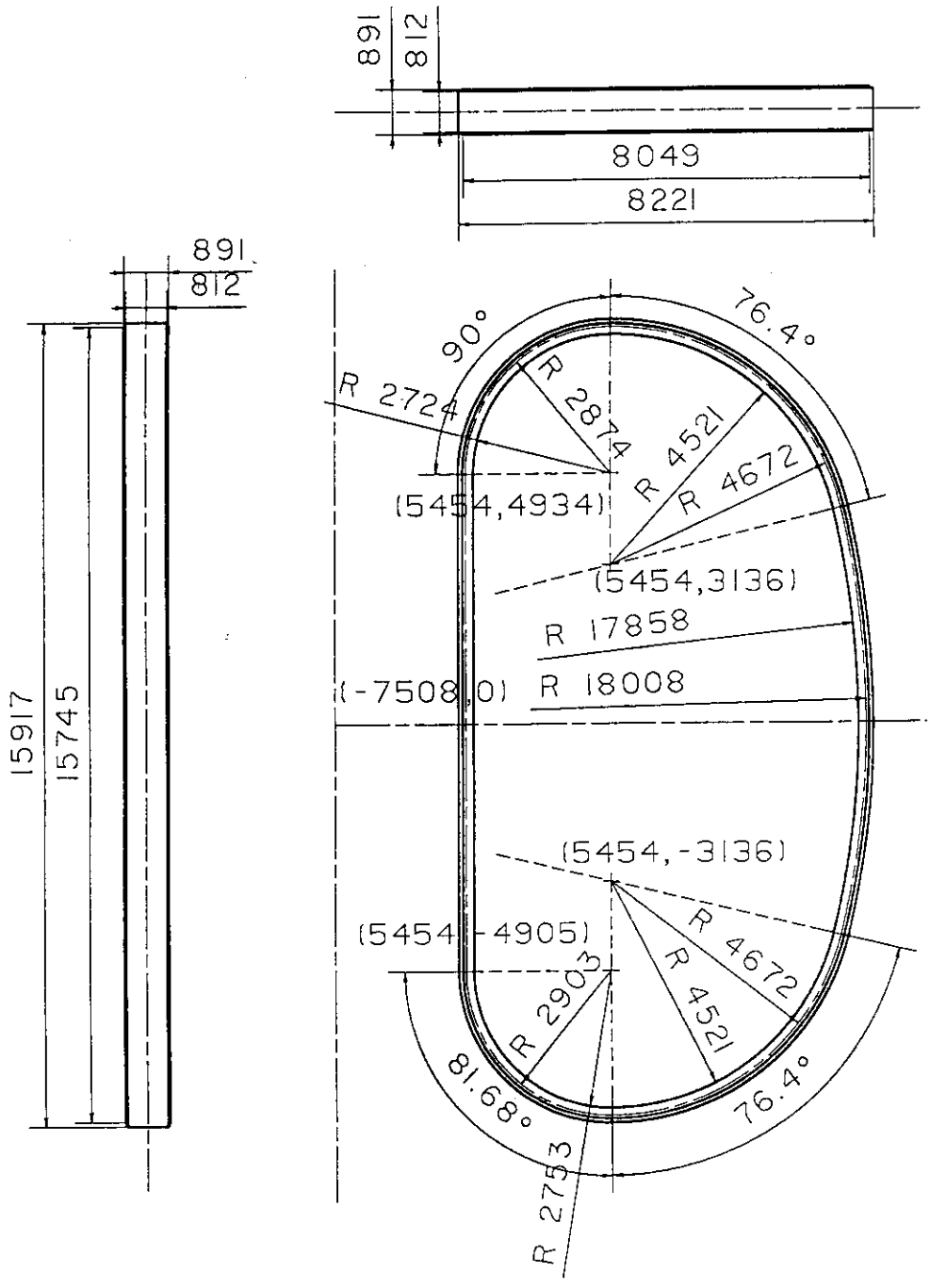

Fig. 3.10 Layout of the TF coil winding

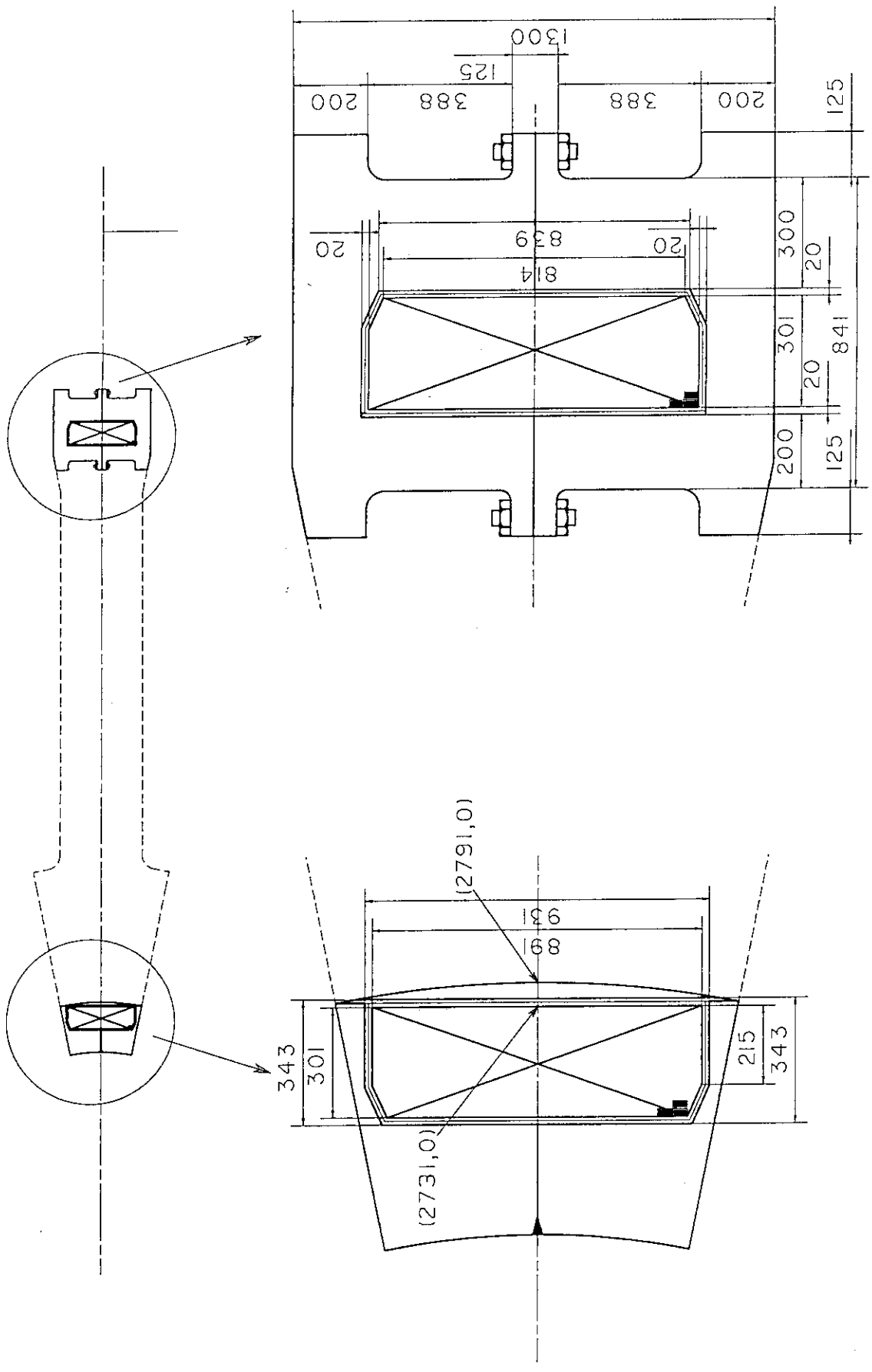

Fig. 3.11 Cross sectional view of the TF coil

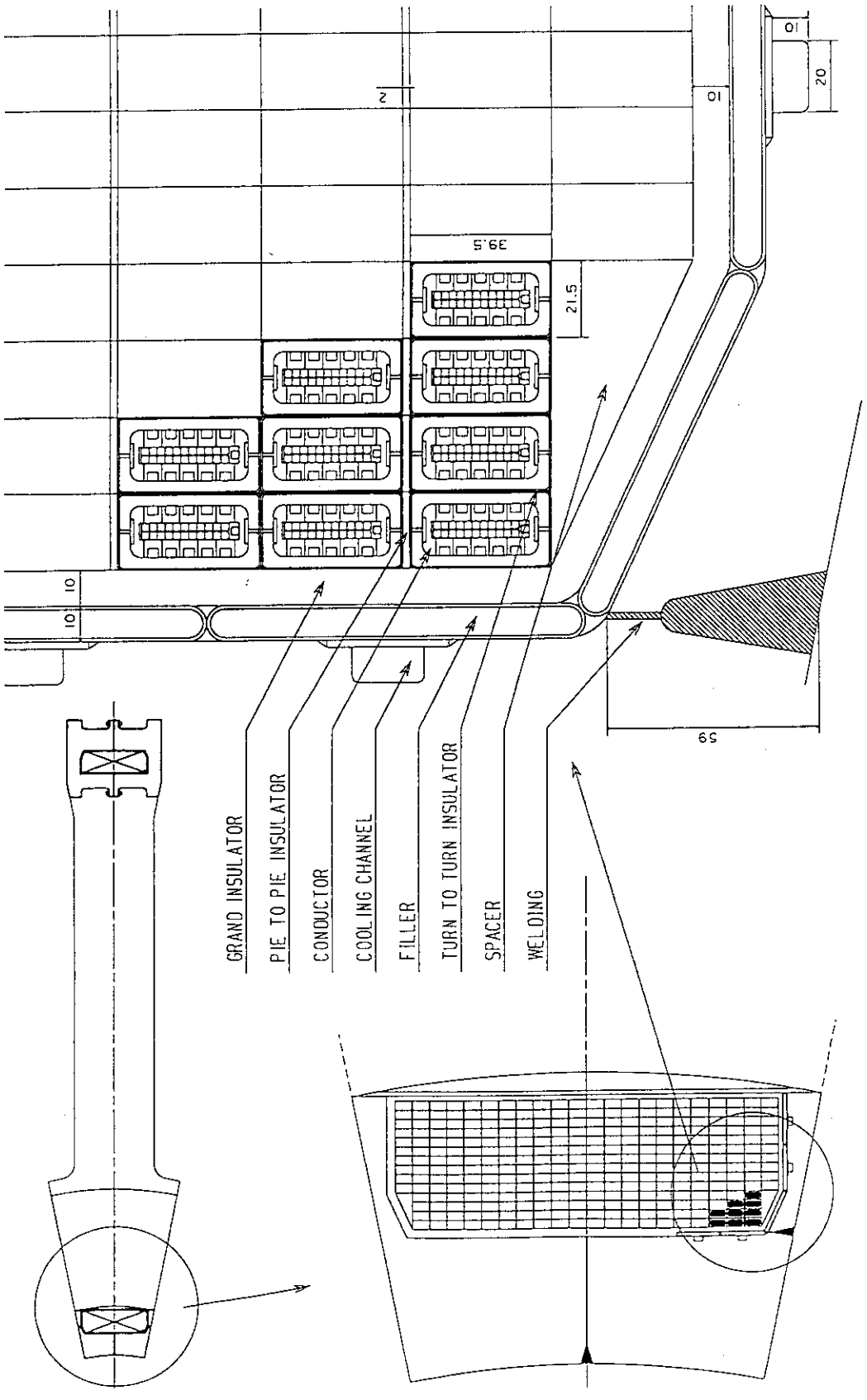

Fig. 3.12 Details of the TF coil winding

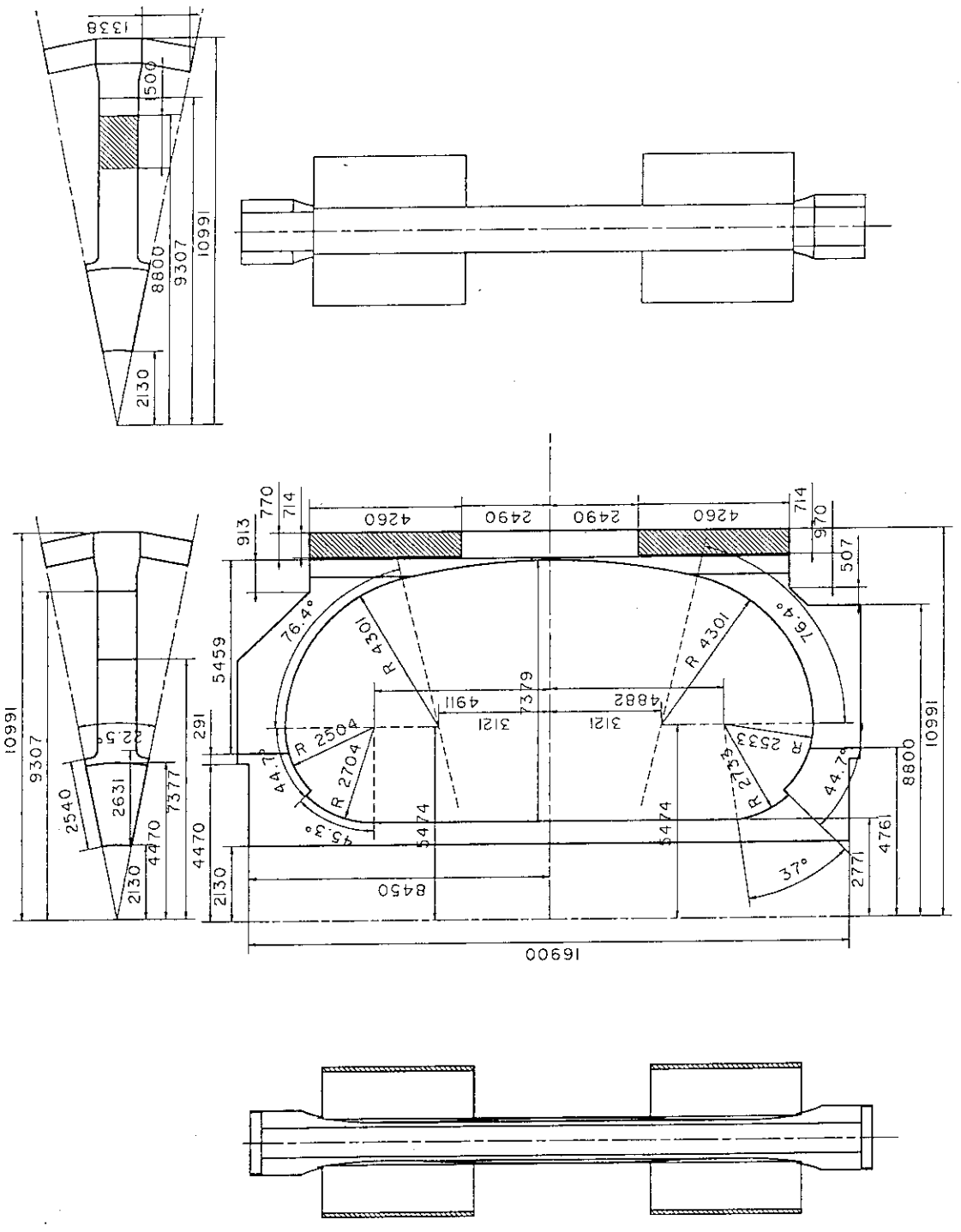

Fig. 3.13 Case of the TF coil

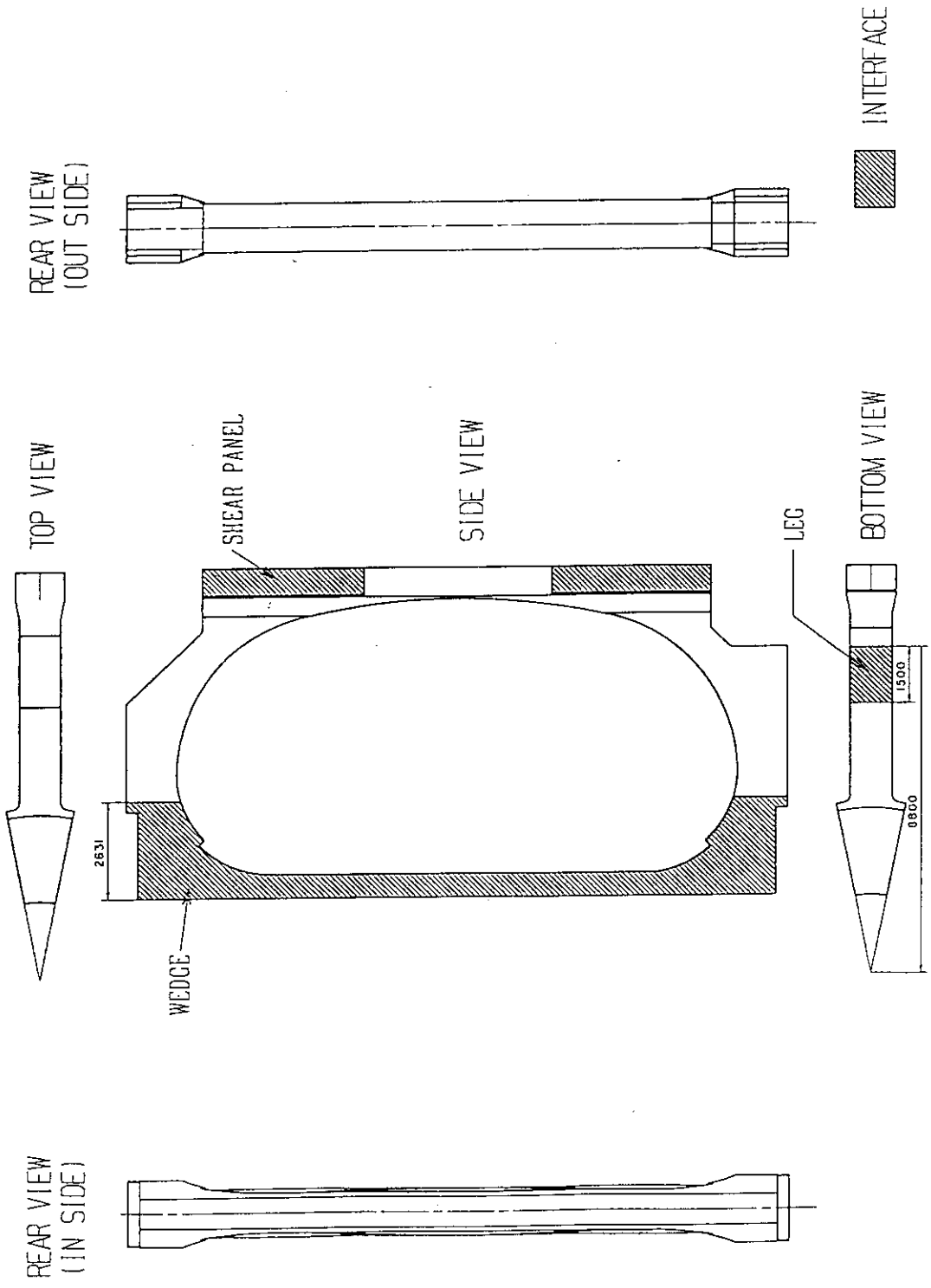

Fig. 3.14 Interface to structural support of the TF coil

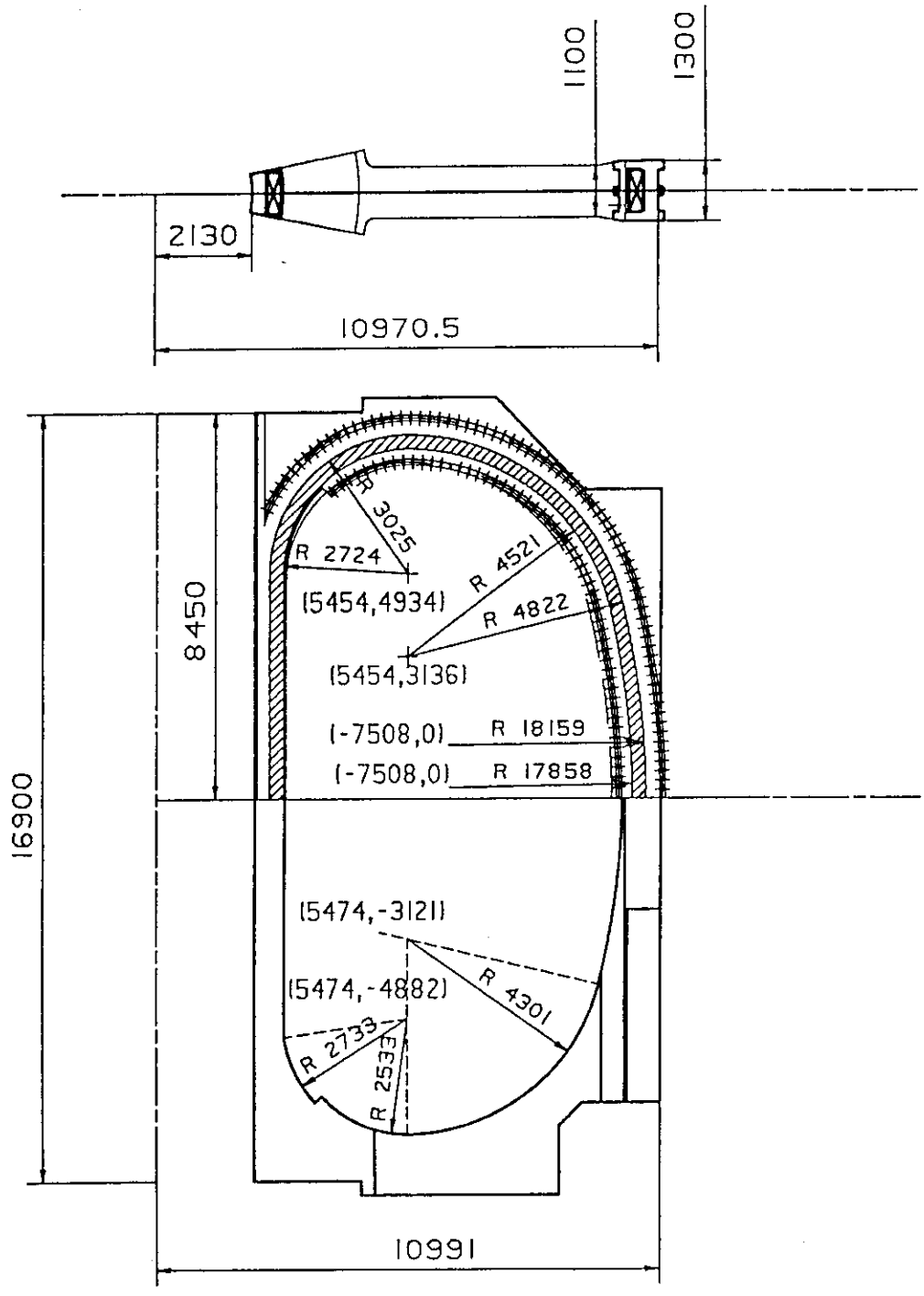

Fig. 3.15 Cross sectional view of the TF coil

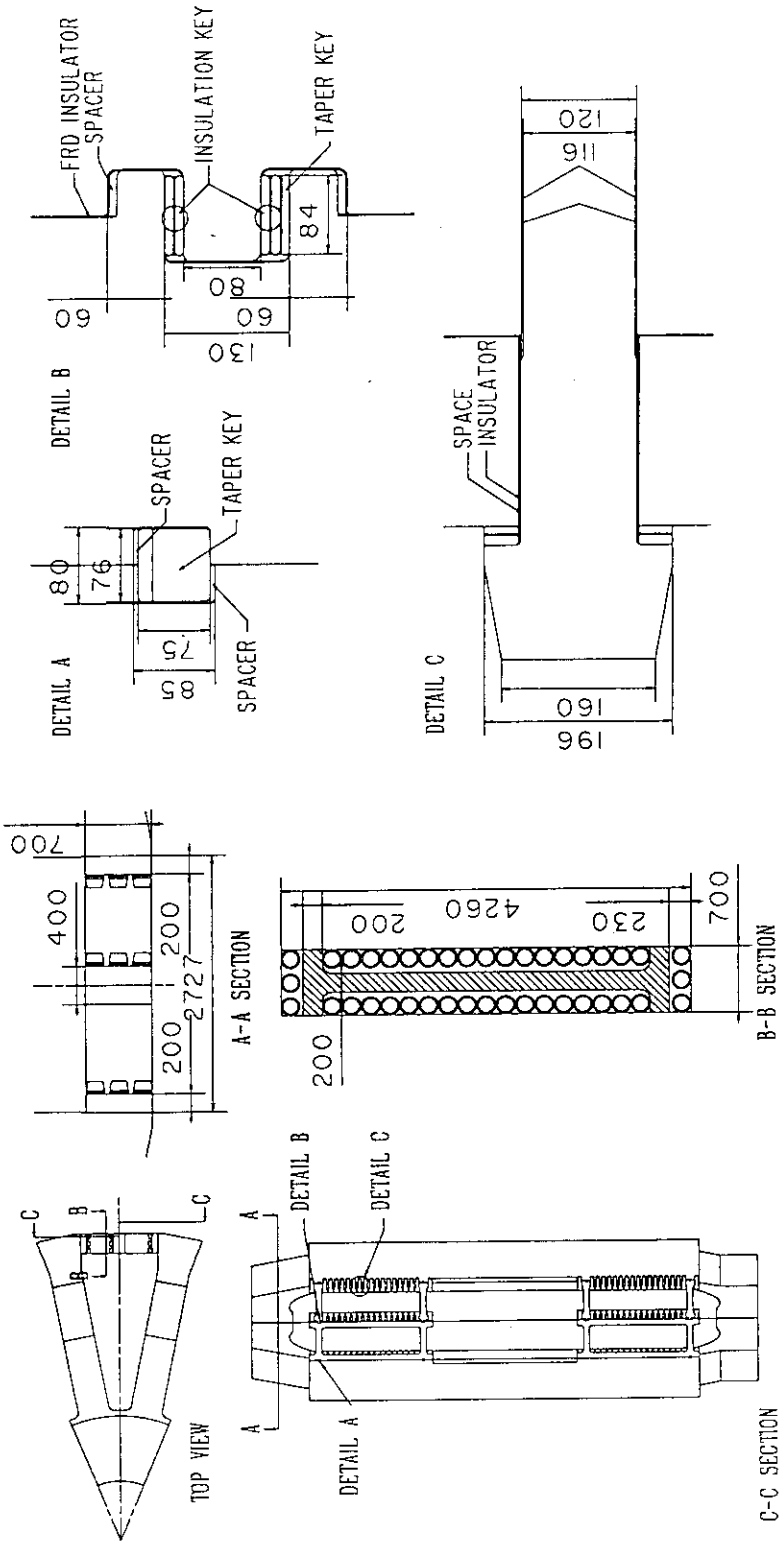

Fig. 3.16 Outer inter-coil structure

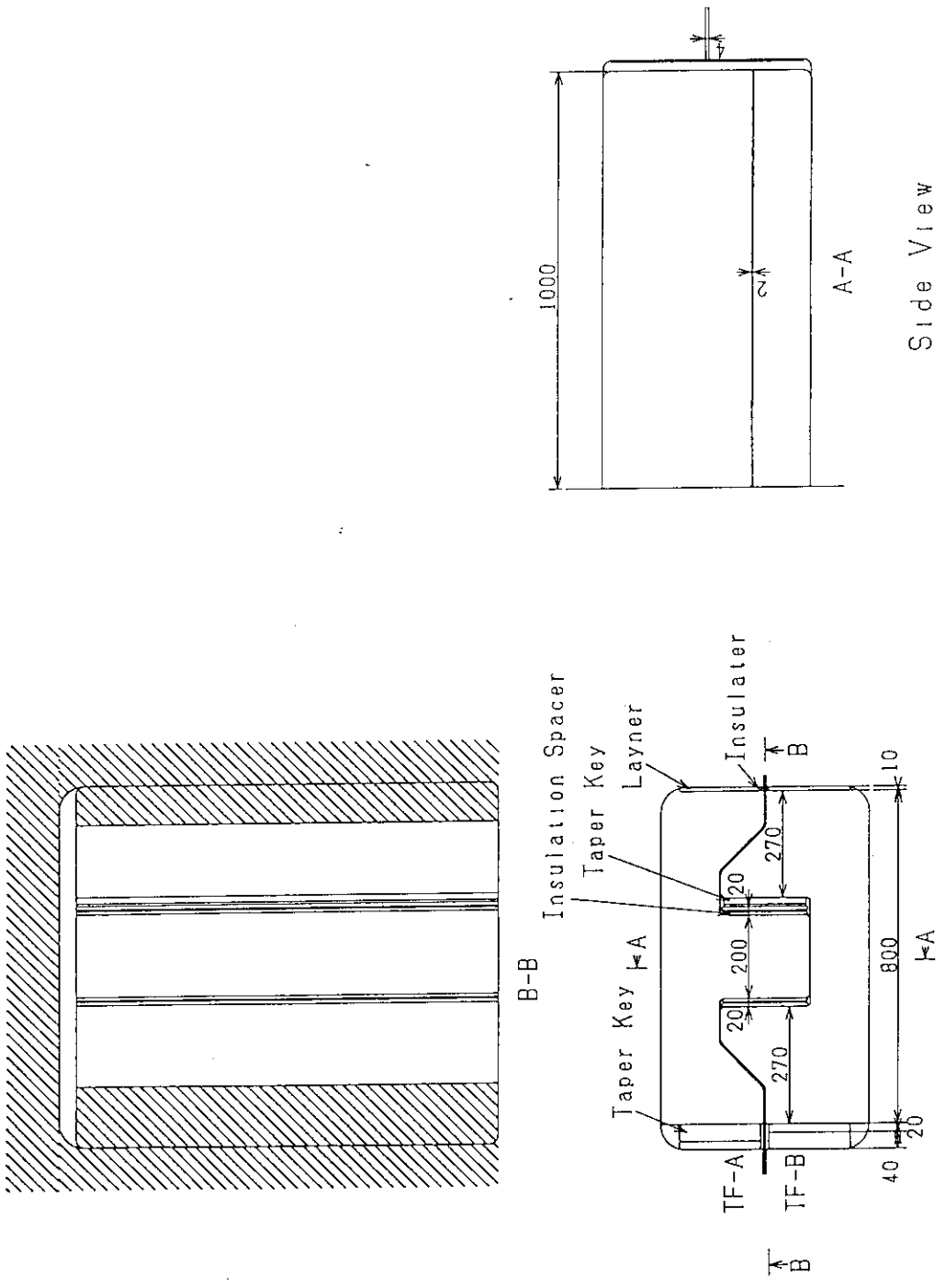

Fig. 3.17 Inner inter-coil structure

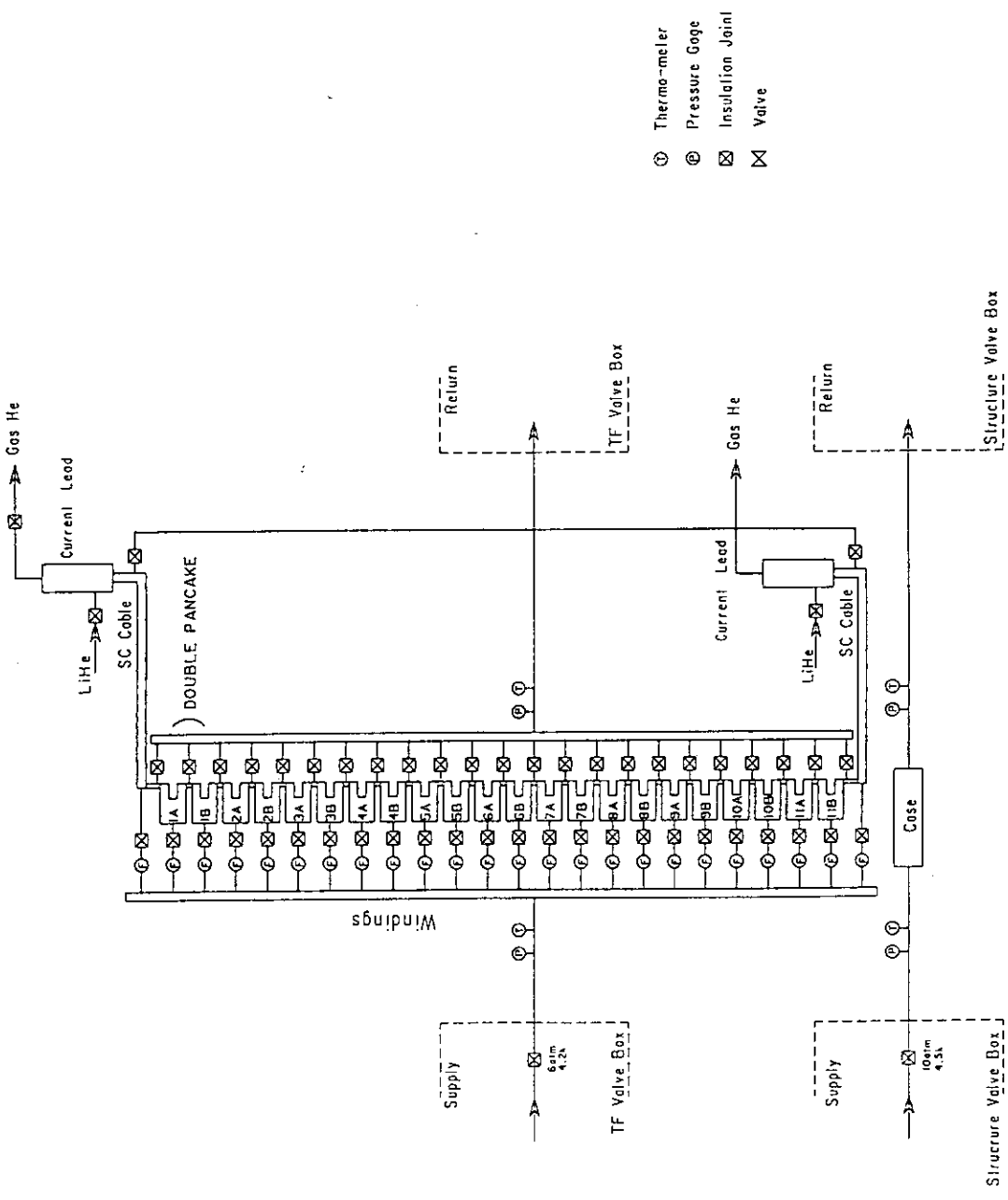

Fig. 3.18 Cooling pass of the TF winding and case

4. CENTRAL SOLENOID COIL

4.1 Introduction

The top view and the cross section of the Center Solenoid(CS) coils are shown in Fig.4.1. The CS coils have following properties:

(1) Function

The center solenoid coils' functions are to generate the equilibrium field and to supply magnetic flux to the plasma. The supplied flux was 128.6 Vs at initial magnetization and -186.6 Vs at "end of burn". The total flux swing is about 315 Vs. The maximum field is 13.5 T at "initial magnetization". The maximum averaged current density of winding is 20.6 A/mm^2 in 12.5 T at "end of burn".

(2) Dimension and configuration

The outer and the inner diameters of CS coil are 4.23 m and 2.820 m, respectively. The height of one CS coil is 1.90 m and 8 CS coils stacked . The total height is 15.2 m.

(3) Conductor

The forced flow cooling technique was adopted for all conductors because of the requirements of the mechanical properties and electrical insulation.

(4) Maintenance

Since the CS coils might be replaced more than once during 100,000 cycles operation, they should be designed with the consideration replaceability.

4.2 Design Concept

Design parameters of the center solenoid coil are listed in Table 4.1. Design parameters of the diverter coils (PF-5)are also listed in Table 4.2 as a reference.

(1) Conductor

- Preformed Armor Bundle type conductor : PF-CS40
- Superconducting material : $(NbTi)_3Sn$
- Each strand is insulated with Cr plating to decrease AC losses.

(2) Winding

- Preformed Armor type winding technique
- Rigid winding : Cured by semi-cured tape

(3) Case
- No steel coil case.
- Only 10 mm thickness for the ground insulation and the protection.

(4) Support structure
- Stainless support structure for the initial compression.
- Circumferentially insulated to decrease AC losses.

4.3. Basic Analysis

4.3.1. Magnetic Field

(1) Condition

Coil configurations and operating current patterns that were used for analysis are listed in Table 4.3 and 4.4, respectively. Operating current scenarios are:

(a) Initial Magnetization. (reference scenario [1])

(b) EOB1 (end of burn for reference scenario)

(2) Maximum magnetic field

Maximum magnetic field is 13.6 T during initial magnetization and 12.5 T at EOB1.

(3) Distribution of the magnetic field

Magnetic field distribution on the inner surface of CS coil in the vertical direction at initial magnetization and end of Burn are shown in Fig. 4.2 (a) & (b), respectively. The distribution in the radial direction on the horizontal plane, including the maximum field point, is shown in Fig. 4.3 (a) & (b). The field distribution cross section of each center solenoid coil at Initial Magnetization is shown in Fig. 4.4 (a), (b), (c) and (d). The corresponding figures at end of burn are shown in Fig. 4.5 (a), (b), (c) and (d). The field distribution in PF-5 coil is shown in Fig. 4.6 for a reference.

4.3.2. Magnetic Loads

(1) Condition

Operating current scenario.

(a) Initial Magnetization. (reference scenario)

(b) EOB1 (end of burn for reference scenario)

(c) EOB2 (the largest compressive condition)

(2) Radial and vertical force

The electromagnetic forces for initial magnetization, EOB1 and EOB2 are listed in Table 4.5.

4.3.3 Inductance

(1) Self and the mutual inductance are shown in Table 4.6. The plasma position was set to be that at EOB.

(2) Stored energy.

Initial Magnetization	:	12.42 (GJ)
EOB1	:	11.01 (GJ)

4.4 Cable

4.4.1 Preformed Armor Type[2][3]

The preformed armor type CICC is a conductor developed especially for large-size large-current coils whose conductors experience strong electromagnetic forces. This type of conductor is composed of a normal CICC with a thin first conduit and with a thick second conduit (armor) (shown in Fig. 4.7).

The two halves of armor are preliminarily formed into a coil shape by methods other than bending, such as milling, The Nb_3Sn CICC to the first conduit, which is already heat-treated with exact coil shape, is then put in the armor. Finally, the two halves of armor are welded onto each other. The major advantages of this type conductor in comparison with ordinary CICC are as follows:

(1)The armor can have any thickness, without any special manufacturing considerations.

(2) All the difficulties associated with the winding procedure, such as the protection of the insulator from the damage and winding tolerances, have been eliminated.

(3) The armor, whose role is to provide mechanical support, can be made by strong materials This armor is free from the severe heat treatment for Nb_3Sn formation.

(4) Sharp and thick corners of the armor, by reducing excess volume of the insulator, increase the rigidity of the

coil.

(5) The thin first conduit, which behaves as a helium sealer, has such advantages as easy seal-welding and low thermal contraction influence on the critical current capacity of Nb_3Sn.

(6) The Nb_3Sn superconductor does not suffer bending stress during the manufacturing process of the coil.

The detail design results of conductors for PF-1 to PF-5 are listed in Table 4.7.

4.4.2 Hot Spot Temperature

(1) Maximum temperature

The maximum hot spot temperature is designed to be 150 K.

(2) Protection condition

It is required that the dead time from initiation of normalcy to dump resistor current decay is 1.0 sec.

(3) Results

The dump time constant is 12.2 sec, which is over than the limited time (10 s) from terminal voltage (20 kV). The temperature rise during quench and protection is calculated as shown in Fig. 4.8.

4.4.3 AC Loss

(1) Equation : See Volume III (AC LOSS).

(2) Results : See Volume III (AC LOSS).

4.4.4 Stability

(1) Requirement

The stability is over 200 mJ and the limiting current over than the rated current.

(2) Stability margin

Temperature Margin is 3 K.

(3) Limiting current

Calculated limiting current at 13.5 T is 65.2 kA, This

value is over than rated current of 37.4 kA.

4.4.5 Hydraulic

(1) Requirement

The pressure drop is less than 2 bar

(2) Calculation

The experimental factor of friction is 2.0.

(3) Results

Pressure drop of PF-1,4 is 0.60 bar per coil. The pressure drop of PF-5 is 1.06 bar per coil.

4.5 **Winding Pack**

4.5.1 Layout

(1)The top view and the cross section is shown Fig. 4.9. The width of the insulation is about 10 mm. The center of the winding was located about 50 mm shifted from the center of the coil. However, the offset of the current center from the coil center is about 7 mm considering a traverse and a joint of the conductor. The radius of the current center is 1773 mm.

(2) Three types of the structural gradings are shown in Fig. 4.10.

(a) Non grading

(b) Grading

(c) Linear grading

For the calculation of the magnetic field , the (c) grading model was used for the calculation.

(3) The winding layout of the one double pancake is shown in Fig. 4.11. Since a double pancake has a traverse part, there is a cross-section in which the upper pancake piles up on the lower one.This results in a displacement of a half or less than a half width of conduit as shown in Fig. 4.11. In this report, the names of 'ordinary part' and 'extraordinary part' are used to distinguish such a part from another part. The ordinary part has no such a displacement, while the extraordinary part has half of the conduit width displacement.

4.5.2 Stress

The stresses of the winding are pictorially described in Volume II (STRESS ANALYSIS). The maximum stress is about 600 MPa for the reference scenario and 650 MPa for the most severe operation with flexibility. The maximum stresses at EOB2 are

Ordinary part : 615 MPa
Extraordinary part : 654 MPa

The stress in the extraordinary part, in which the conduits pile up with a half of the conduit width displacement, is larger than that of the ordinary part.

The stainless filler, which is packed in the empty space between the top and the bottom pancakes in the extraordinary part is required to reduce the stresses down to allowable values.

4.5.3 Pancake connection

One double pancake with the coil connection is shown in outside of D-D' section of fig. 4.11 and Fig 4.13.

4.6 Support structure

(1) Structure

The CS coil support structure is shown in Fig. 4.12. The stainless support structure is composed of the upper and the lower compression part and the center cylindrical part. This structure is insulated circumferentially to decrease AC loss. A section of the upper part consists of an assembly of the radial stainless channel.

(2) Initial compression

The initial compression of 180 MN is required to prevent separation of the CS coils. The resulting amount of the compression is about 16 mm.

The thermal shrinkage method was adopted for the initial compression. About 60 degree temperature difference is required between the CS coils and the support structure for the initial compression.

(3) Stress

The details of the stress analysis are described in Volume II (STRESS ANALYSIS). The stress due to the initial compression during initial assembly at room temperature is most severe. The maximum Tresca stresses of the upper and the lower part of the support structure are 206 MPa and 197 MPa at initial compression, respectively.

4.7 Connection to piping

(1) The top view and the development drawing of the pancake and the pancake connections are shown in Fig. 4.13. The pancake connections are located helically around the CS coil for two purposes. One is to reduce the error field due to the non coaxial (~7mm) location between the coil and torus center. The other is to prevent pile up vertically of the connection parts, which are mechanically weak parts.

(2) The helium supply inlet is located at the inner part and the outlet is at the outer part, as shown in Fig. 4.13.

(3) The schematic drawing of the concepts for the current lead and the coolant supply are shown in Fig. 4.14.

(4) The overview of the He piping and the current supply is shown in Fig. 4.15.

(5) The helium piping and the current supply in the building are shown in Fig. 4.16 (a),(b).

4.8 Manufacturing

Preformed Armor type CICC is the new type conductor developed especially for large-size large-current coils whose conductors expérience strong electromagnetic forces. This type of conductor is composed of (1) a normal CICC with thin first conduit and (2) a thick second conduit (armor) (shown in Fig. 4.7). The halves of coil-shaped armors are manufactured by milling or another method besides bending. The Nb_3Sn CICC with first conduit, which is already heat-treated with exact coil shape is put in them, is inserted into the two halves of the armor and it is welded together. Then, turn-to-turn insulation and ground insulation is done. Finally, the coil is epoxy-impregnated. Figure 4.17 shows the schematic flow chart of

this manufacturing process. Major advantages of this type of conductor compared with the ordinary CICC are as follows:

(1) The armor can have any thickness required without any special manufacturing considerations.

(2) All difficulties attended with winding procedure, such as the protection of the insulator from the damage and the winding tolerance, are eliminated.

(3) The armor, whose role is mechanical supporter, can be made with a strong material, since the armor is free from the severe heat treatment during Nb_3Sn formation.

(4) Sharp and thick corners of the armor reduce excess volume of the insulator this adding rigidity to the coil.

(5) The thin first conduit, which behaves as a helium sealer, has advantages of easy seal-welding. It also less creates thermal-contraction-influence on the critical current capacity of Nb_3Sn.

(6) Nb_3Sn superconductor does not suffer bending stress during manufacturing process of the coil.

This type of manufacturing process was developed and was established in the DPC-TJ program [3,4,5,6,] and the prototoroidal conductor project [7,8,9]. The first preformed-armor type superconducting coil, the DPC-TJ coil (1.0 m-ID, 1.8 m-OD, 0.11 m-H, 12 T, 24 kA, 1.7 MAT), is already completed and is being tested.

4.9 **Instrumentation**

4.9.1 Voltage Monitor (See Table 4.8 and 4.9)

Voltage taps should be attached directly to the conductor conduit or preferably a superconducting cable inside a conduit. The functions of the voltage taps are to monitor pancake voltages and coil terminal voltages during operation The voltages are analyzed to check if there are anomalous conditions inside coils, and to detect normal voltages so that the coil protection circuit can be initiate. To avoid electrical shorts inside a coil, voltage taps should not be attached inside the coil winding. Each voltage tap should have two instrumentation

wires for redundancy. It is not necessary to monitor the voltage of an electrical joint itself, since excessive joule heating at this part can be detected by downstream temperature rises or normal voltages inside coil.

To detect normal transition of a coil, the compensation method, can be used by using a compensation coil that is co-wound with a conductor. Each pancake should have two compensation coils inside its winding. A schematic configuration is given in Fig. 4.18.

4.9.2 Fluid Monitor (See Table 4.10 and 4.11)

To monitor the operating conditions of the coil, temperature, pressure, mass flow rate, and differential pressure of coolant helium should be monitored. A schematic drawing is shown in Fig. 4.19. These sensors should be located in the cryogenic piping at a low-potential region which is electrically insulated by insulation joints. Monitoring of flow rate can also be used for detecting coil quenches as shown in Fig. 4.20.

4.9.3 Others

To monitor strains of the coil structure, strain gauges (rosette) may be attached on the surface of the structures. In addition, to investigate the displacements and deformation of coils, displacement transducers may be installed. In any case, these sensors should be located at low-potential region.

4.10 **Interpolation of Summary**

The conceptual design of the CS coil is completed.

(1) The stored energies of the PF coils are

Initial Magnetization : 12.42 (GJ)

EOB (Reference) : 11.01 (GJ).

(2)The Maximum Tresca stress was 615 MPa in the ordinary part and 654 MPa at extraordinary part.

(3) The initial compression of 180 MN is required to prevent separation of the CS coils.

(4) The preformed armor type conductor was adopted for the CS coils conductor.

References

[1]ITER-CDA PF Group,"ITER Poloidal Field System", ITER Document Series, No-27 IAEA, Vienna Austria 1990.
[2] Yoshida, M. F. Nishi, Y Takahashi, et al.," DESIGN OF THE PROTOTYPE CONDUCTORS FOR THE FUSION EXPERIMENTAL REACTOR", IEEE Transactions on Magnetics 25-2 (1989) 1488
[3] H. Mukai, O. Osaki, T. Hamajima, et al., "Fabrication of DPC-TJ, a Forced-cooled Large Superconducting Coil", Proc of MT-11 (1990) 852
[4] Y. Sanada, et al., "Development of a Forced-cooling Cable-in-conduit Superconducting Coil (DPC-TJ)", Proc. of ICEC-12, 1988, pp. 789-793
[5] T. Hamajima, et al., "Development of a Forced-cooled Superconducting Coil with High Average Current Density (DPC-TJ)", IEEE Trans. on Magnetics, Vol. 25, 1989, pp. 1721-1724
[6]M. Nishi, et al., "Results of Verification Tests and Coil Test of DPC-TJ", Proc., of MT-11, (1990) 856
[7] K. Yoshida, et al., "Design of the Proto-type Conductors for the Fusion Experimental Reactor", IEEE Trans. on Magnetics, Vol. 25, 1989, pp. 1488-1491
[8] K. Yoshida, et al., "Developments of the Prototype Conductors and Design of the Proto Toroidal Coil for the Fusion Experimental Reactor", Proc. of MT-11, (1990) 890
[9] M. F. Nishi et al., "Development of the Proto-type Conductors and Design of the Test Coil for the Fusion Experimental Reactor", Proc of 13th symp. on Fusion Eng. (1990) 780.

Table 4.1 Design Parameter of the Centeral Solenoid Coil (ITER-PF-1,4)

	INIT	EOB	
Max. Field	13.5	12.5	T
Rated Current	37.4	40.7	kA
Margin of Ic		1.71	
Current Density of Coil Space		19.0	A/mm^2
Ampere-turn / Coil	20.6	22.4	MAT
Mean Diameter		3.50	m
Thickness		0.590	m
Height		1.846	m
Number of Total Turns		550 (12.5x2x22)	
Double Pancakes		22	
Cooling Passages		44	
Dump Time		10	s
Length of Cooling Pass		137	m
Mass Flow Rate		10.0	g/s
Inlet Temperature		4.5	K
Pressure		6.0	bar
Pressure Drop		0.60	bar
Poloidal Cycle	< 5,000		
Cool-down Cycle	< 20		

Table 4.2 Design Parameters of the Divertor Field Coil (ITER-PF-5)

Max. Field		8.5	T
Rated Current		40.7	kA
Margin of Ic		2.	
Current Density of Coil Space		22.8	A/mm^2
Ampere-turn / Coil		18.5	MAT
Mean Diameter		7.80	m
Thickness		0.752	m
Height		0.850	m
Number of Total Turns		400 (10x2x10x2)	
Double Pancakes		10	
Cooling Passages		40	
Dump Time		10	s
Length of Cooling Pass		245	m
Mass Flow Rate		10.0	g/s
Inlet Temperature		4.5	K
Pressure		6.0	bar
Pressure Drop		1.06	bar
Poloidal Cycle	< 10,000		
Cool-down Cycle	< 20		

Table 4.3 Sizes and Location of PF Coils

	R(m)	Z(m)	DR(m)	DZ(m)
PF-1	1755	950	590	1848
PF-2	1755	2850	590	1848
PF-3	1755	4750	590	1848
PF-4	1755	6650	590	1848
PF-5	3900	9000	900	900
PF-6	11500	6000	500	1500
PF-7	11500	3000	500	900
PLASMA	6000	0	2150	4773

Table 4.4 Currect Variations of PF coils

	IMAG(MA)	SOFT1(MA)	SOFT2(MA)	EOB1(MA)	EOB2(MA)
PF-1	20.41	-16.79	-17.46	-22.30	-22.42
PF-2	20.41	-16.79	-17.46	-22.30	-22.42
PF-3	20.41	2.85	4.47	-9.14	-11.45
PF-4	20.41	0.00	5.25	0.0	2.61
PF-5	14.53	13.60	9.32	6.25	11.71
PF-6	0.25	-8.95	-5.03	-6.49	-13.61
PF-7	0.25	-2.72	-5.09	-5.25	0.36
PLASMA	0.00	22.00	22.00	22.00	22.00

Analysis parameter: IMAG, SOFT1, EOB1:Refernce,
SOFT2:Li=0.75, Bp=0.0, EOB2:1i=0.55, Bp=0.0

Table 4.5 Electromagnetic force per one turn

[IMAG]	FR(MN)	FZ(MN)			
PF 4U	1333.1	-362.9			
PF 3U	1422.2	-36.8			
PF 2U	1436.6	-4.9			
PF 1U	1438.9	-0.6			
[SOFT1]	FR(MN)	FZ(MN)	**[SOFT2]**	FR(MN)	FZ(MN)
PF 4U	0.0	0.0		73.1	8.4
PF 3U	-7.1	53.2		5.8	105.1
PF 2U	410.3	-322.0		421.4	-382.3
PF 1U	513.6	-29.4		551.7	-36.9
[EOB1]	FR(MN)	FZ(MN)	**[EOB2]**	FR(MN)	FZ(MN)
PF 4U	0.0	0.0		-4.0	46.8
PF 3U	264.7	-216.8		326.2	-308.5
PF 2U	1069.0	-313.9		1069.1	-284.2
PF 1U	1163.1	-26.3		1154.6	-23.2

Table 4.6 PF-Coil and Plasma Self and Mutual inductance matrix.

PF1U	PF2U	PF3U	PF4U	PF5U	PF6U	PF7U	PF7L	PF6L	PF5L	PF4L	PF3L	PF2L	PF1L	PLASMA
8.95D-01	2.94D-01	7.18D-02	2.59D-02	2.79D-02	7.21D-02	5.62D-02	4.98D-02	5.88D-02	1.65D-02	1.18D-02	2.59D-02	7.18D-02	2.94D-01	5.26D-04
2.94D-01	8.95D-01	2.94D-01	7.18D-02	5.13D-02	8.45D-02	5.90D-02	4.16D-02	4.66D-02	1.04D-02	6.28D-03	1.18D-02	2.59D-02	7.18D-02	4.14D-04
7.18D-02	2.94D-01	8.95D-01	2.94D-01	1.03D-01	9.26D-02	5.70D-02	3.34D-02	3.65D-02	6.96D-03	3.71D-03	6.28D-03	1.18D-02	2.59D-02	2.76D-04
2.59D-02	7.18D-02	2.94D-01	8.95D-01	2.15D-01	9.38D-02	5.10D-02	2.63D-02	2.85D-02	4.85D-03	2.37D-03	3.71D-03	6.28D-03	1.18D-02	1.73D-04
2.79D-02	5.13D-02	1.03D-01	2.15D-01	1.95D+00	3.12D-01	1.45D-01	6.71D-02	7.30D-02	1.11D-02	4.85D-03	6.96D-03	1.04D-02	1.65D-02	3.16D-04
7.21D-02	8.45D-02	9.26D-02	9.38D-02	3.12D-01	4.95D+00	1.37D+00	5.07D-01	5.48D-01	7.30D-02	2.85D-02	3.65D-02	4.66D-02	5.88D-02	1.38D-03
5.62D-02	5.90D-02	5.70D-02	5.10D-02	1.45D-01	1.37D+00	2.13D+00	4.93D-01	5.07D-01	6.71D-02	2.63D-02	3.34D-02	4.16D-02	4.98D-02	1.20D-03
4.98D-02	4.16D-02	3.34D-02	2.63D-02	6.71D-02	5.07D-01	4.93D-01	2.13D+00	1.37D+00	1.45D-01	5.10D-02	5.70D-02	5.90D-02	5.62D-02	1.20D-03
5.88D-02	4.66D-02	3.65D-02	2.85D-02	7.30D-02	5.48D-01	5.07D-01	1.37D+00	4.95D+00	3.12D-01	9.38D-02	9.26D-02	8.45D-02	7.21D-02	1.38D-03
1.65D-02	1.04D-02	6.96D-03	4.85D-03	1.11D-02	7.30D-02	6.71D-02	1.45D-01	3.12D-01	1.95D+00	2.15D-01	1.03D-01	5.13D-02	2.79D-02	3.16D-04
1.18D-02	6.28D-03	3.71D-03	2.37D-03	4.85D-03	2.85D-02	2.63D-02	5.10D-02	9.38D-02	2.15D-01	8.95D-01	2.94D-01	7.18D-02	2.59D-02	1.73D-04
2.59D-02	1.18D-02	6.28D-03	3.71D-03	6.96D-03	3.65D-02	3.34D-02	5.70D-02	9.26D-02	1.03D-01	2.94D-01	8.95D-01	2.94D-01	7.18D-02	2.76D-04
7.18D-02	2.59D-02	1.18D-02	6.28D-03	1.04D-02	4.66D-02	4.16D-02	5.90D-02	8.45D-02	5.13D-02	7.18D-02	2.94D-01	8.95D-01	2.94D-01	4.14D-04
2.94D-01	7.18D-02	2.59D-02	1.18D-02	1.65D-02	5.88D-02	4.98D-02	5.62D-02	7.21D-02	2.79D-02	2.59D-02	7.18D-02	2.94D-01	8.95D-01	5.26D-04
5.26D-04	4.14D-04	2.76D-04	1.73D-04	3.16D-04	1.38D-03	1.20D-03	1.20D-03	1.38D-03	3.16D-04	1.73D-04	2.76D-04	4.14D-04	5.26D-04	1.18D-05

(UNIT : H)

Table 4.7 Conductor Details for ITER PF-1 to PF-5

[Type]	:	PA-40 type	
[Cable]			
- Condition			
Bop	:	13.5	T
Iop	:	37400	A
Top	:	4.5	K
Jc	:	525	A/mm^2
Rou Cu	:	7.8E-10	Ohm-m
HeatFlax	:	1000	$W/m^2/K$
Density He	:	0.143	g/cc
Viscosity	:	4.247E-05	g/cm/s
- Design Parameter			
Temp Margin	:	3	K
Damage of Cabling	:	0.25	
Number of Strand	:	648	
Rate of Cu/Sc	:	1.6	
Thick of Cr	:	0.005	mm
Mass Flow	:	10	g/s
- Results			
Tc	:	11.745	K
Tcs	:	7.5	K
JcSC	:	393.75	A/mm^2
Iop/Ic	:	0.585	
JopSC	:	230.706	A/mm^2
J cable spce	:	48.685	A/mm^2
Score	:	162.110	mm^2
Scu	:	259.377	mm^2
Scr	:	9.313	mm^2
Sstrand	:	421.487	mm^2
Diam. of core	:	0.564	mm
Diam. of strand	:	0.920	mm
Area of He	:	291.914	mm^2
Area of Cable Space	:	768.195	mm^2
- Pressure Drop			
Pcool	:	1763.715	mm
Hydroric Diameter	:	0.662	mm
He Velocity	:	23.955	cm/s
Reynold's Number	:	5340.099	
Friction Factor	:	8.890E-03	
Press. Drop	:	4.35E-03	bar/m
- Limiting Current			
I-limit	:	65185.65	A
Jcs-limit	:	84.855	A/mm^2
- Hot Spot Temperature			
Tau	:	12.2	s
Dead Time	:	1.0	s
Hot Spot Temperature	:	150.0	K

Table 4.8 Location of voltage taps.

current feeder terminal	
coil terminal	
pancake	pancake-to-pancake joint
	center of pancake (if necessary)

Table 4.9 Monitoring of voltages.

Item	Voltage Monitor	Protection
Crrent feeder	no	yes
Pancake	choice	choice
Coil	yes	yes(compensated)

Table 4.10 Type of sensors for fluid monitor.

Temperature	Platinum resistance thermometer
	Carbon resistance thermometer
Pressure	Pressure transducer at room temperature
Mass flow rate	Orifice flowmeter

Table 4.11 Fluid monitor.

Item	Location	Function
Temperature	inlet and outlet of each pancake inlet of a coil	@monitor cooldown and warmup @monitor coolant temperature during operation
Pressure	inlet of a coil outlet of each pancake	@monitor coolant pressure
Differential pressure	each pancake or coil	@detect anomalous pressure drop
Mass flow rate	inlet of each pancake and of a coil	@monitor coolant flow rate and flow balance @detect choking of channel @detect normal transition of a coil

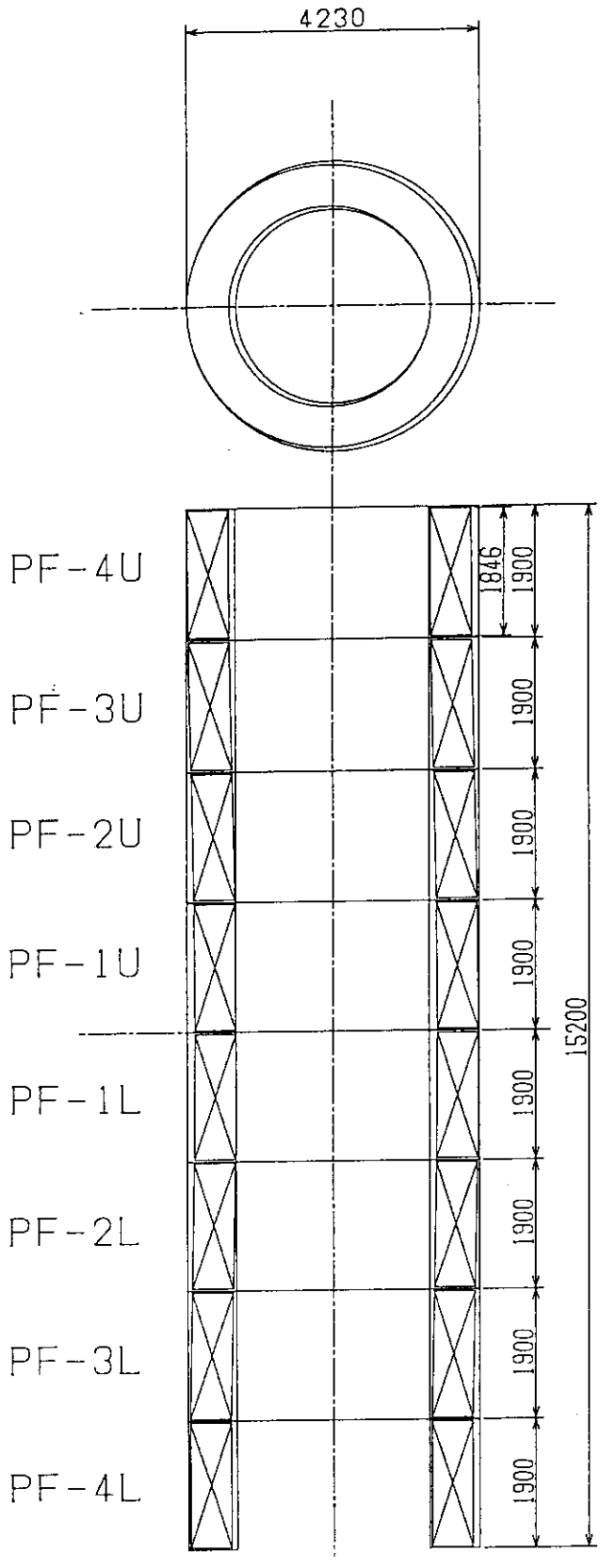

Fig.4.1 Top view and the cross section of the whole CS coils.

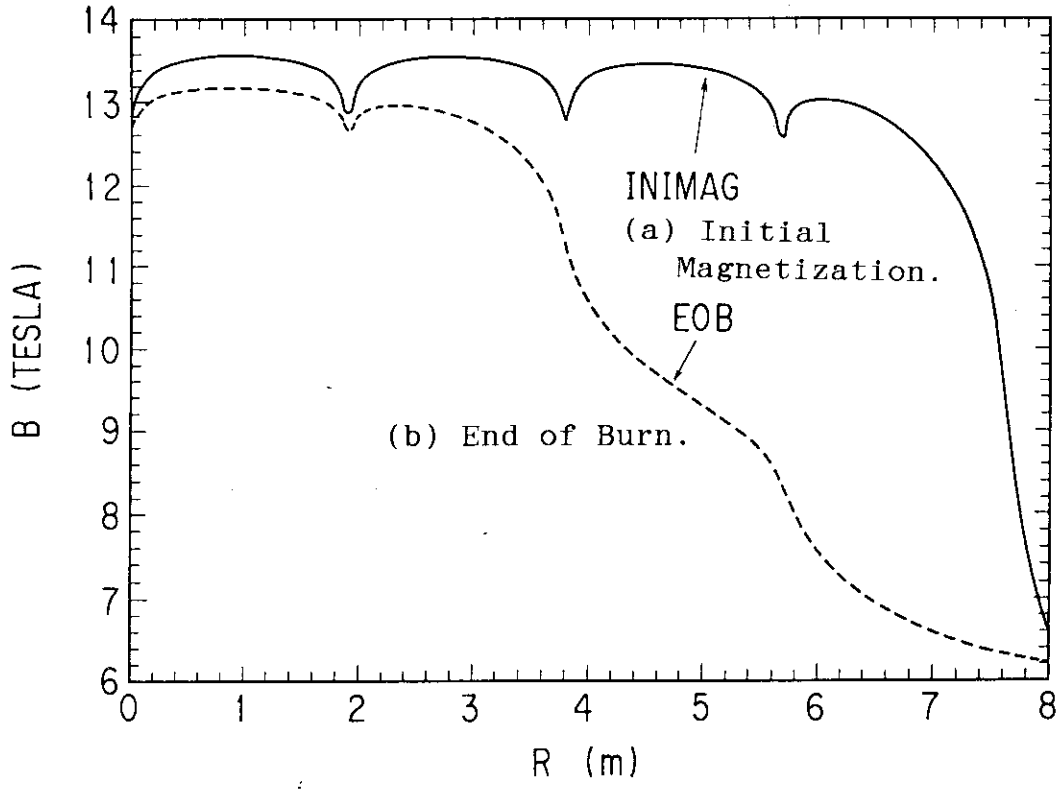

Fig.4.2 Magnetic field distribution on the inner surface of CS coil in the vertical direction

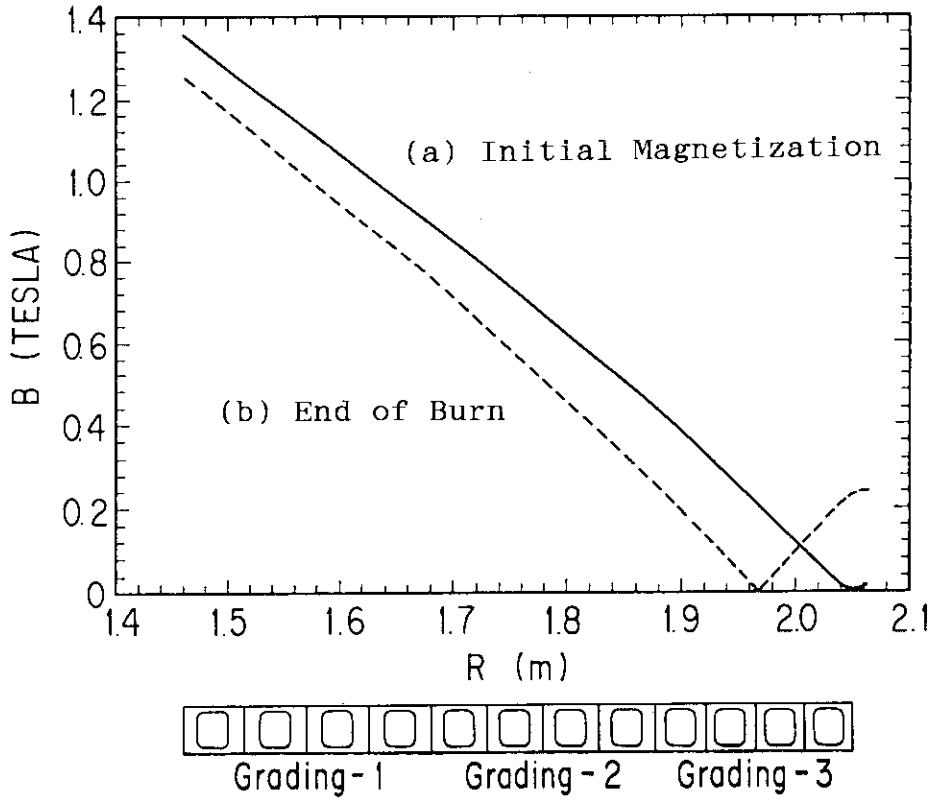

Fig.4.3 Distribution in the radial direction on the horizontal plane including the maximum field point

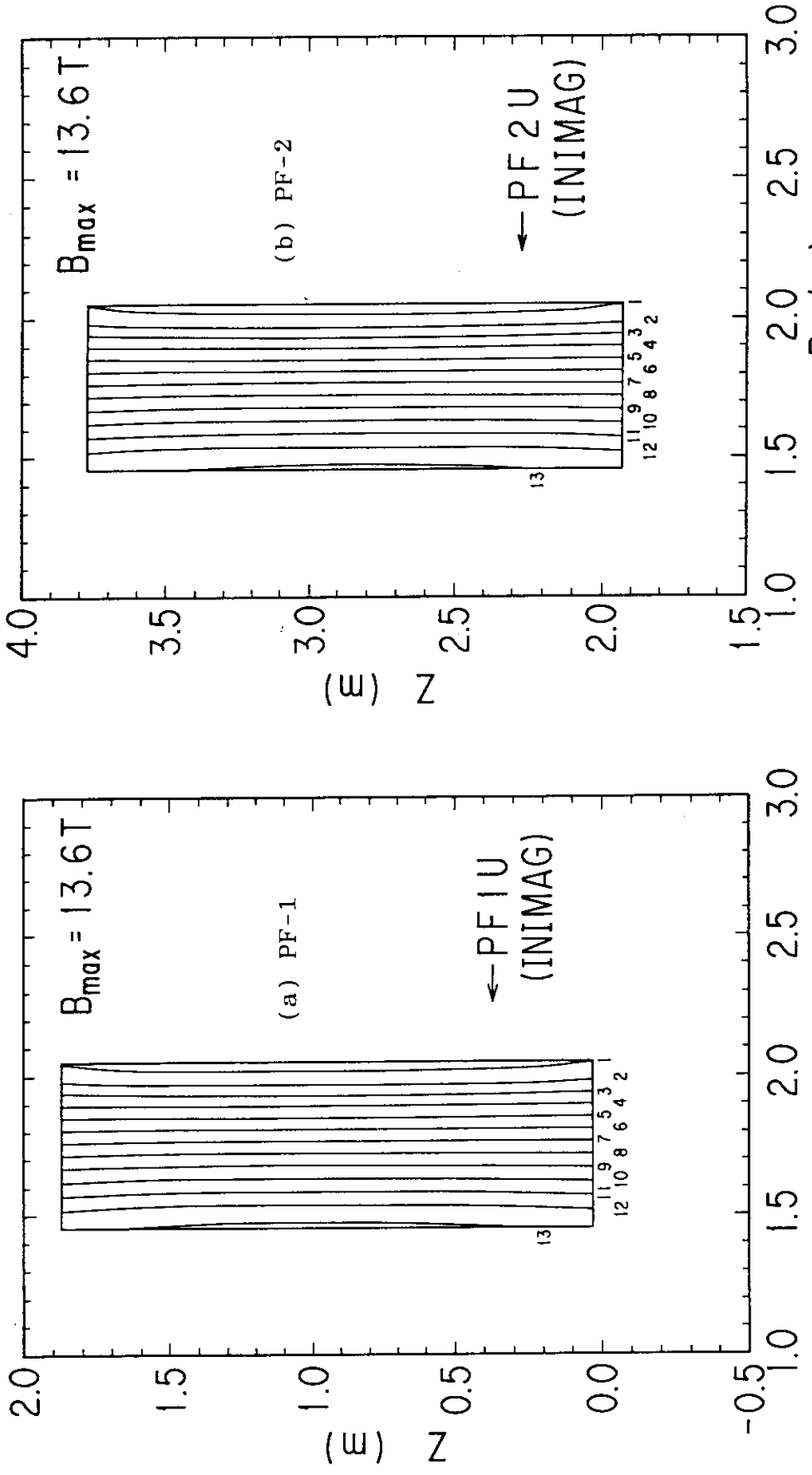

Fig.4.4 Field distribution in the cross section of each center solenoid coil at Initial Magnetization (1/2)

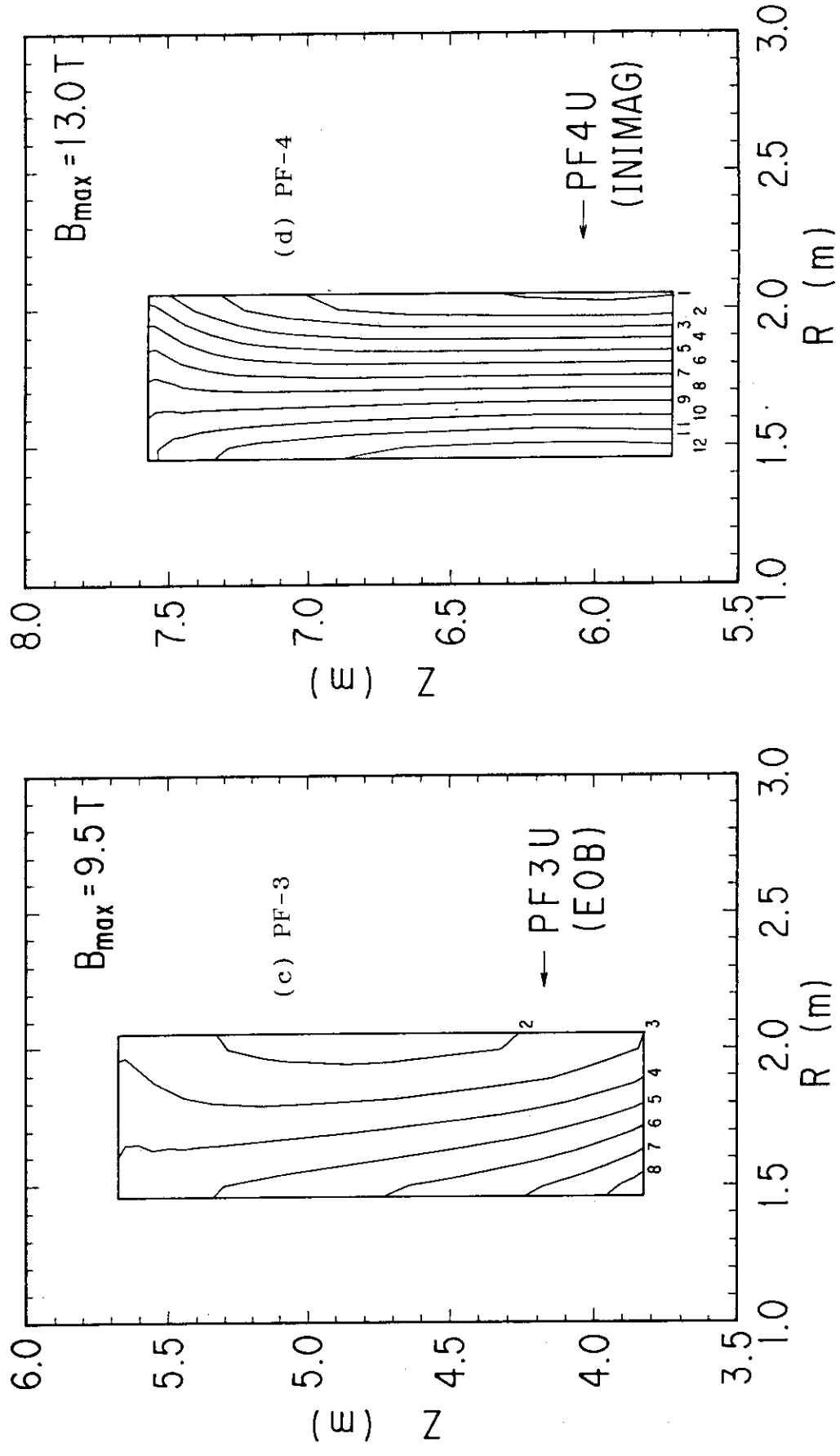

Fig.4.4 Field distribution in the cross section of each center solenoid coil at Initial Magnetization (2/2)

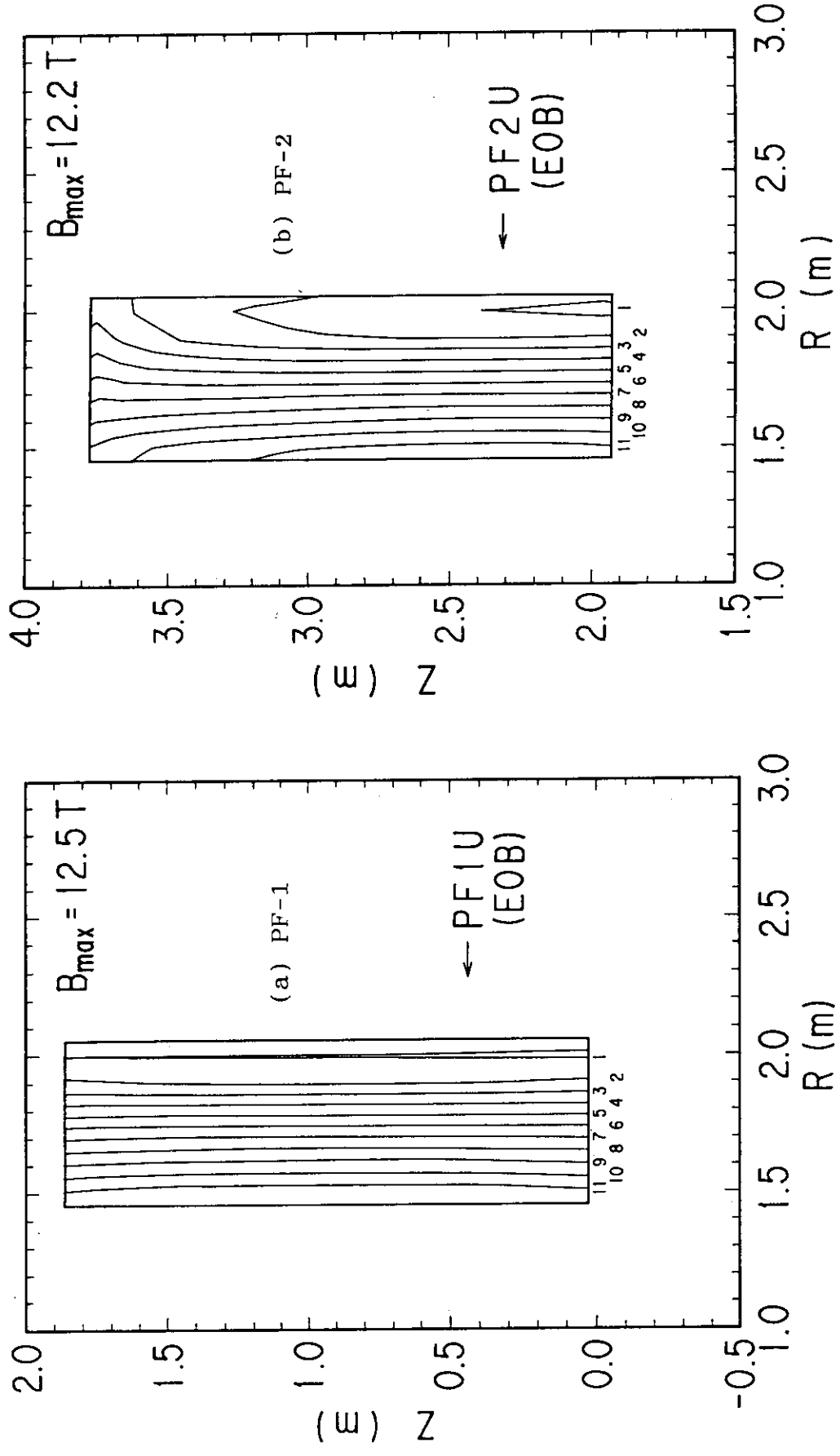

Fig.4.5 Field distributions in the cross section of each center solenoid coil at End of Burn (1/2)

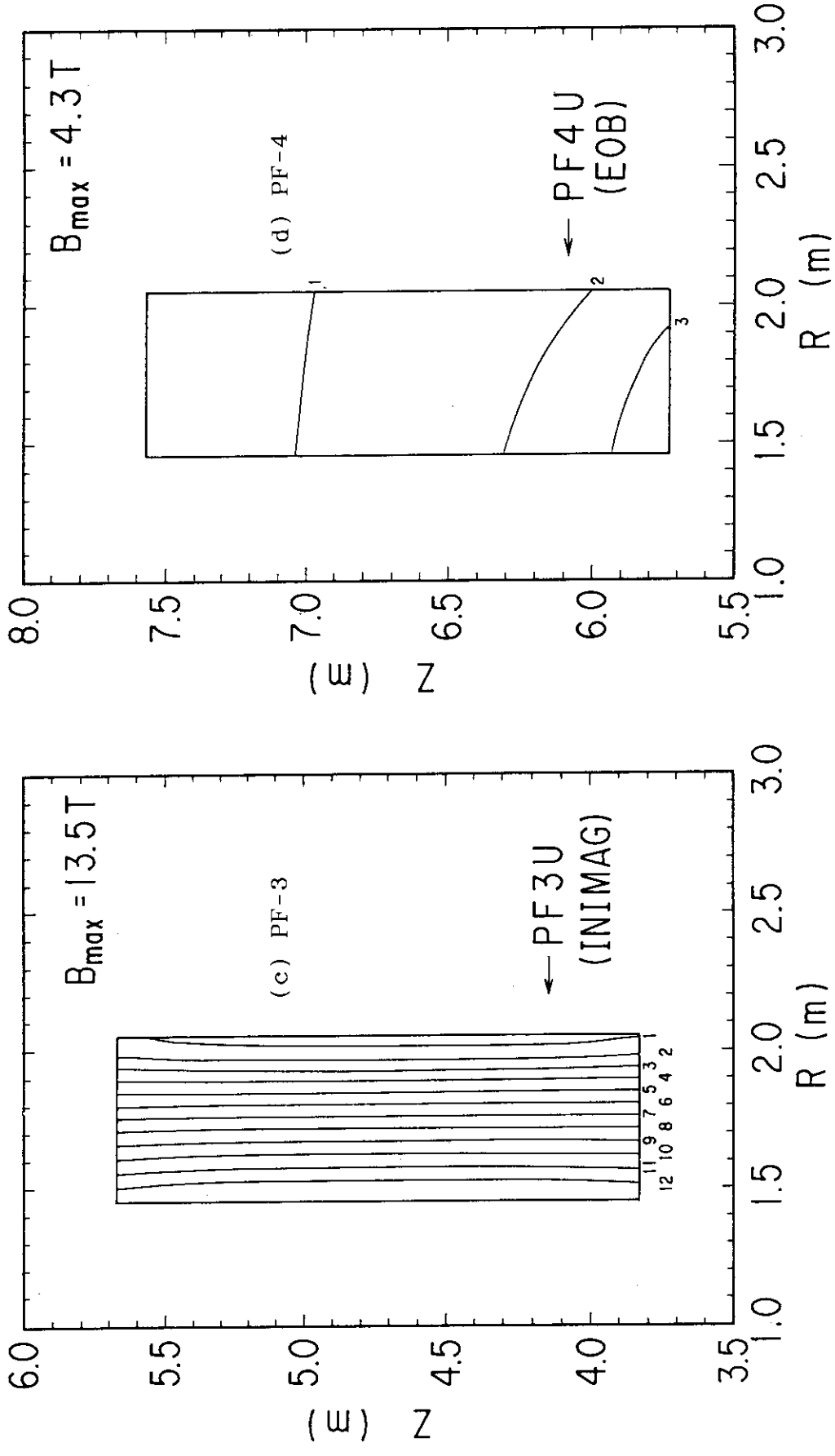

Fig.4.5 Field distribution in the cross section of each center solenoid coil at End of Burn (2/2)

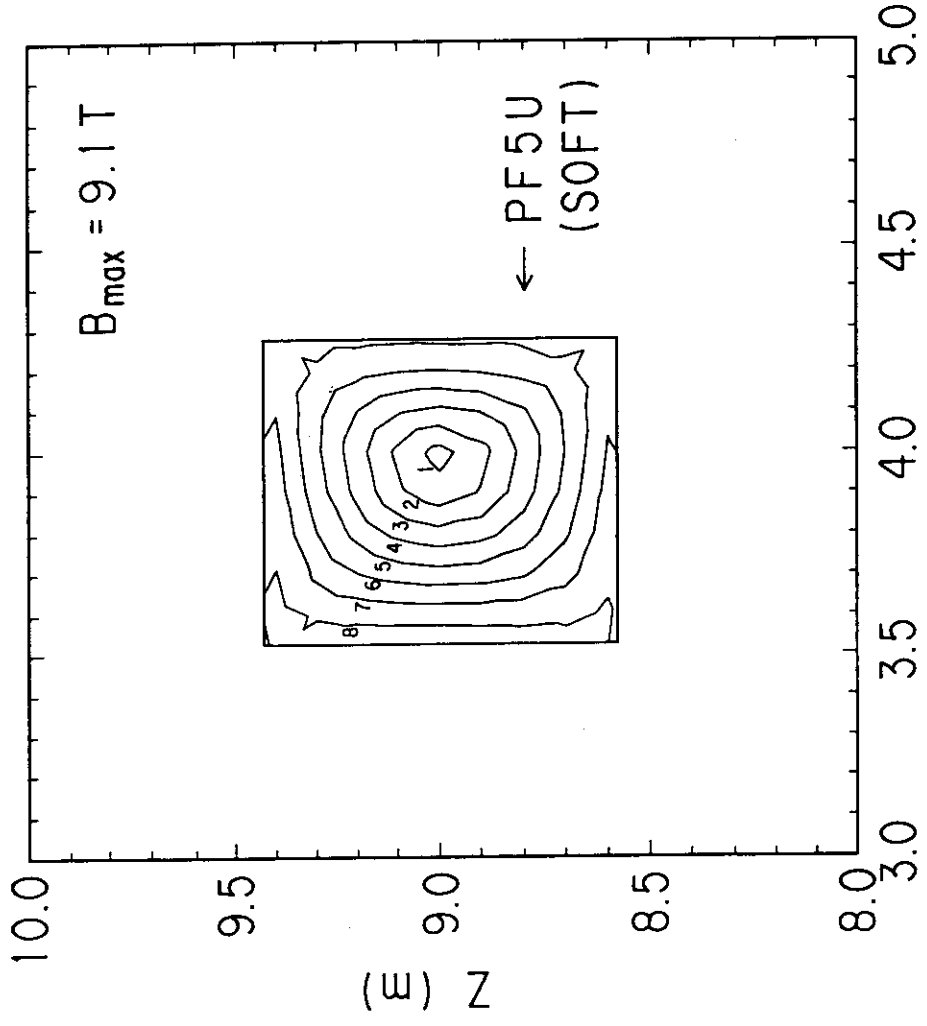

Fig.4.6 Field distribution in the cross section of PF-5 at SOFT (β_p=0, l_i=0.55)

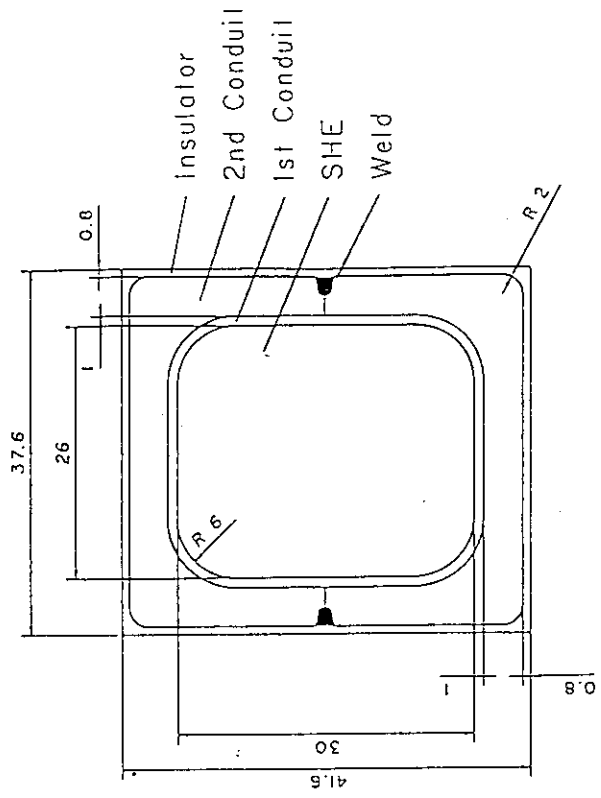

CONDUCTOR FOR PF5

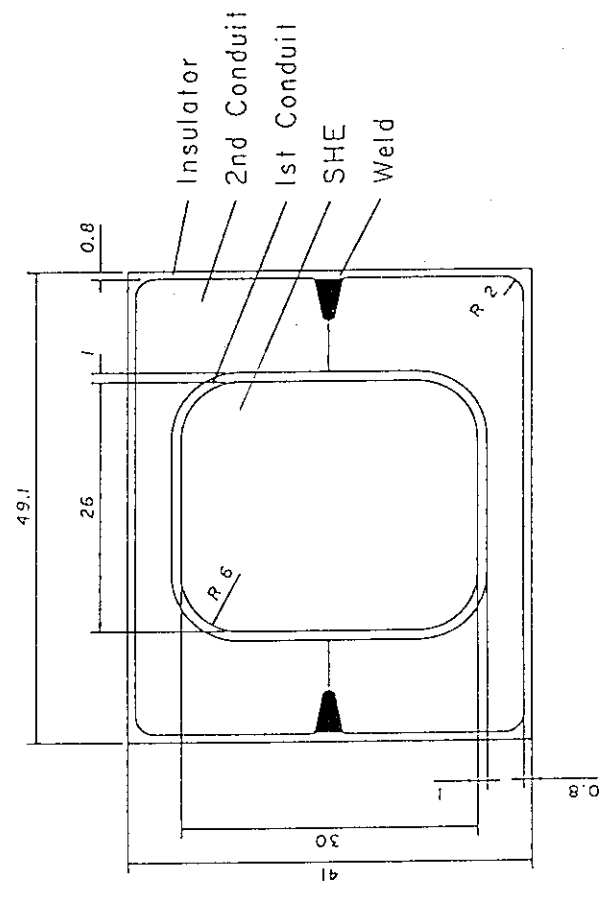

CONDUCTOR FOR PF1-PF4

Fig.4.7 Cross-sectional view of the Preformed Armor type Cable-in-Conduit Conductor and PF-5 conductor

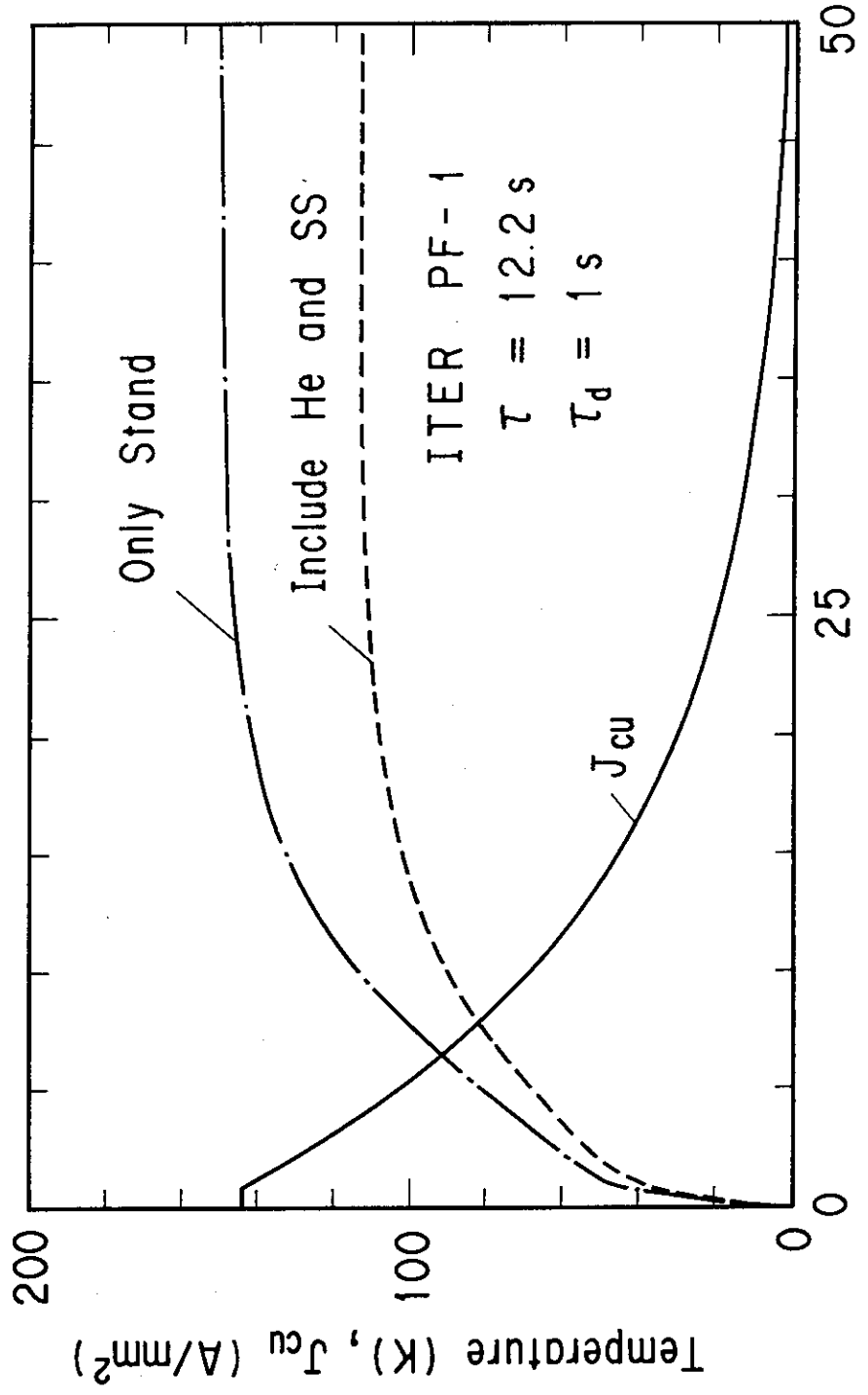

Fig.4.8 Temperature rise during quench and protection

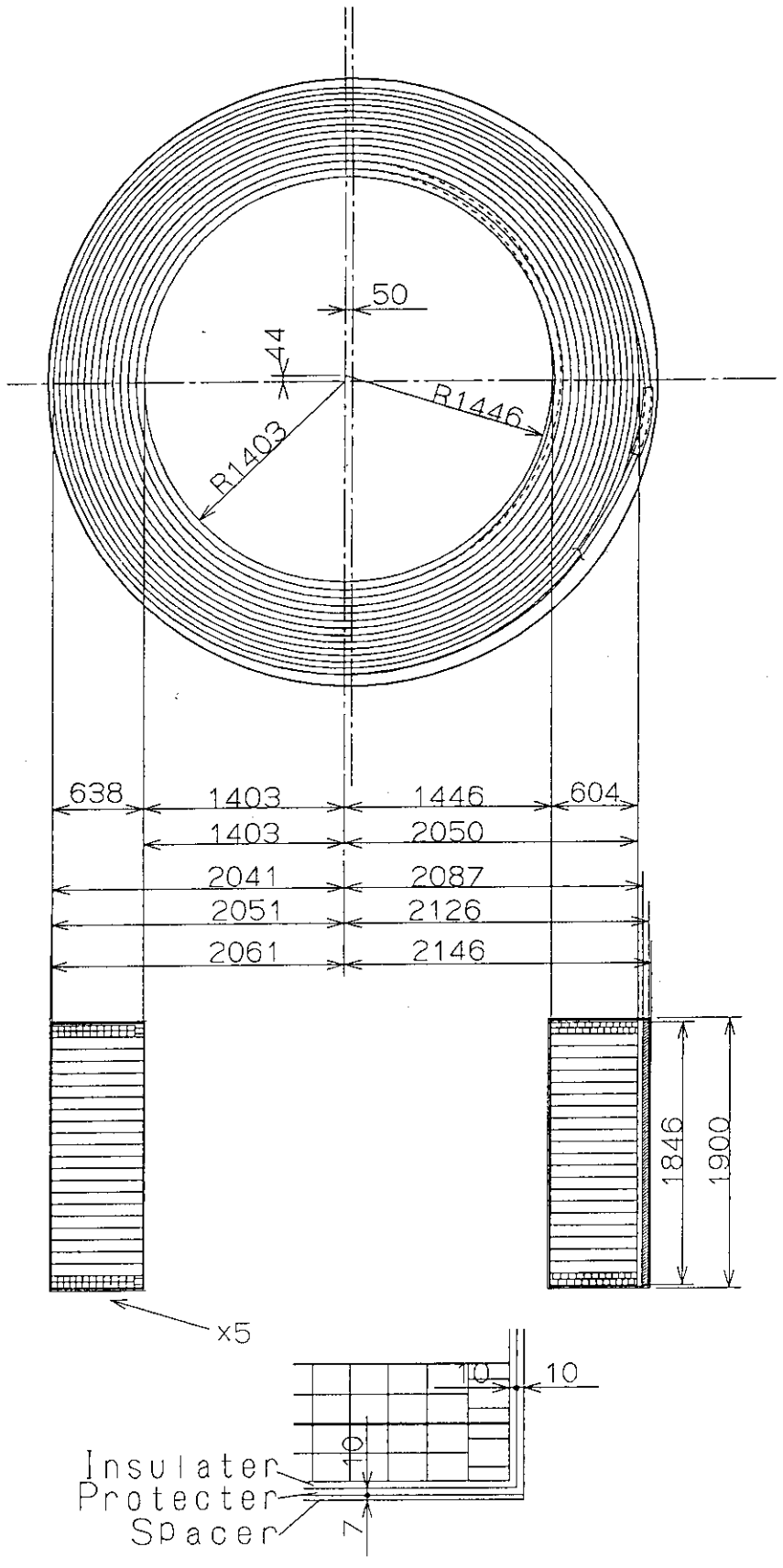

Fig.4.9 Top view and the cross section of one CS coil.

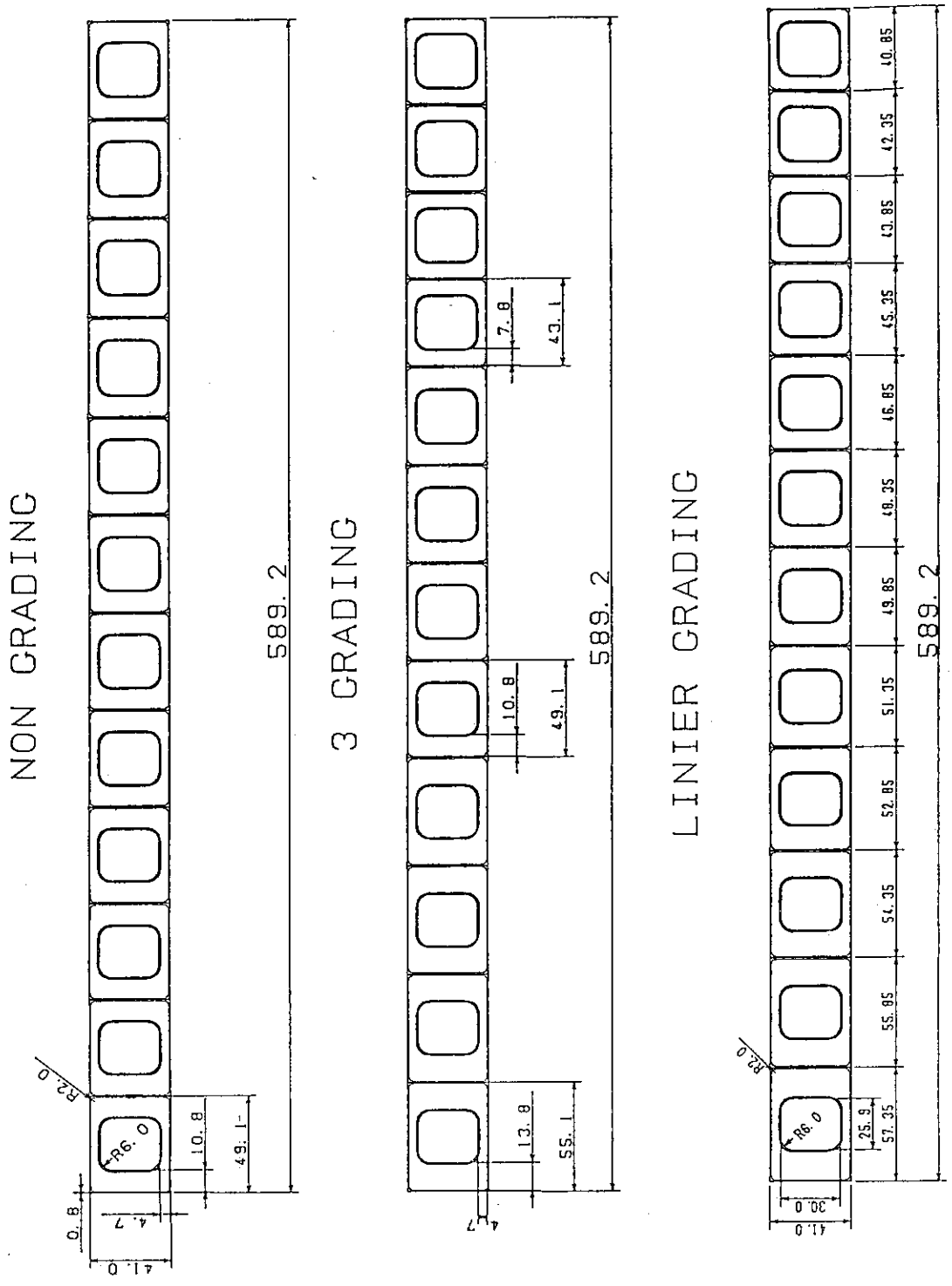

Fig.4.10 Three types of the structural gradings.

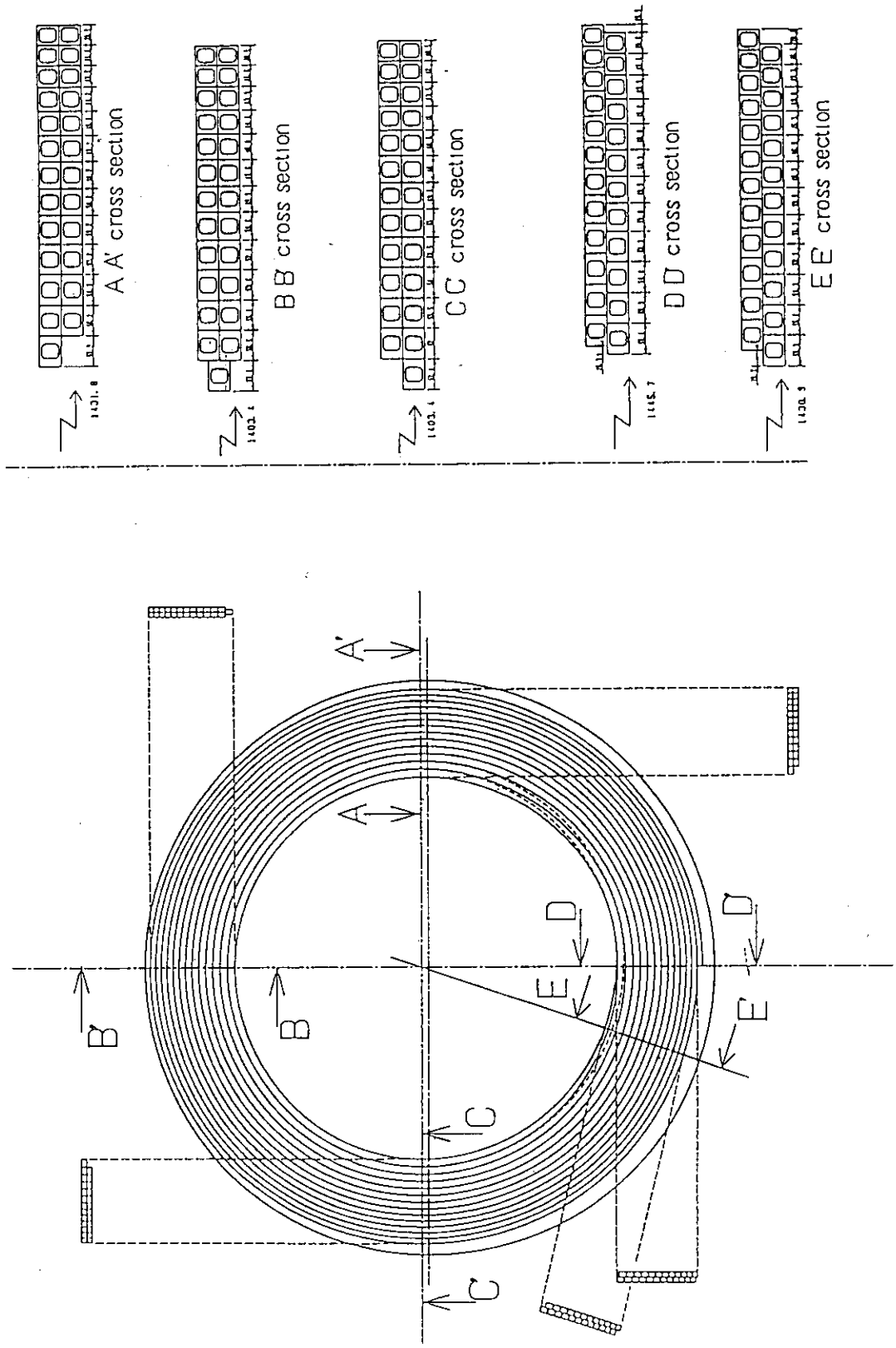

Fig.4.11 Winding layout and the cross section of the several parts of the one double pancake.

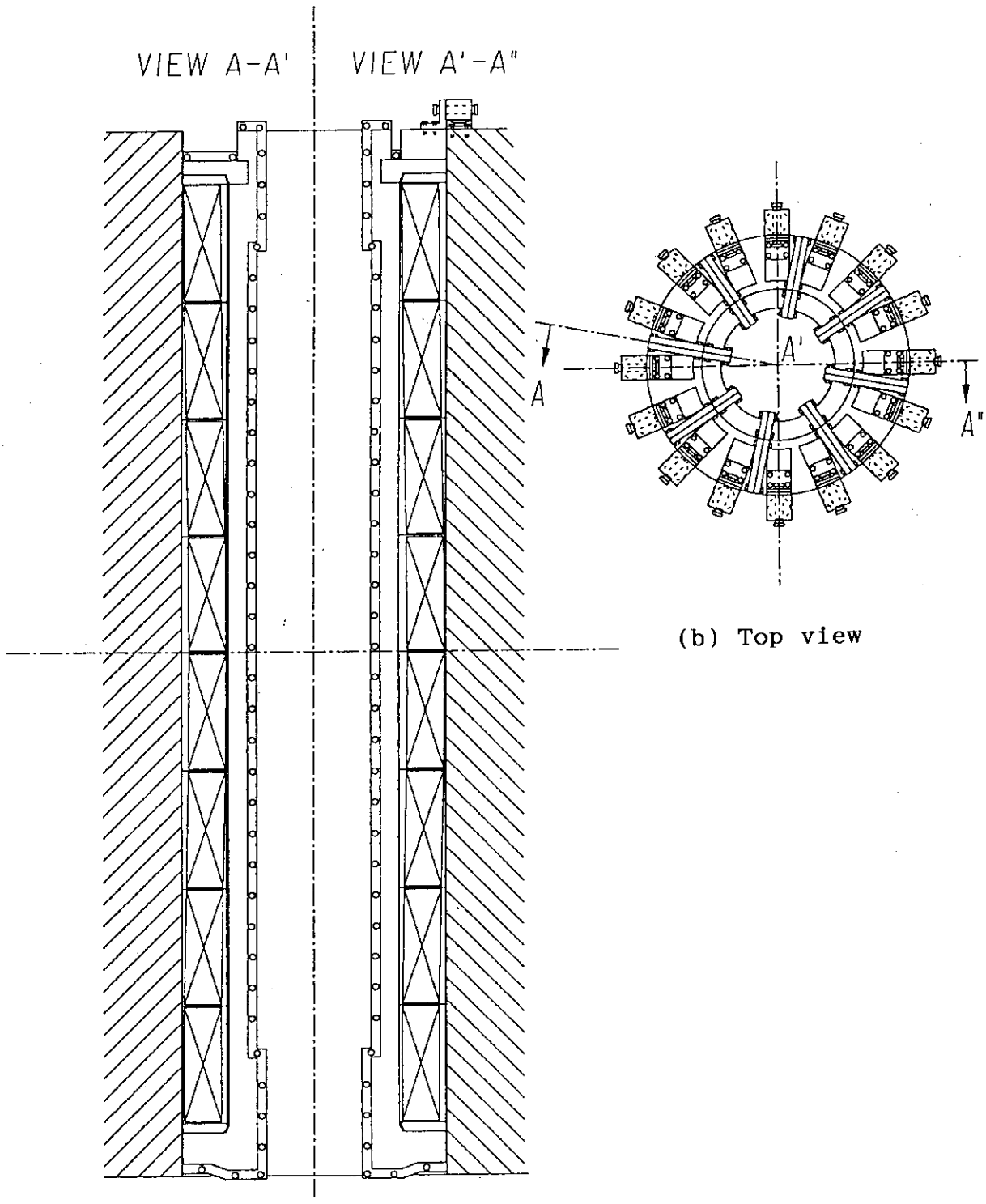

(a) Cross section

(b) Top view

Fig.4.12 The structure of CS coil support structure.

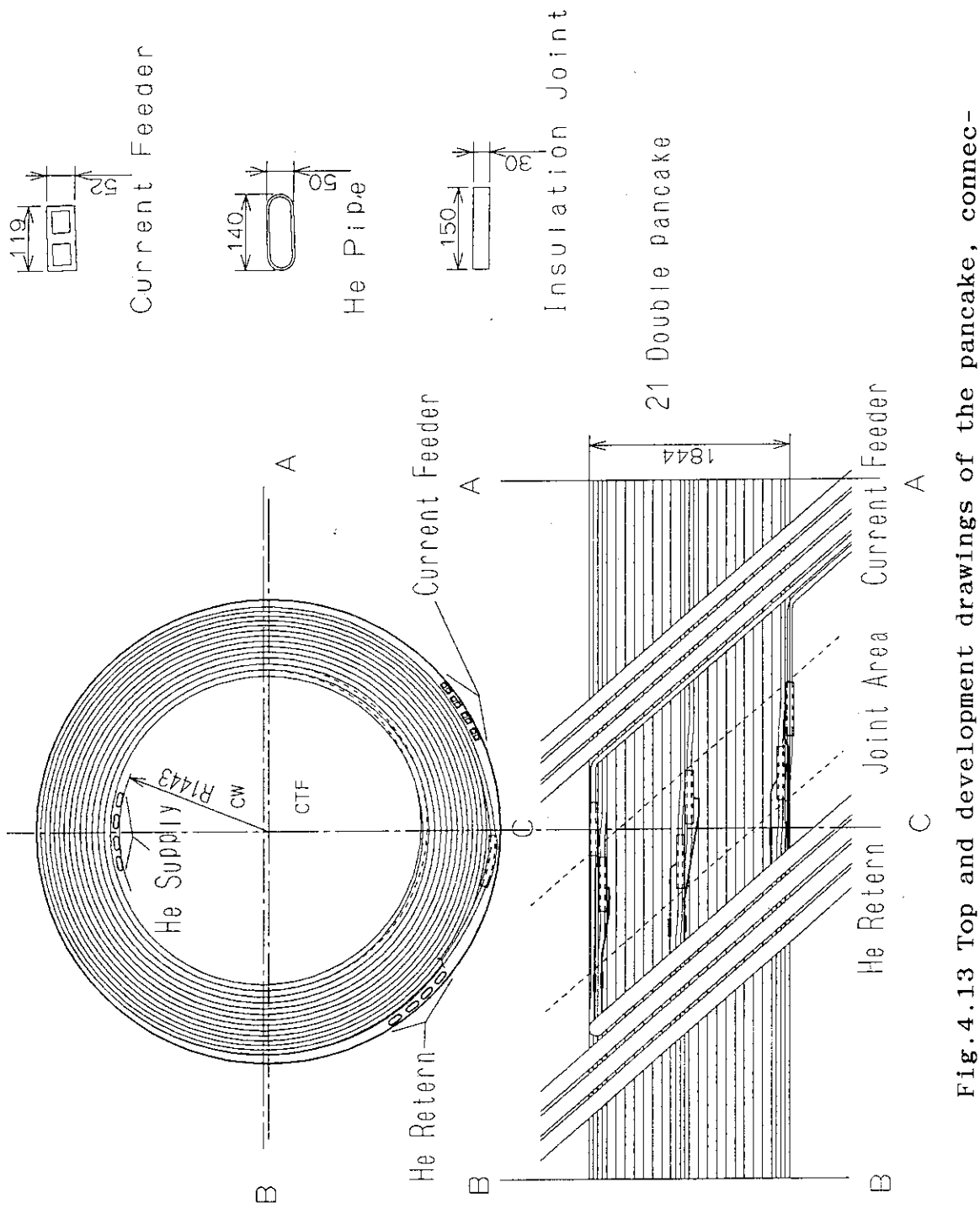

Fig.4.13 Top and development drawings of the pancake, connections and pipings

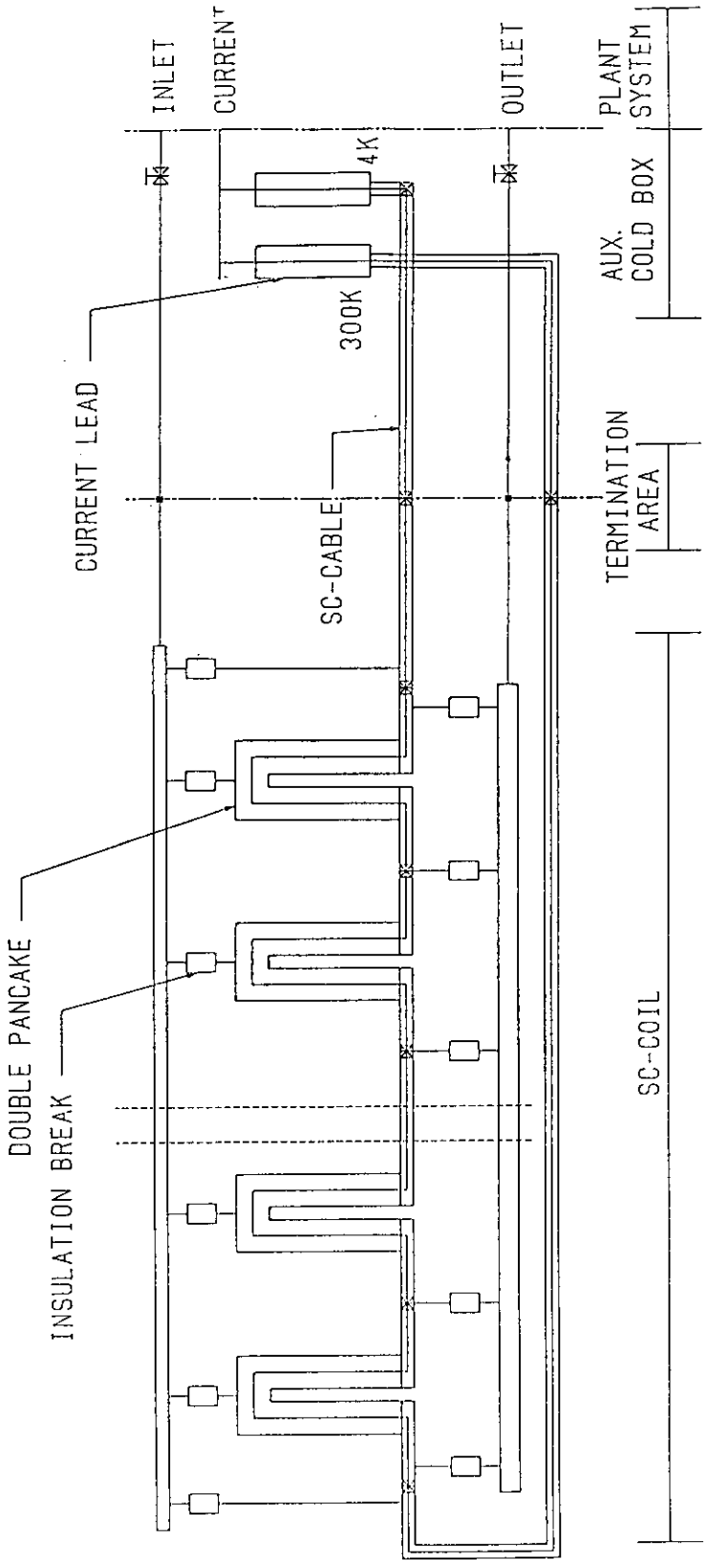

Fig.4.14 Schematic drawing of the concepts for the current lead and the coolant supply.

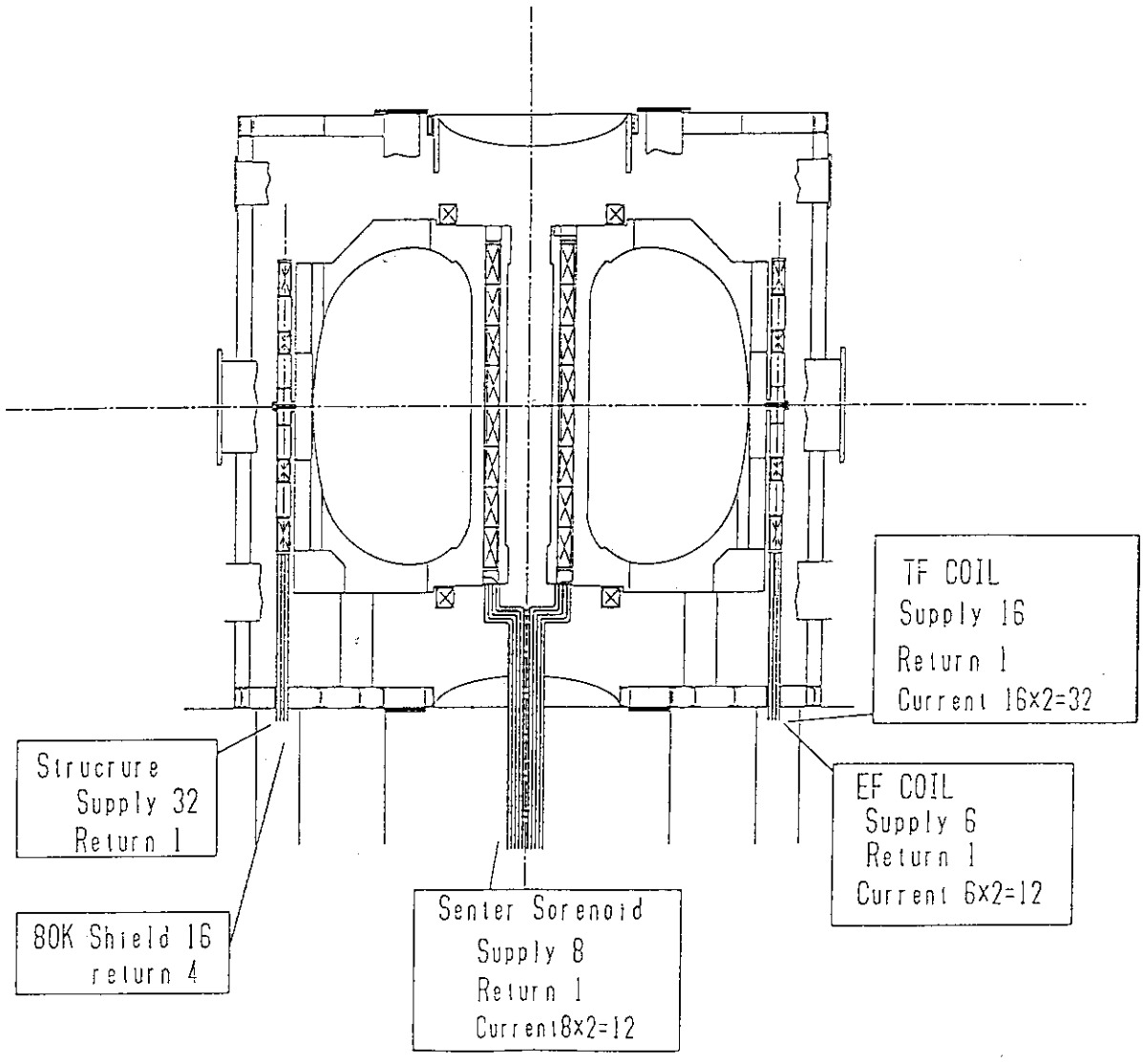

Fig.4.15 Overview of the He piping and the current supply.

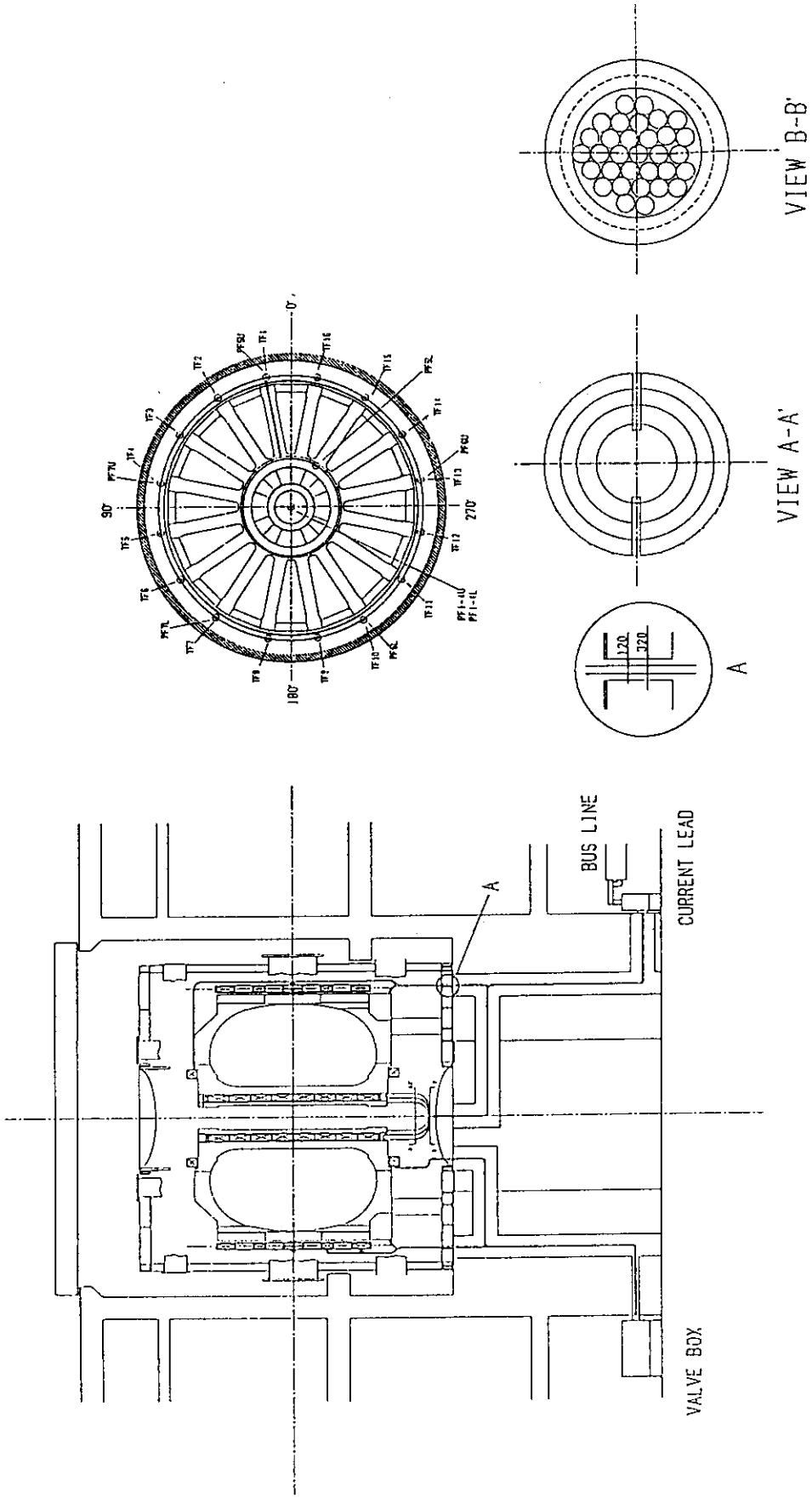

(a) Elevation view.

Fig.4.16 He piping and the current supply in the building.(1/2)

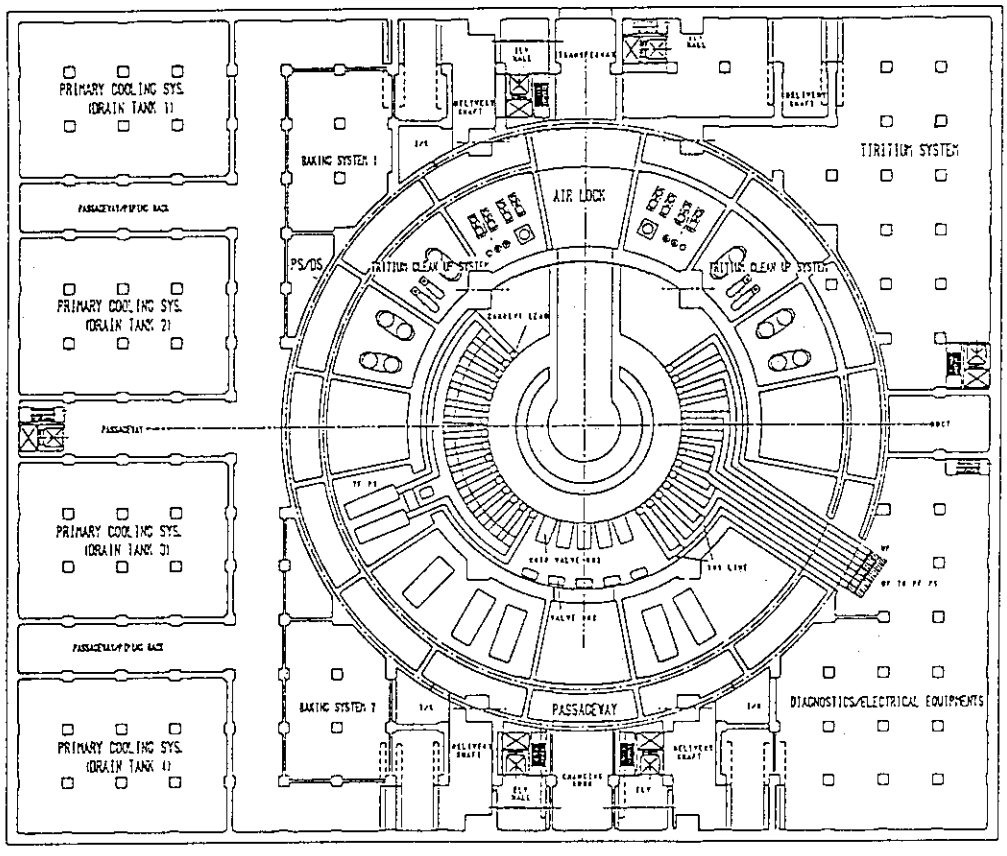

(b) Plan view.

Fig.4.16 He piping and the current supply in the building.(2/2)

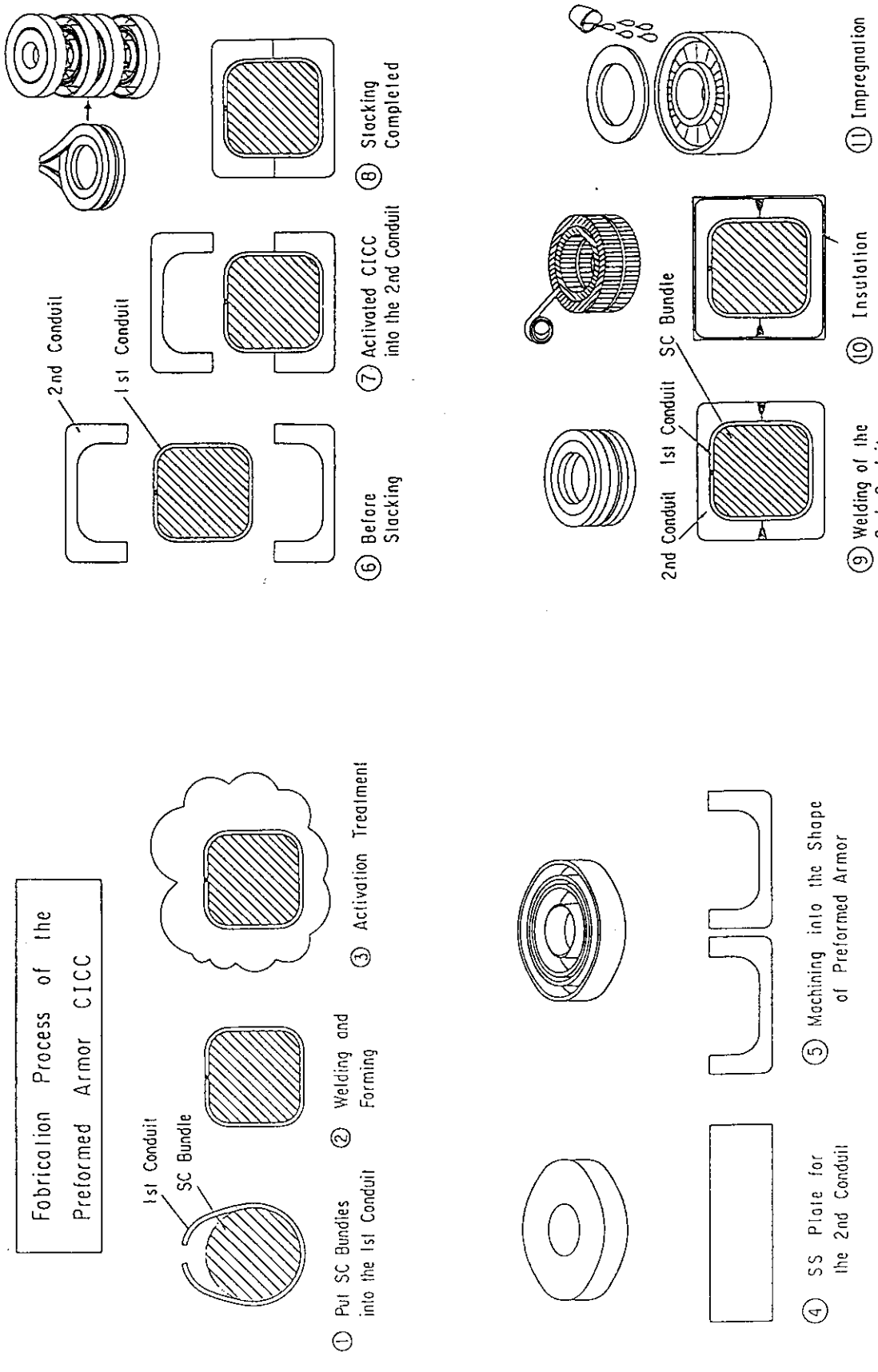

Fig.4.17 Schematic flow chart of the preformed-armor type coil.

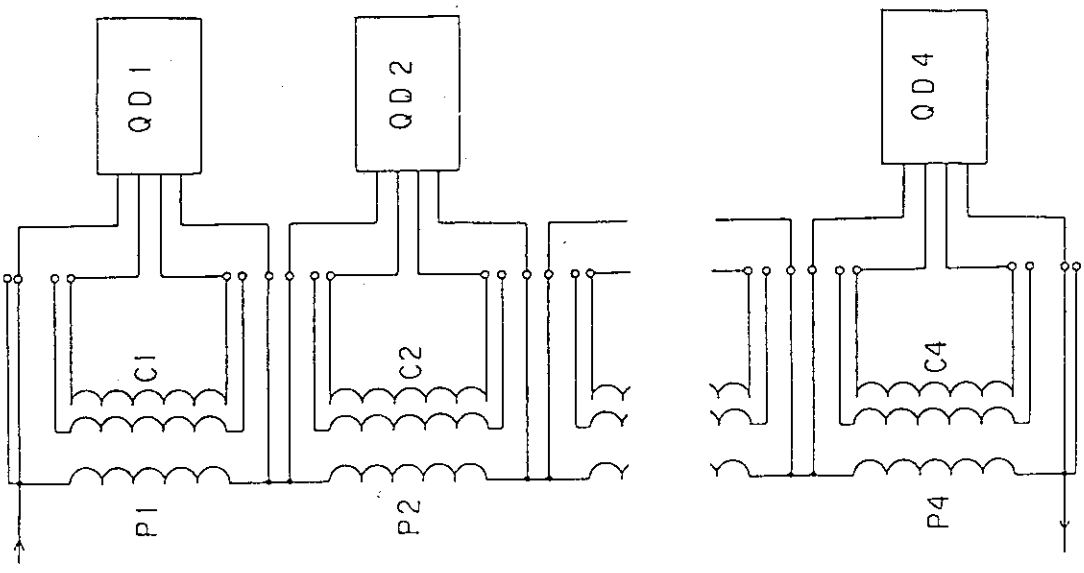

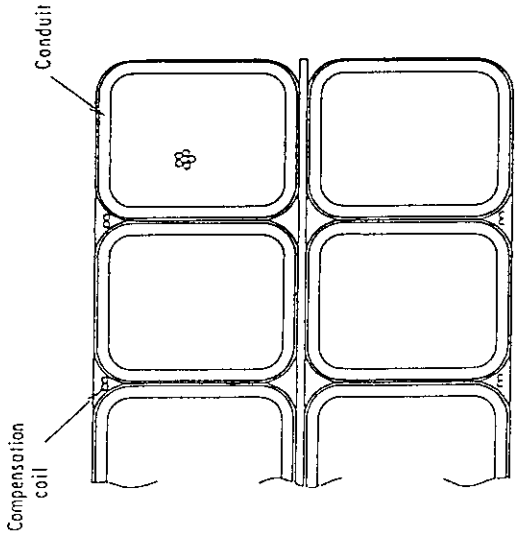

Fig.4.18 Schematic configuration of the voltage monitor.

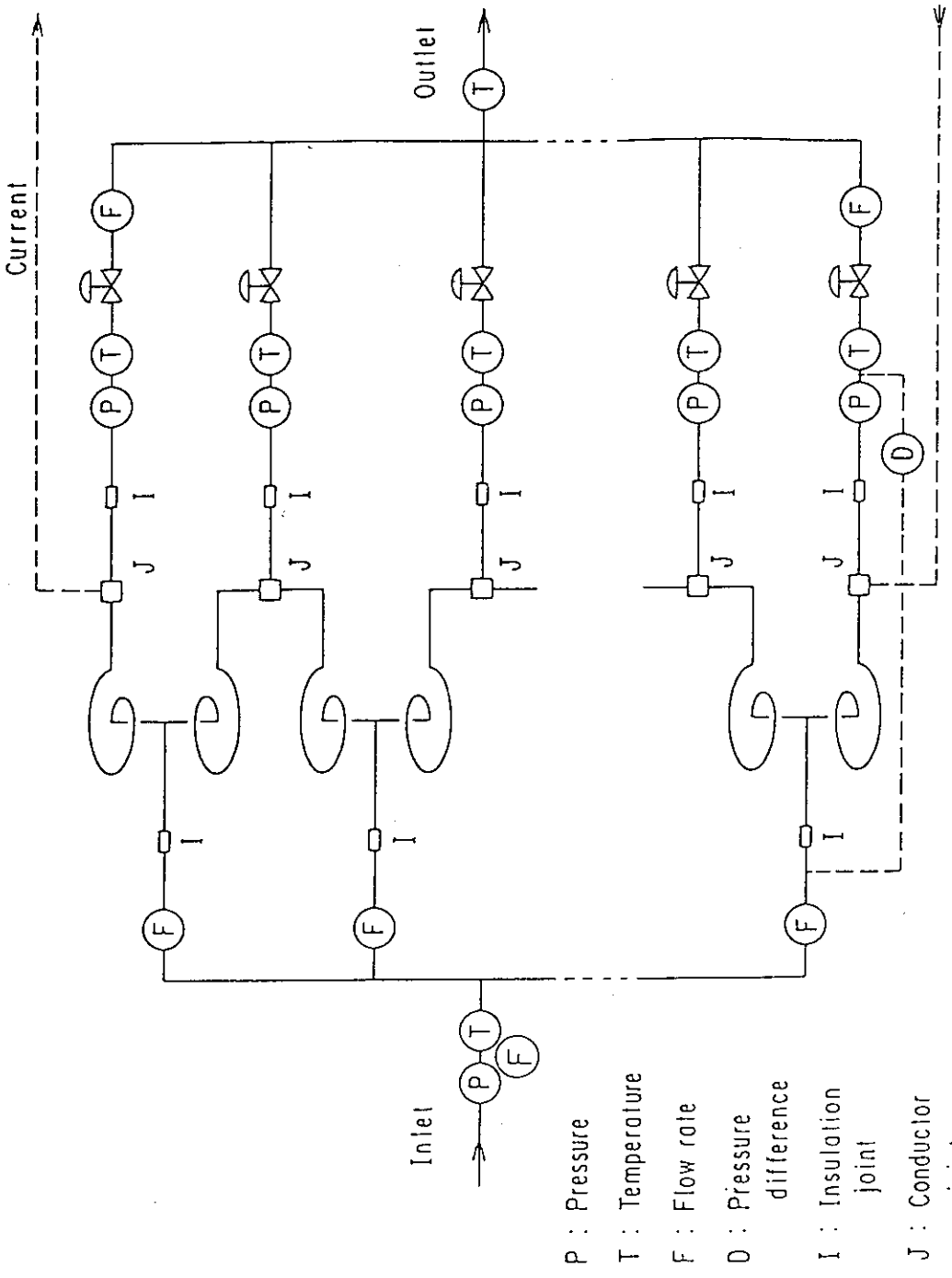

Fig.4.19 Schematic configuration of the fluid monitor.

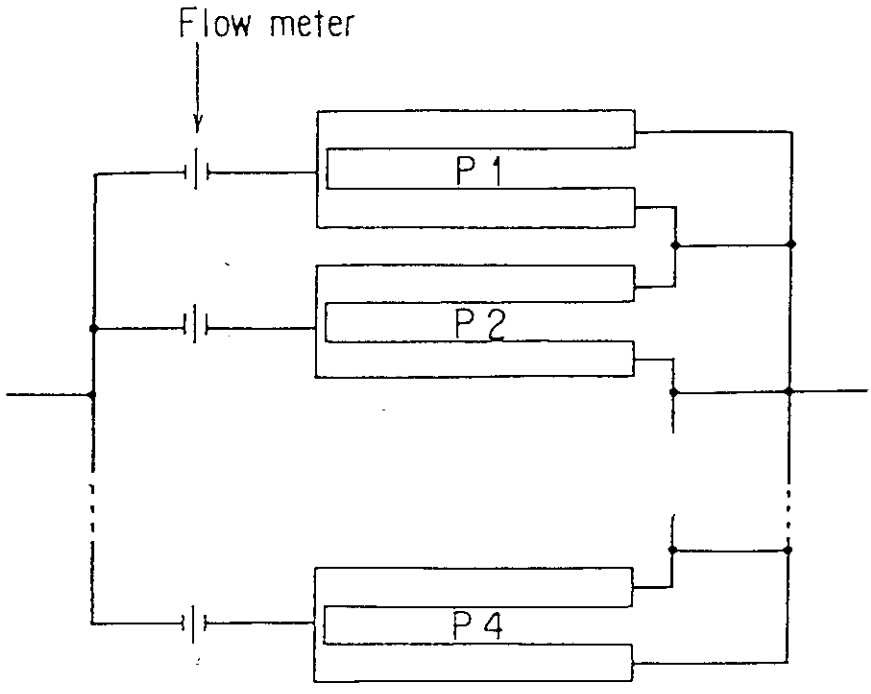

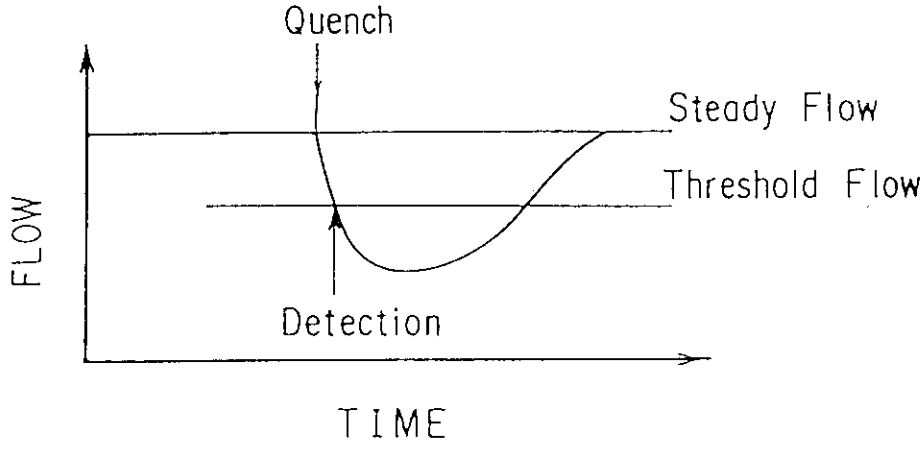

Fig.4.20 Quench detection by the flow detection.

5. OUTER RING COIL

5.1 Introduction

The top view and the cross section of the whole PF coil system are shown in Fig. 5.1. The outer ring coil (OR) has following properties.

(1) Function

The outer ring coil's functions are to generate an equilibrium field and to control the shape of the plasma.
The maximum fields of the PF-6 and PF-7 coils are 5.5 T and 4.9 T, respectively. The maximum averaged current densities of PF6 and PF7 coils are 19.8 A/mm^2 and 19.9 A/mm^2, respectively.

(2) Dimensions and configuration

The radius of PF-6 and PF-7 coils are same,11.5 m. Their heights are 3 m and 6 m, respectively. The radial and the vertical widths of the PF-6 coil are 466 mm and 1,522 mm, respectively. Those of the PF-7 coil are 466 mm and 950 mm, respectively.

(3) Conductor

The forced flow cooling technique was adopted for all conductors because of the required mechanical properties and the electrical insulation properties. The sub-He channel was made to avoid high pressure, since the cooling path is very long.

(4) Maintenance

It is very difficult to replace the outer ring coils, since the ports and the cooling pipe of the reactor need to be removed during replacement. Therefore, the reliability should be such that it equals that of the semi-permanent components. The requirement of high reliability is considered in this design.

5.2 Design Concept

Design parameters of the outer ring coils are listed in Table 5.1 and 5.2.

(1) Conductor

- Sub-channel type conductor : EF-40
- Superconducting material : NbTi

- Each strand is insulated by Cr plating to decrease AC losses.

(2) Winding

- Rigid winding : Cured by semi-cured tape

(3) Case

- 50 mm thick insulation case.

(4) Support structure

- Stainless support structure.

5.3 Basic Analysis

5.3.1 Magnetic Field

(1) Condition

The coil configuration and operating current patterns that were used for analysis are listed in Table 5.3. Operating current scenarios. are:

(1) SOFT3 (l_i=0.55, β_p=0.0 : The case of the maximum current for PF-6)

(2) EOB4 (l_i=0.75, β_p=1.0 : The case of the maximum current for PF-7)

(2) Maximum magnetic field

Maximum magnetic field is 5.5 T for PF-6 and 4.9 T for PF-7.

(3) Distribution of the magnetic field

The field distributions in the cross sections of PF-6 at SOFT3 and PF-7 at EOB4 (for which operation the operating currents of PF-6 and PF-7 are largest), respectively, are shown in Fig. 5.2 (a) & (b). The maximum field is 5.2 T for PF-6 at SOFT3 and 4.6 T for PF-7 at EOB4.

5.3.2 Magnetic Loads

(1) Condition

Operating current scenarios. are:

(1) EOB1 (End of Burn for Reference Scenario)

(2) EOB3 (l_i=0.6, β_p=1.0 : The maximum vertical force for PF-6)

(2) Radial and vertical force

The electromagnetic forces for EOB1 and EOB3 are listed in Table 5.4.

The distributions of the radial and the vertical electromagnetic forces for EOB1 vary from 11.25 degree to 56.25 degree along the circumference of the coils, as shown in Fig. 5.3 (a) and (b), respectively. Those for EOB3 are shown in Fig. 5.4 (a) and (b). The toroidal coils are located at 22.5 and 45.0 degrees in Fig 5.3 and 5.4.

5.4 Cable

5.4.1 Sub-channel added modified DPC-U type[2]

(1) Modified DPC-U type

NbTi filament is selected for the outer ring coil because the relatively low maximum field is 5.5 T. And NbTi strands have the benefits of reliability and cost. The DPC-U type conductor is under development in the Demo Poloidal Program in Japan. The following modifications can be added to original design. The details of the design are listed in Table 5.5.

(2) Sub-channel

The outer Ring coil has a long cooling path (400 m). Heat remove from conductor is most essential to the low Tc material (NbTi). The sub-channel, as shown in Fig. 5.5, can be added to center of wire. The coolant is flowed as mixed between a sub-cannel and a main channel, verified in the DPC-EX coil[3].

(3) Strand

The strand of DPC-U has weak heat transfer to coolant because of the thermal barriers CuNi and formvar that are used. Cr plating is used for new design to reduce strand coupling loss. Also, diameter of strand is 0.91 mm which increases cooling surface, as shown in Fig. 5.6.

5.4.2 Hot Spot Temperature

(1) Maximum Temperature

The maximum hot spot temperature is designed to be 150 K.

(2) Protection condition

It is required that the dead time from initiation of normalcy to dump resister current decay be 1.0 sec.

(3) Results

The dump time constant is 16.0 sec which is over than the

limited time (10 s) from terminal voltage (20 kV). The temperature rise during quench and protection is calculated as shown in Fig. 5.7.

5.4.3 AC Loss

(1) Equation : See Volume III. (AC LOSS).

(2) Results : See Volume III. (AC LOSS).

5.4.4 Stability

(1) Requirement

The stability is over 200 mJ and the limiting current over than the rated current.

(2) Stability margin

Temperature Margin 2 K.

(3) Limiting current

Calculated limiting current at 5.5 T is 64.1 kA, which is over than rated current 43.8 kA.

5.4.5 Hydraulic

(1) Requirement

The pressure drop is less than 2 bar

(2) Calculation

The experimental factor of friction is 2.0.

(3) Results

Pressure drop of PF-6,7 is 0.092 bar per coil.

5.5 **Winding Pack**

5.5.1 Layout

(1) The overall layout is shown in Fig. 5.8.

(2) The cross sections of the PF-6 and PF-7 coils are shown in Fig. 5.9. The thickness of the insulator is about 10 mm. 50 mm thick insulation support structure (Young's Modulus ~ 20 GPa) surrounds the coil serving as a coil case.

5.5.2 Stress

The stresses of the winding are described in Volume II (STRESS ANALYSIS) in detail. The maximum tensile stress for winding is about 95 MPa. This value can be transformed to the

stress of the conduits. The maximum tensile stress for the conduits is about 212 MPa.

5.6. **Support structure**

(1) Structure

The outer ring coil support structure is shown in Fig. 5.10. The support structures consists of 16 individual support structures. Each support structure is fixed to one toroidal coil by a column which prevents radial and rotational free doms. Each support structure can be divided into two parts due to the limitation of the capacity of the building's crane.

(2) Stress

The details of the stress analyses are described in Volume II. (STRSS ANALYSIS). The maximum Tresca stresses are about 120 MPa for the support structure.

5.7 **Manufacturing**

Since the diameters of the outer ring coils are 23 m, manufacturing on site should be considered.

5.8 **Instruments**

See section 4.8.

5.9 **Summary**

The conceptual design and analysis of the outer ring coil has been completed.

(1) Sub-channel added modified DPC-U type NbTi conductor is selected for the outer ring coil conductor.

(2) The maximum tensile stress for winding is about 95 MPa. This value can be transformed to the stress of the conduits. The maximum tensile stress for the conduits was about 212 MPa.

(3) The maximum Tresca stresses is about 120 MPa for the support structure.

References

[1] ITER-CDA PF Group, "ITER Poloidal Field System", ITER Document Series, No. 27, IAEA, Viena, Austria, 1990
[2] H. Tsuji, et.al.,"Evolutions of the Demo Poloidal Coil Program", Proc, of MT-11 (1990) 806.
[3] T. Ando, et.al.,"Design of the Nb_3Sn Demo Poloidal Coil (DPC-EX)", IEEE Transactions on Magnetics 24-2 (1988) 1444

Table 5.1 Design Parameter of the Equilibrium Field Coil (ITER-PF-6)

Max. Field	5.5	T
Rated Current	43.75	kA
Margin of Ic	4.45	
Current Density of Coil Space	18.7	A/mm^2
Ampere-turn / Coil	14.0	MAT
Mean Diameter	23.0	m
Thickness	0.466	m
Height	1.522	m
Number of		
Total Turns	320 (5x2x15x2)	
Double Pancakes	15	
Cooling Passages	60	
Dump Time	29	s
Length of Cooling Pass	361	m
Mass Flow Rate	10.0	g/s
Inlet Temperature	4.2	K
Pressure	6.0	bar
Pressure Drop	0.092	bar
Poloidal Cycle	< 10,000	
Cool-down Cycle	< 20	

Table 5.2 Design Parameters of the Equilibrium Field Coil (ITER-PF-7)

Max. Field	4.9	T
Rated Current	43.75	kA
Margin of Ic	4.45	
Current Density of Coil Space	18.9	A/mm^2
Ampere-turn / Coil	8.82	MAT
Mean Diameter	23.0	m
Thickness	0.466	m
Height	0.950	m
Number of		
Total Turns	200 (5x2x10x2)	
Double Pancakes	10	
Cooling Passage	40	
Dump Time	29	s
Length of Cooling Pass	361	m
Mass Flow Rate	10.0	g/s
Inlet Temperature	4.2	K
Pressure	6.0	bar
Pressure Drop	0.092	bar
Poloidal Cycle	< 10,000	
Cool-down Cycle	< 20	

Table 5.3 Current variations of the PF coils

	SOFT3(MA)	EOB1(MA)	EOB3(MA)	EOB4(MA)
PF-1	-13.34	-22.3	-21.81	-22.17
PF-2	-13.34	-22.3	-21.81	-22.17
PF-3	0.02	-9.14	-13.59	-7.06
PF-4	8.59	0.02	-0.10	-0.63
PF-5	18.43	6.25	7.89	3.44
PF-6	-14.01	-6.49	-7.98	-1.93
PF-7	0.83	-5.25	-4.99	-8.82
PLASMA	22.00	22.00	22.00	22.00

Table 5.4 Electromagnetic Forces per one turn

	EOB1		EOB3	(MN)
	FR	FZ	FR	FZ
PF-6	222.8	-175.4	308.8	-213.6
PF-7	222.2	109.0	222.5	131.8

Table 5.5 Conductor Details for ITER-PF-6&7 (1/2)

[Type]	: Sub-Cannel & Modified DPC-U type		
[Cable]			
- Condition			
Bop	:	5.5	T
Iop	:	43750.0	A
Top	:	4.2	K
Jc	:	2200.0	A/mm^2
Rou Cu at 5.5T	:	4.20E-10	Ohm-m
HeatFlux	:	1000.0	$W/m^2/K$
Density He	:	0.143	g/cc
Viscosity	:	4.247E-05	g/cm/s
- Design Parameter			
Temp Margin	:	2.0	K
Damage of Cabling	:	0.1	
Number of Strand	:	810	
Cable pattern	:	3x3x3x5x6	
Rate of Cu/Sc	:	3.2	
Thick of Cr	:	0.005	mm
Rate of CuNi/Sc	:	1.06	
Sub Chan. Diam.	:	12.0	mm
Thick Pipe	:	0.8	mm
Mass Flow	:	10.0	g/s

Table 5.5 Conductor Details for ITER-PF-6&7 (2/2) (continued)

- Results			
Tc	:	6.709	K
Tcs	:	6.2	K
JcSC	:	1980.	A/mm^2
Iop/Ic	:	0.2247	
JopSC	:	444.989	A/mm^2
Jcable-spce	:	46.642	A/mm^2
Snbti	:	98.316	mm^2
Scu	:	314.614	mm^2
Scr	:	11.535	mm^2
Scuni	:	104.215	mm^2
Sstrand	:	528.682	mm^2
Diam. of strand	:	0.9116	mm
Asus-core	:	32.169	mm^2
Area of He in main	:	356.434	mm^2
Area of He in sub	:	113.097	mm^2
Total Area of He	:	469.531	mm^2
A of Cable Space	:	937.984	mm^2
Diam. of Cable	:	37.138	mm
- Pressure Drop-Main			
Pcool	:	2126.455	mm
Hydroric Diameter	:	0.670	mm
He Velocity	:	19.619	cm/s
Reynold's Number	:	4429.	
Friction Factor	:	9.316E-03	
Press. Drop	:	1.509E-03	bar/m
- Pressure Drop-Sub			
He Velocity	:	61.831	cm/s
Reynold's Number	:	249800.	
Friction Factor	:	3.399E-03	
Press. Drop	:	3.056E-04	bar/m
Press. Drop total	:	0.2541E-03	bar/m
- Limiting Current			
I-limit	:	64100.	A
Jcs-limit	:	68.3	A/mm^2
- Hot Spot Temperature			
Tau	:	16.0	s
Dead Time	:	1.0	s
Hot Spot Temperature	:	150.0	K
[Conduit]			
Ass-Total	:	889.8	mm^2
A1ss	:	125.7	mm^2
A2ss	:	713.8	mm^2
Acore	:	50.3	mm^2
[Insulation]			
Thickness	:	0.75	mm
Ains	:	137.6	mm^2

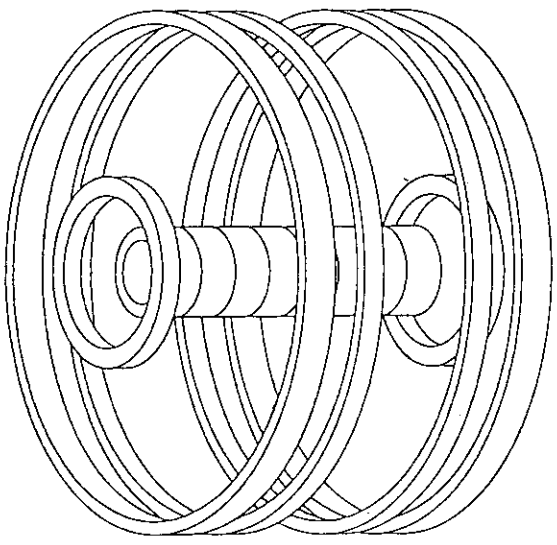

BIRD'S-EYE VIEW

	DR (mm)	DZ (mm)		DR (mm)	DZ (mm)
PF1U	590	1846	PF1L	590	1846
PF2U	590	1846	PF2L	590	1846
PF3U	590	1846	PF3L	590	1846
PF4U	590	1846	PF4L	590	1846
PF5U	752	850	PF5L	752	850
PF6U	466	1522	PF6L	466	1522
PF7U	466	950	PF7L	466	950

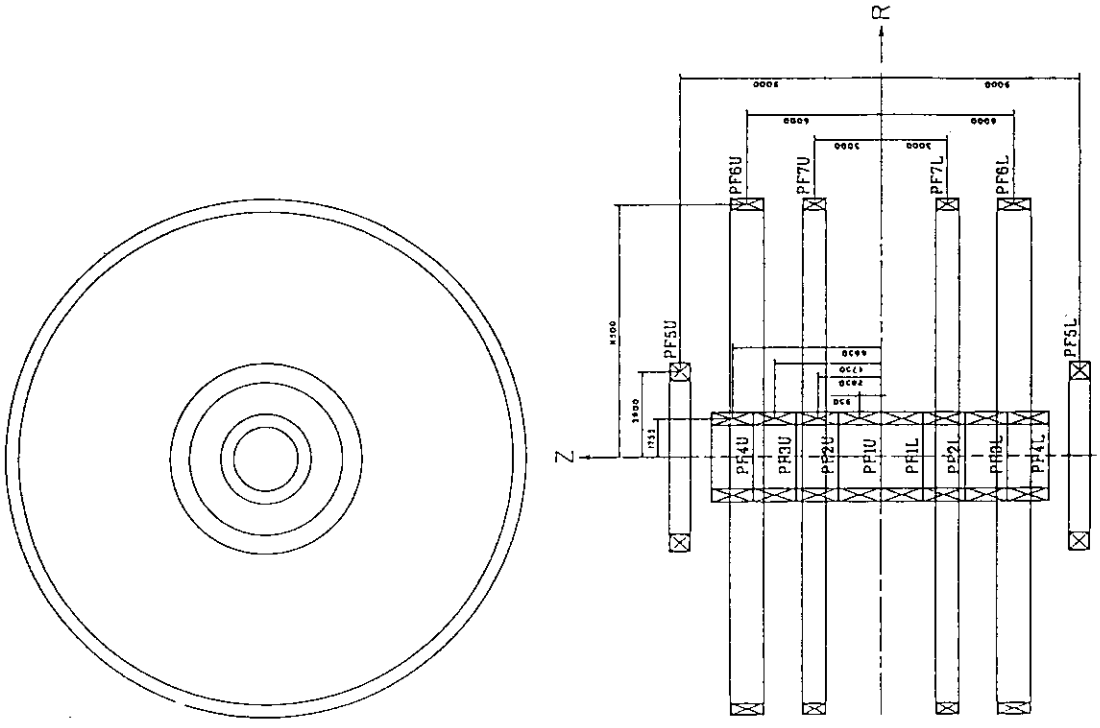

Fig.5.1 Top view, the cross section and the bird's-eye view of the CS coils.

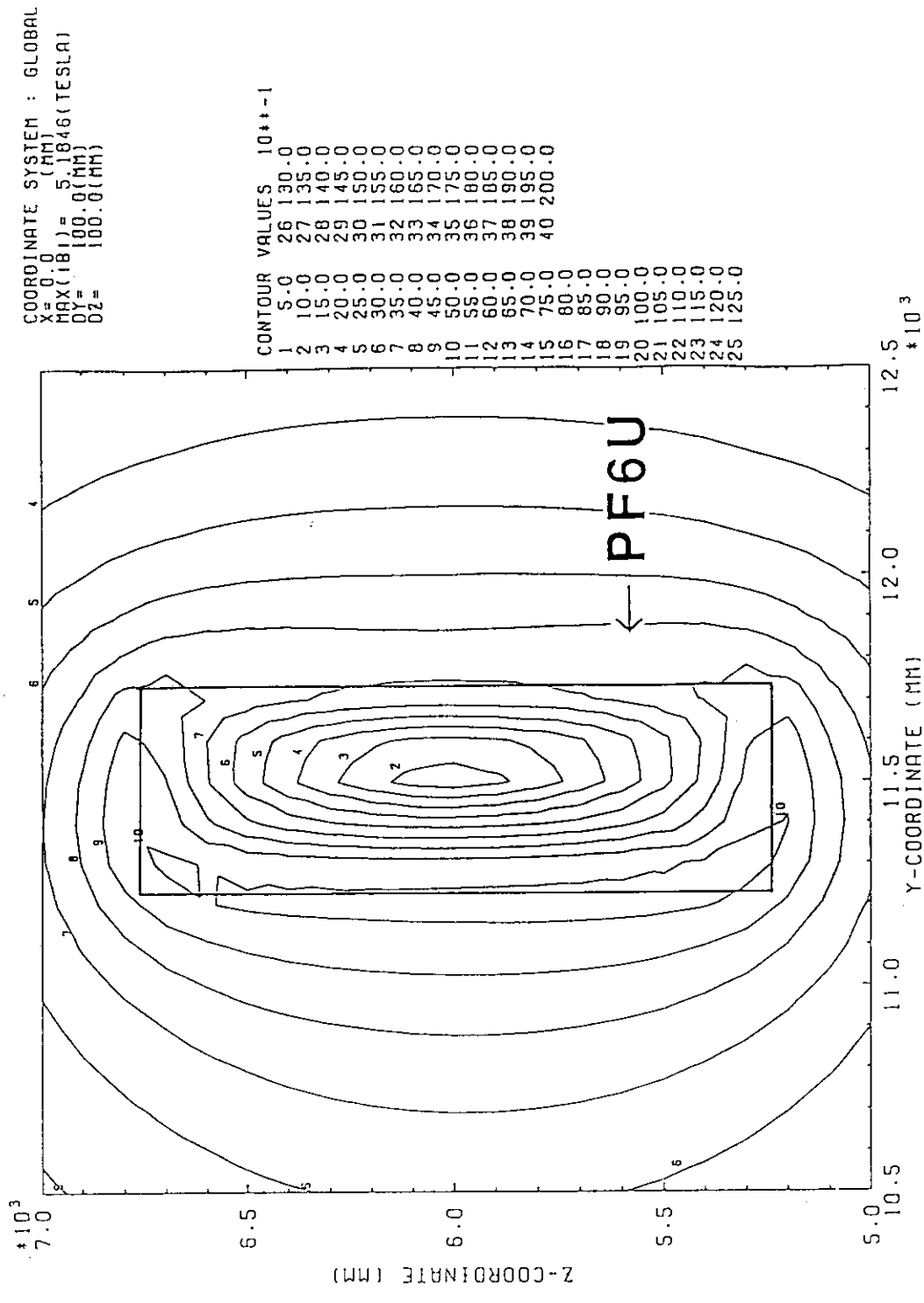

(a) PF-6.

Fig.5.2 Field distribution is cross sections of the outer ring coils at SOFT3. (1/2)

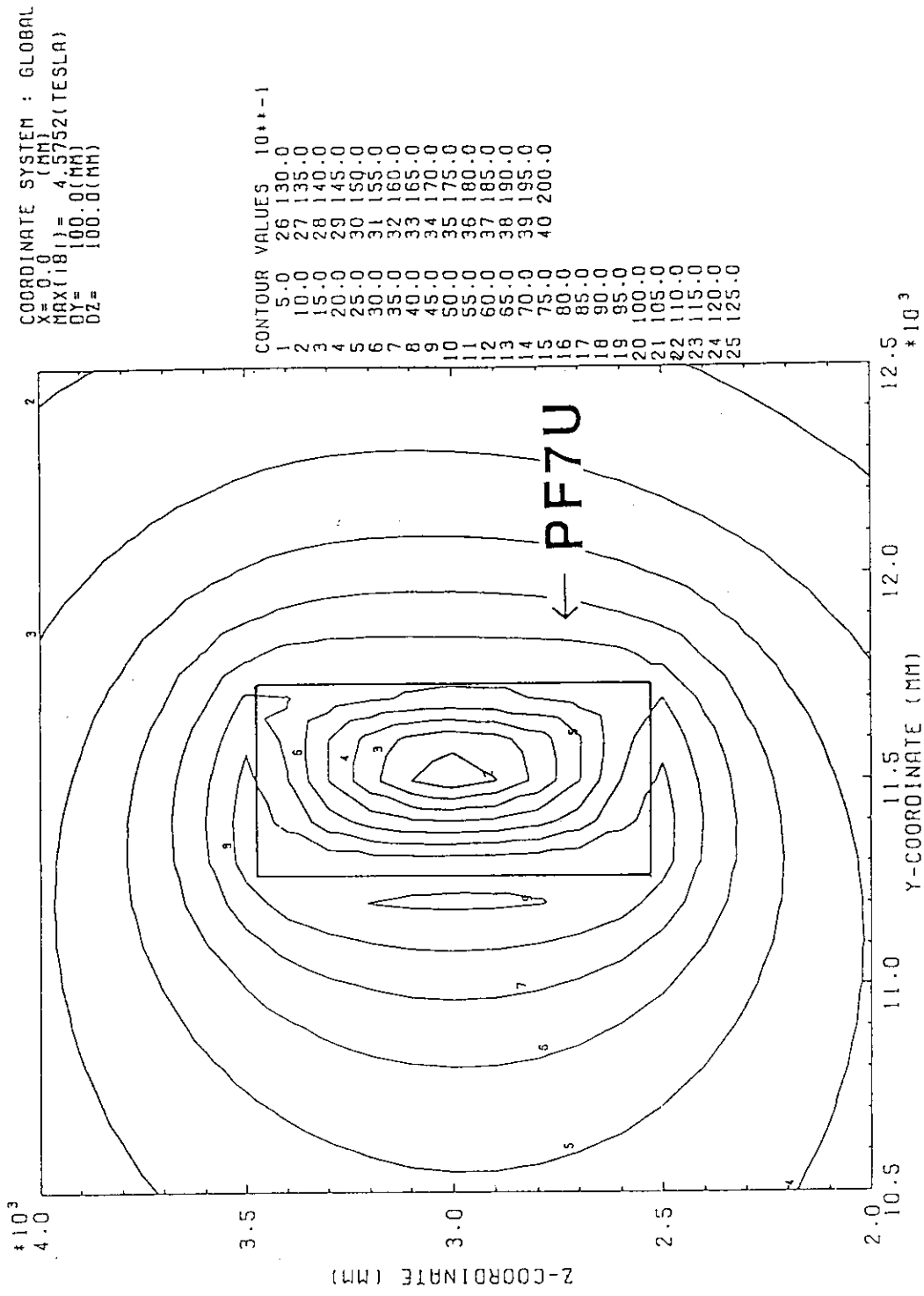

(b) PF-7.

Fig.5.2 Field distribution is cross sections of the outer ring coils at SOFT3. (2/2)

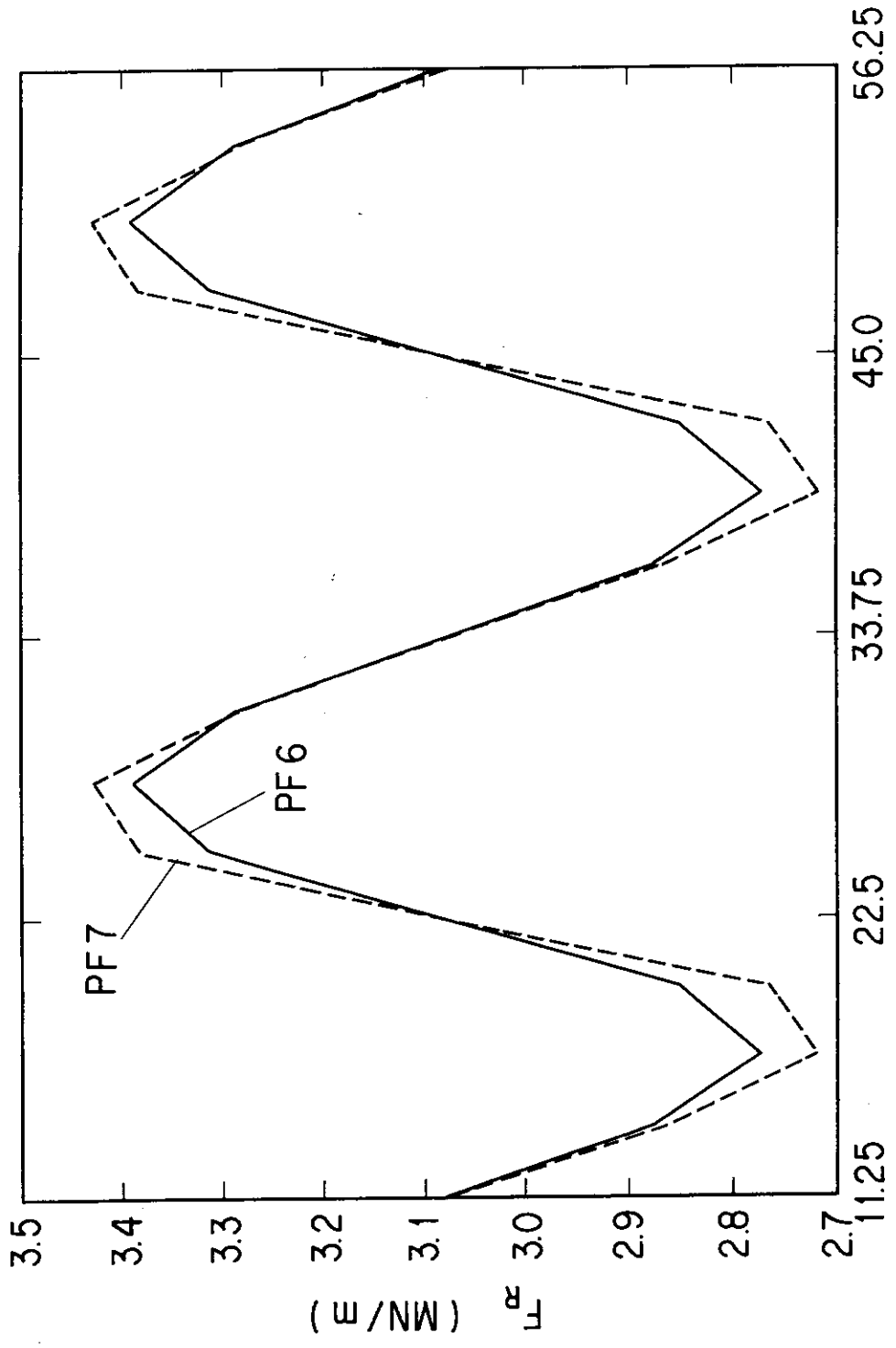

(a) Radial force distribution.

Fig.5.3 Distributions of the radial and the vertical electromagnetic force for EOB1 from 11.25 degree to 56.25 degree along the circumference of the coils. (1/2)

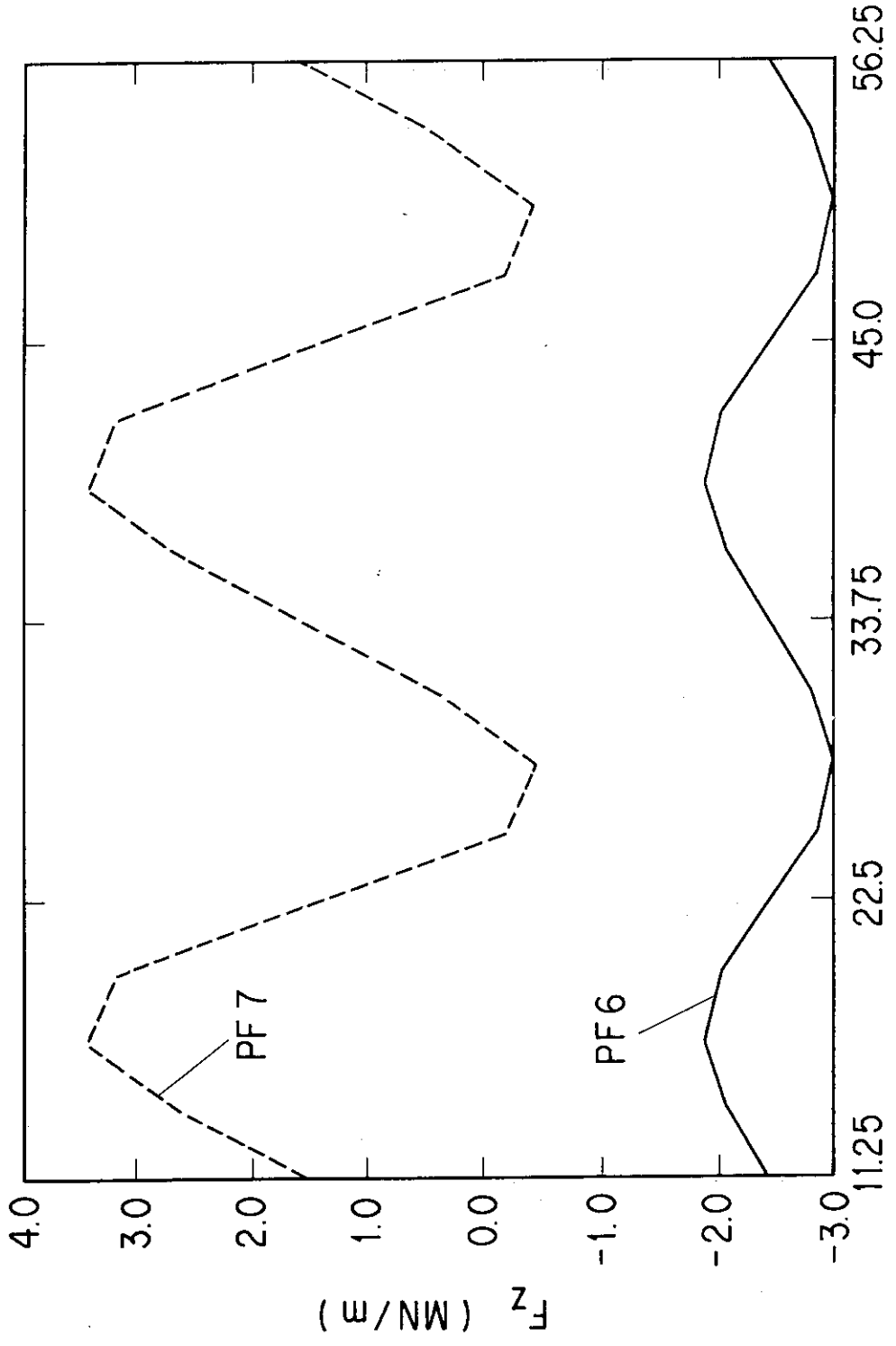

(b) Vertical force distribution.

Fig.5.3 Distributions of the radial and the vertical electromagnetic force for EOB1 from 11.25 degree to 56.25 degree along the circumference of the coils. (2/2)

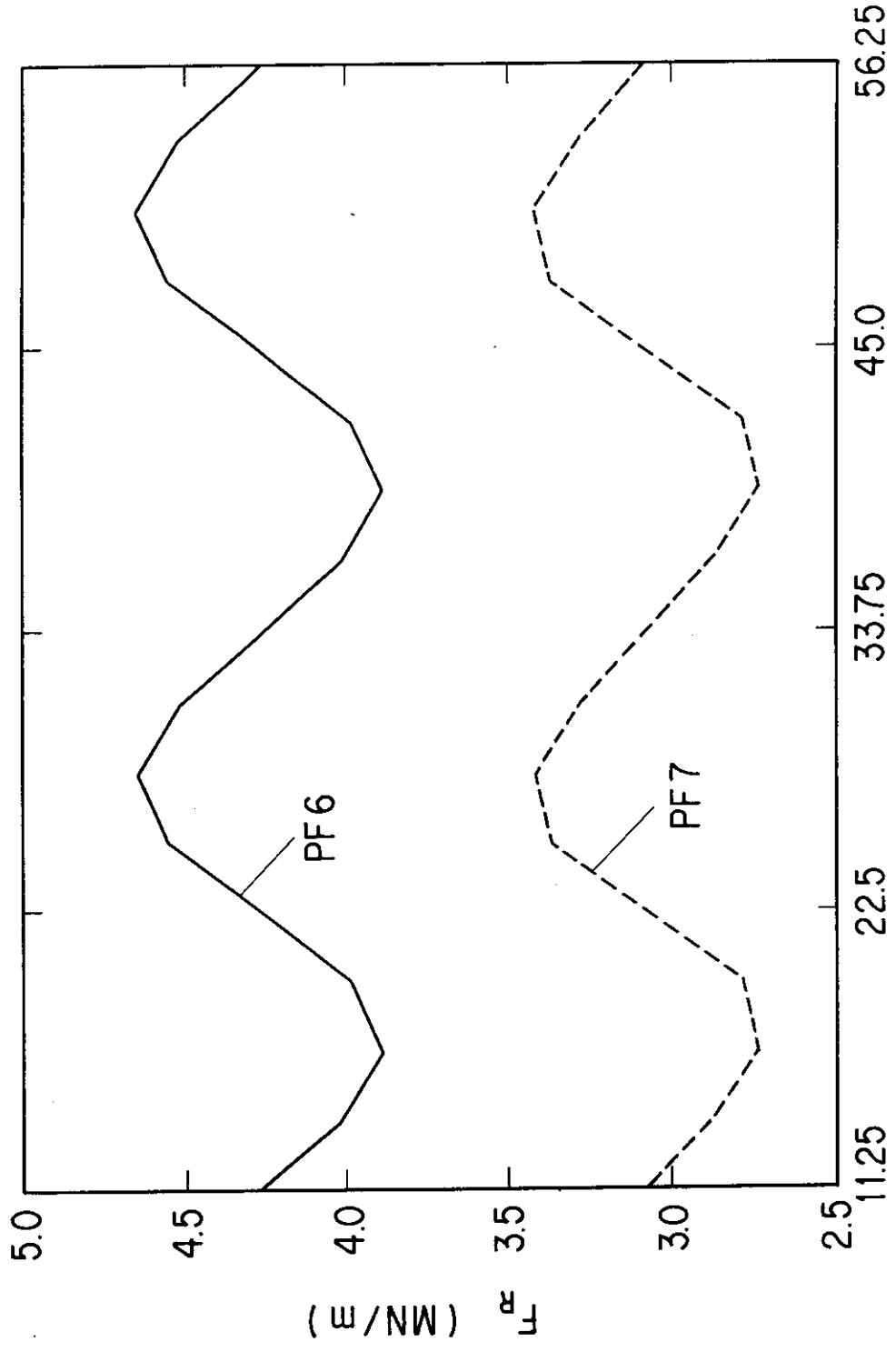

(a) Radial force distribution.

Fig.5.4 Distributions of the radial and the vertical electromagnetic force for EOB3 from 11.25 degree to 56.25 degree along the circumference of the coils. (1/2)

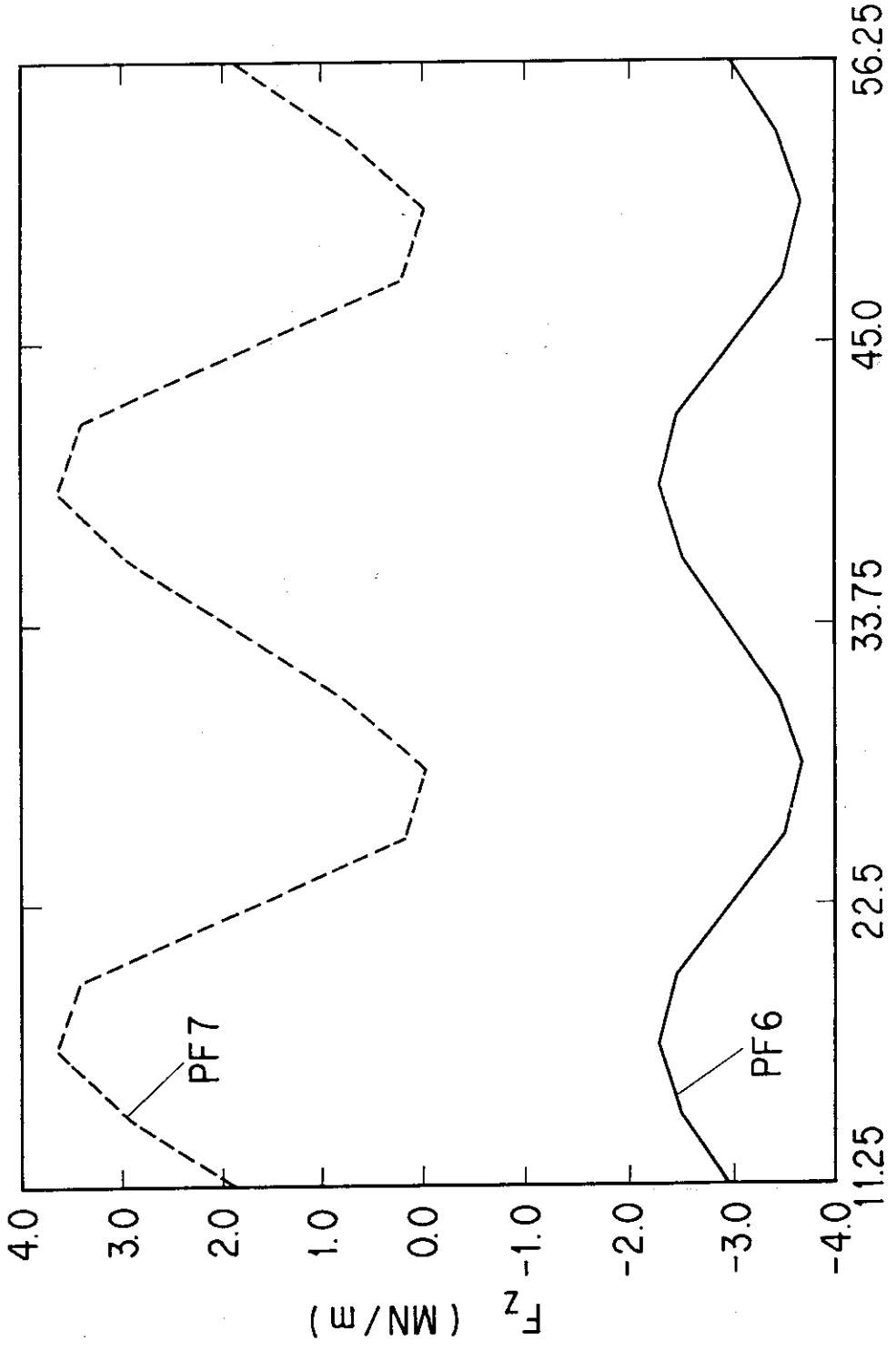

(b) Vertical force distribution.

Fig.5.4 Distributions of the radial and the vertical electromagnetic force for EOB3 from 11.25 degree to 56.25 degree along the circumference of the coils. (2/2)

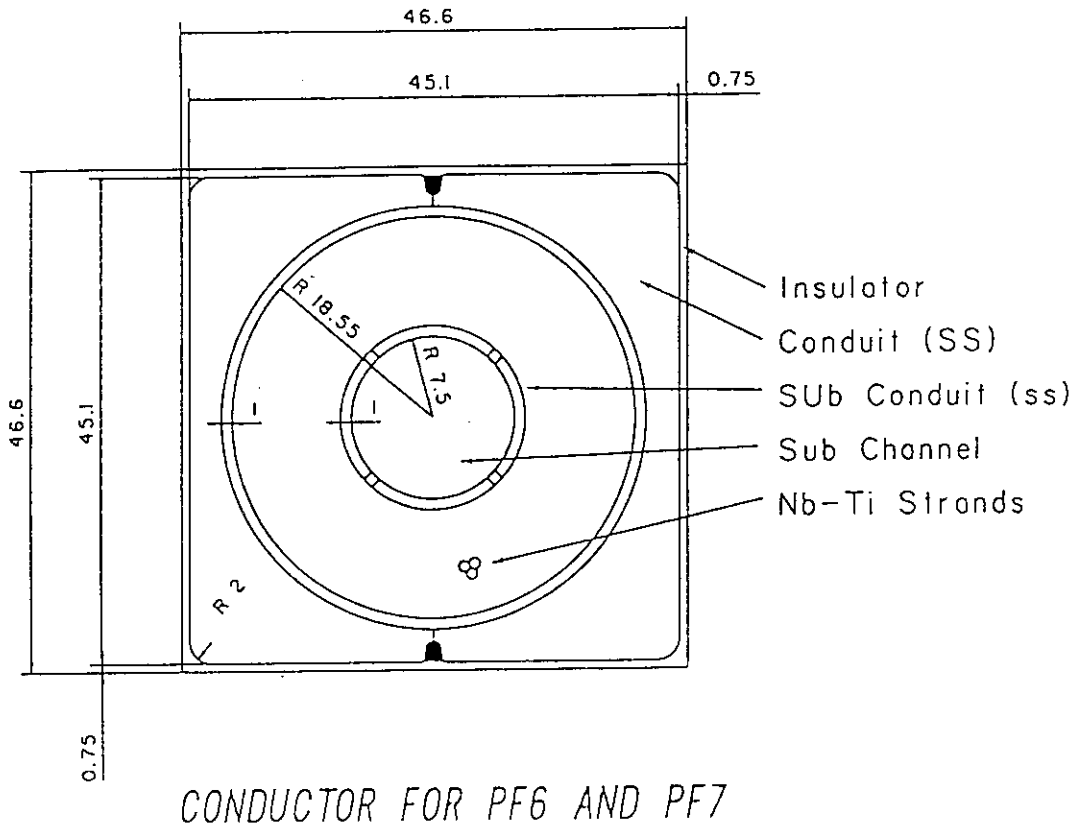

Fig.5.5 Cross-sectional view of sub-channel added modified DPC-U type conductor.

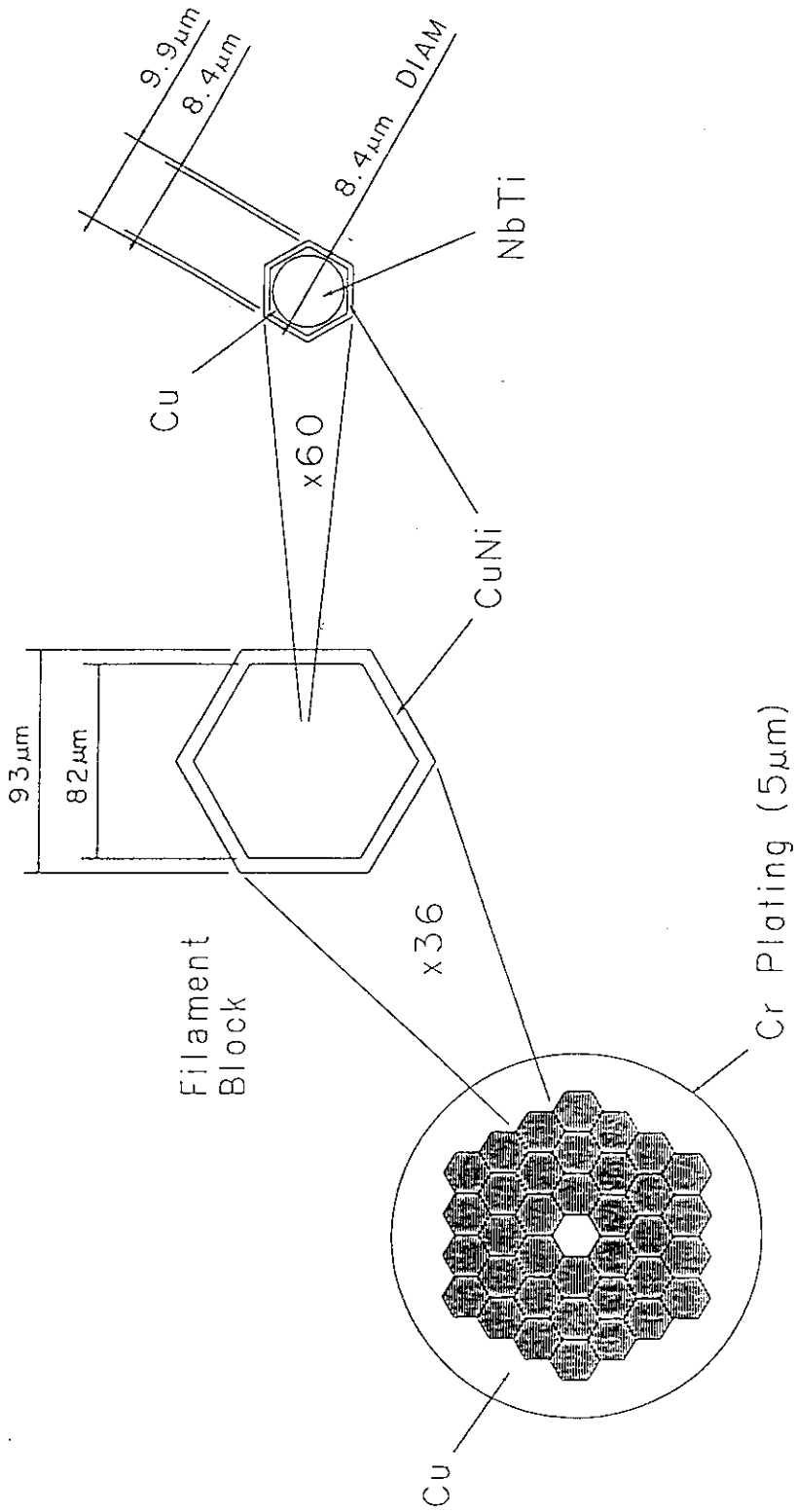

Fig.5.6 Cross sectional view of modified DPC-U strand.

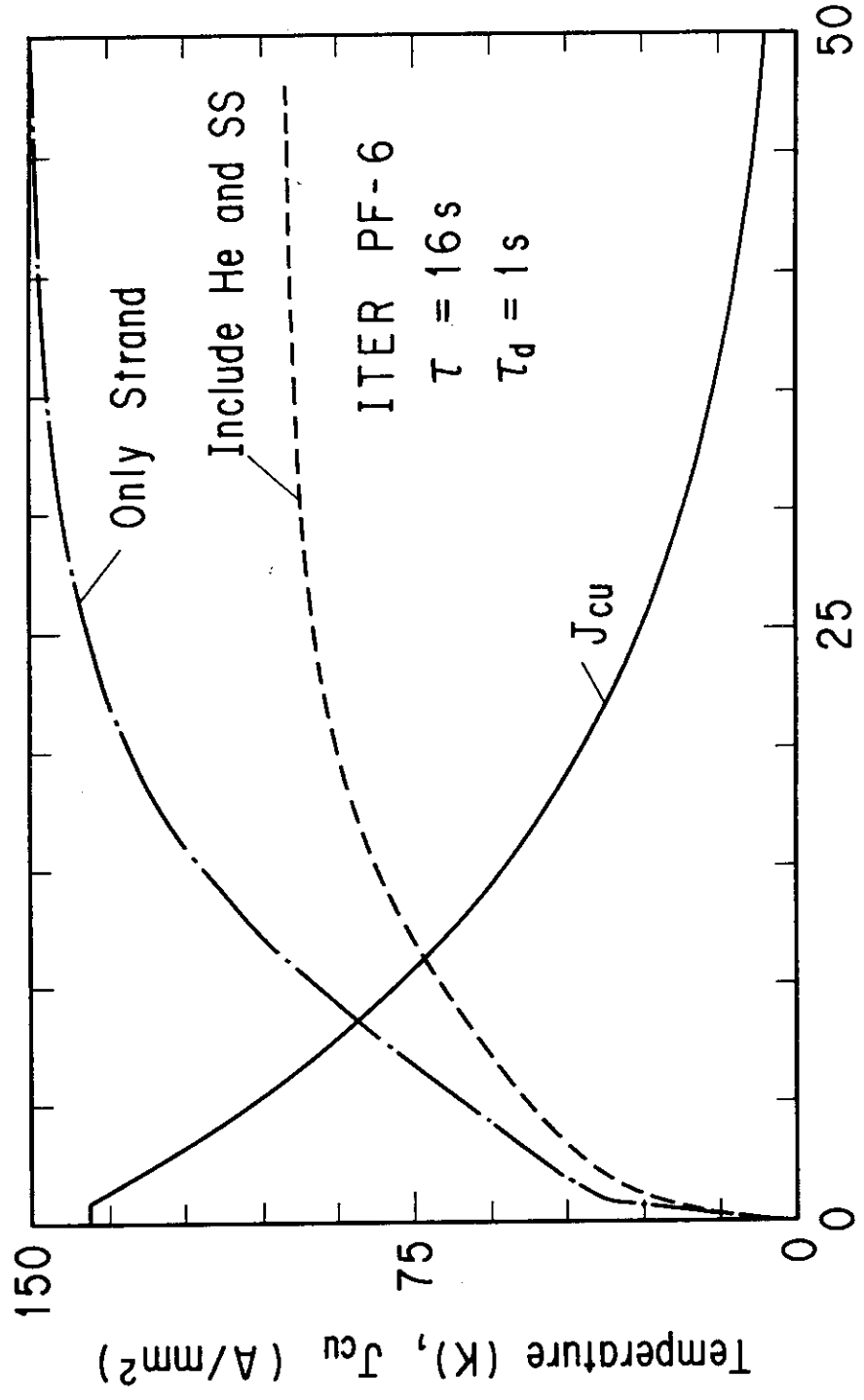

Fig.5.7 Temperature rise during quench and protection of modified DPC-U conductor.

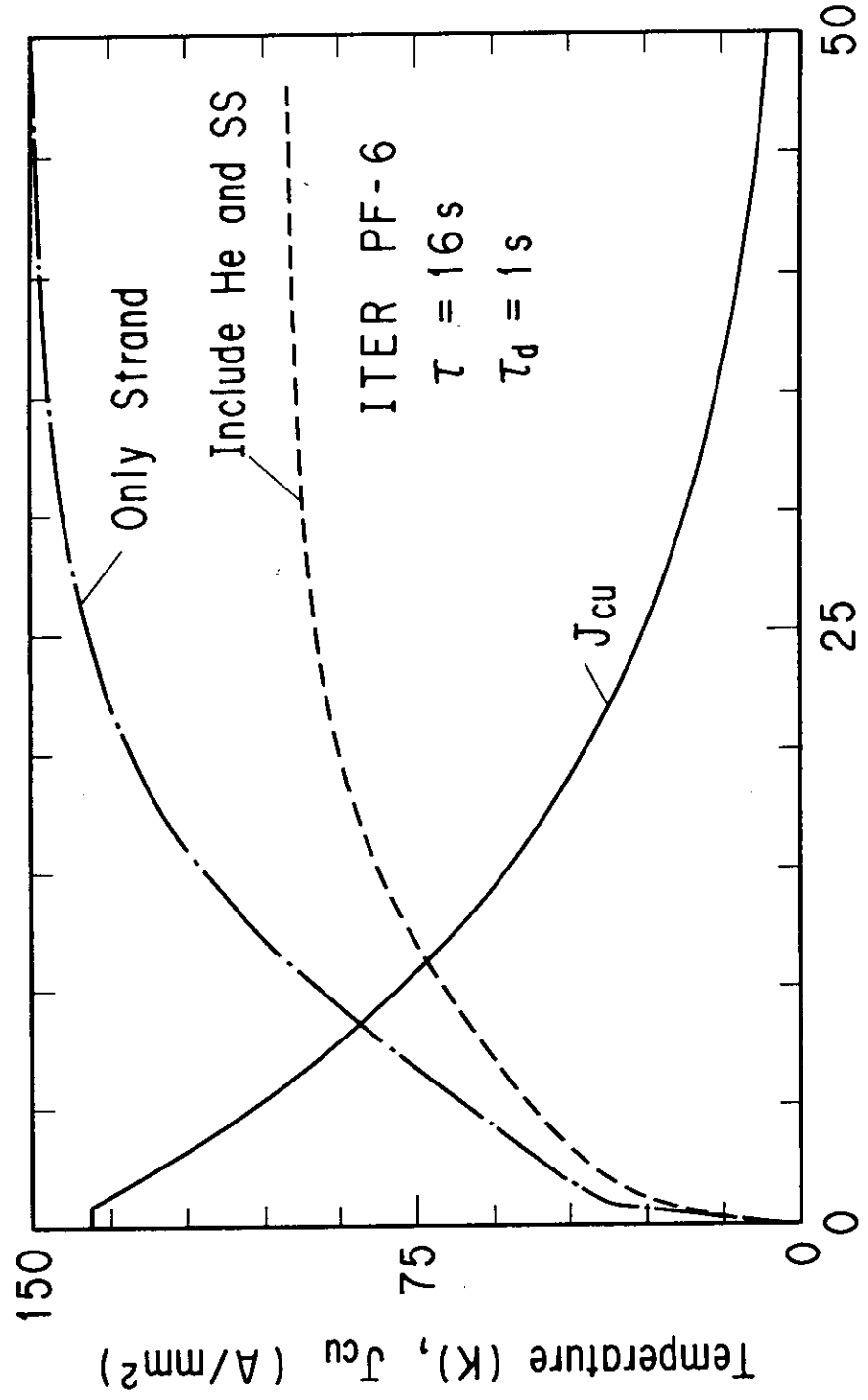

Fig.5.7 Temperature rise during quench and protection of modified DPC-U conductor.

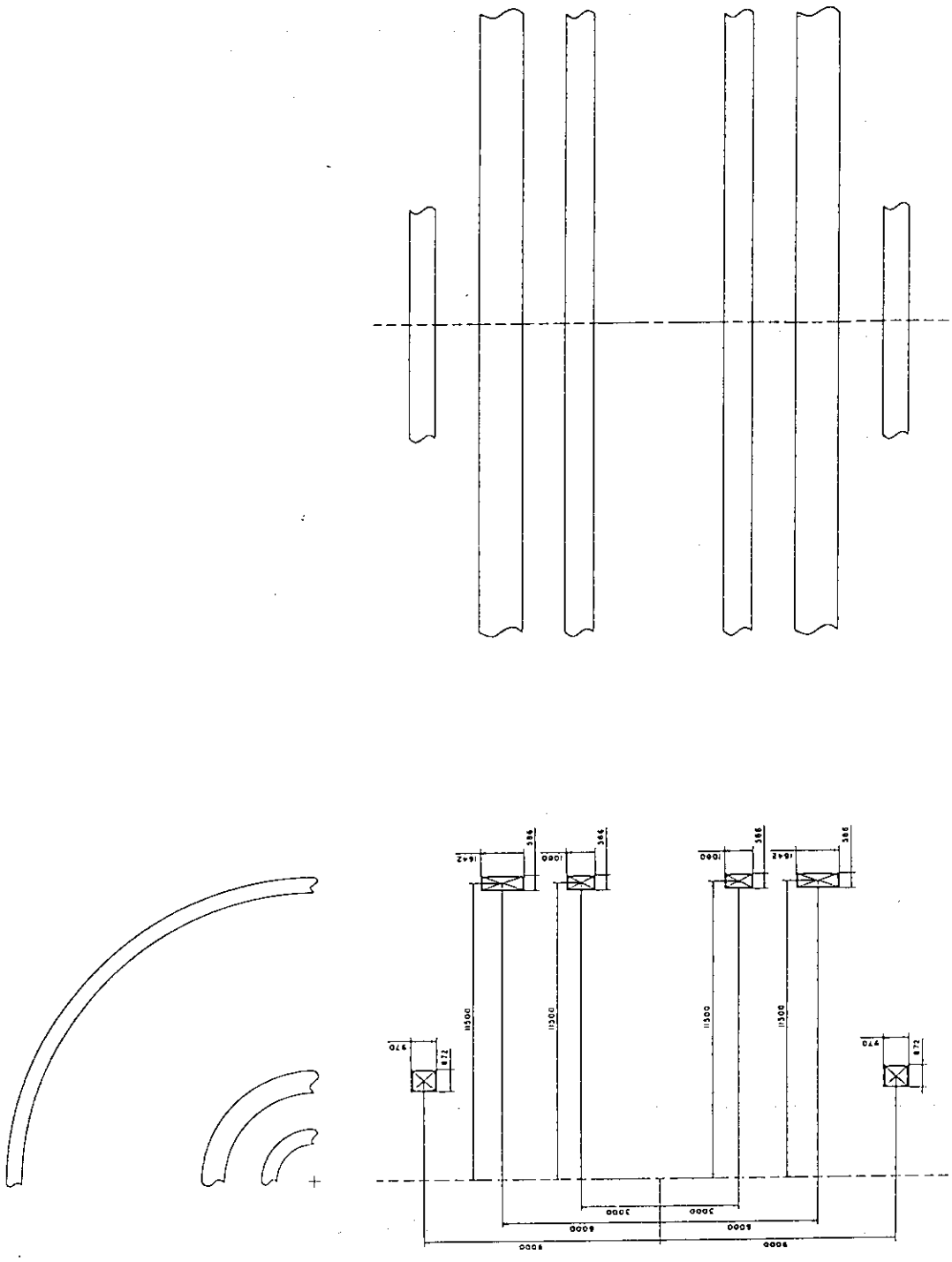

Fig.5.8 Overall layout of the Outer Ring coils.

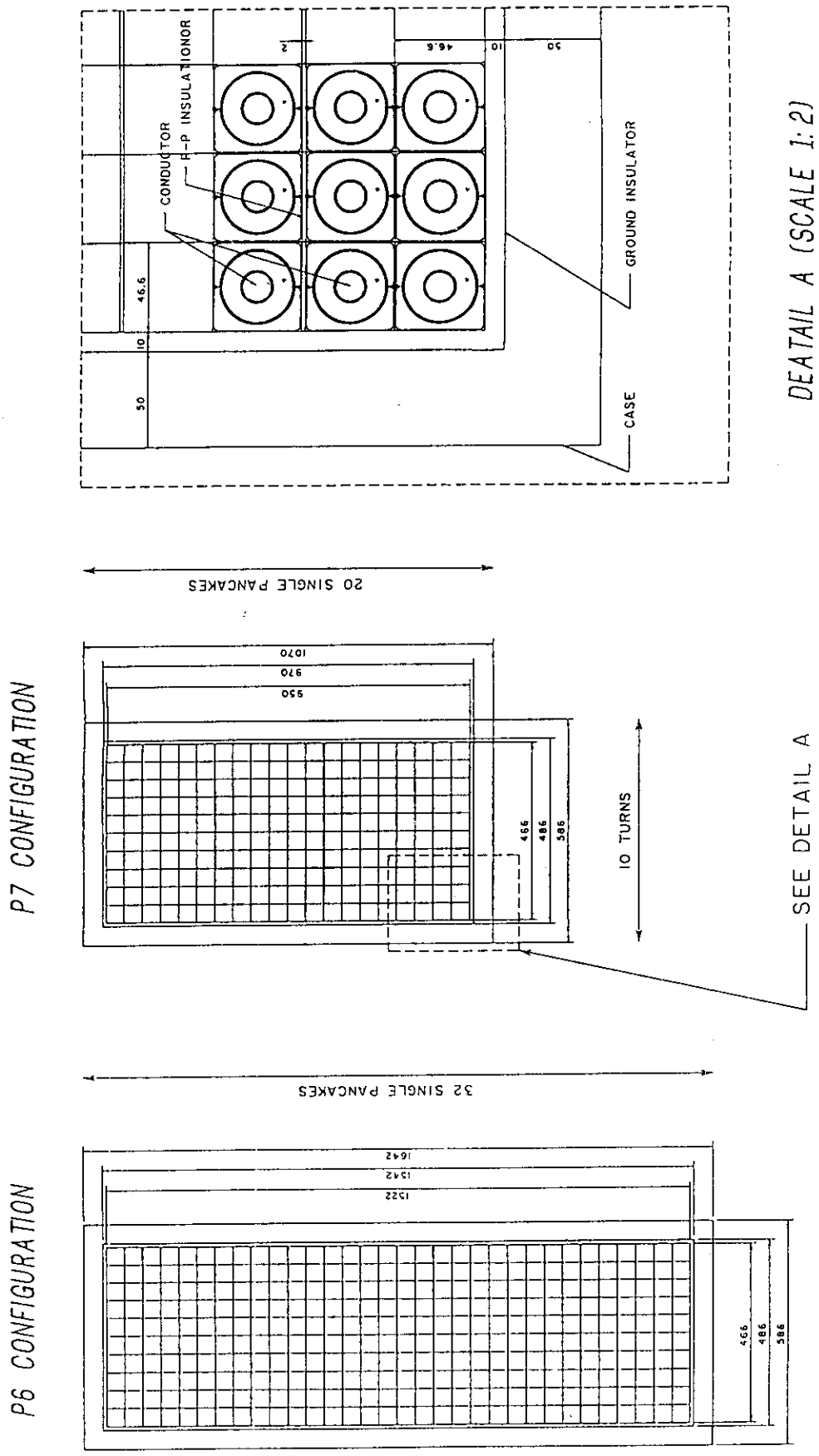

Fig.5.9 Cross sectional views of the PF-6 and PF-7 coils.

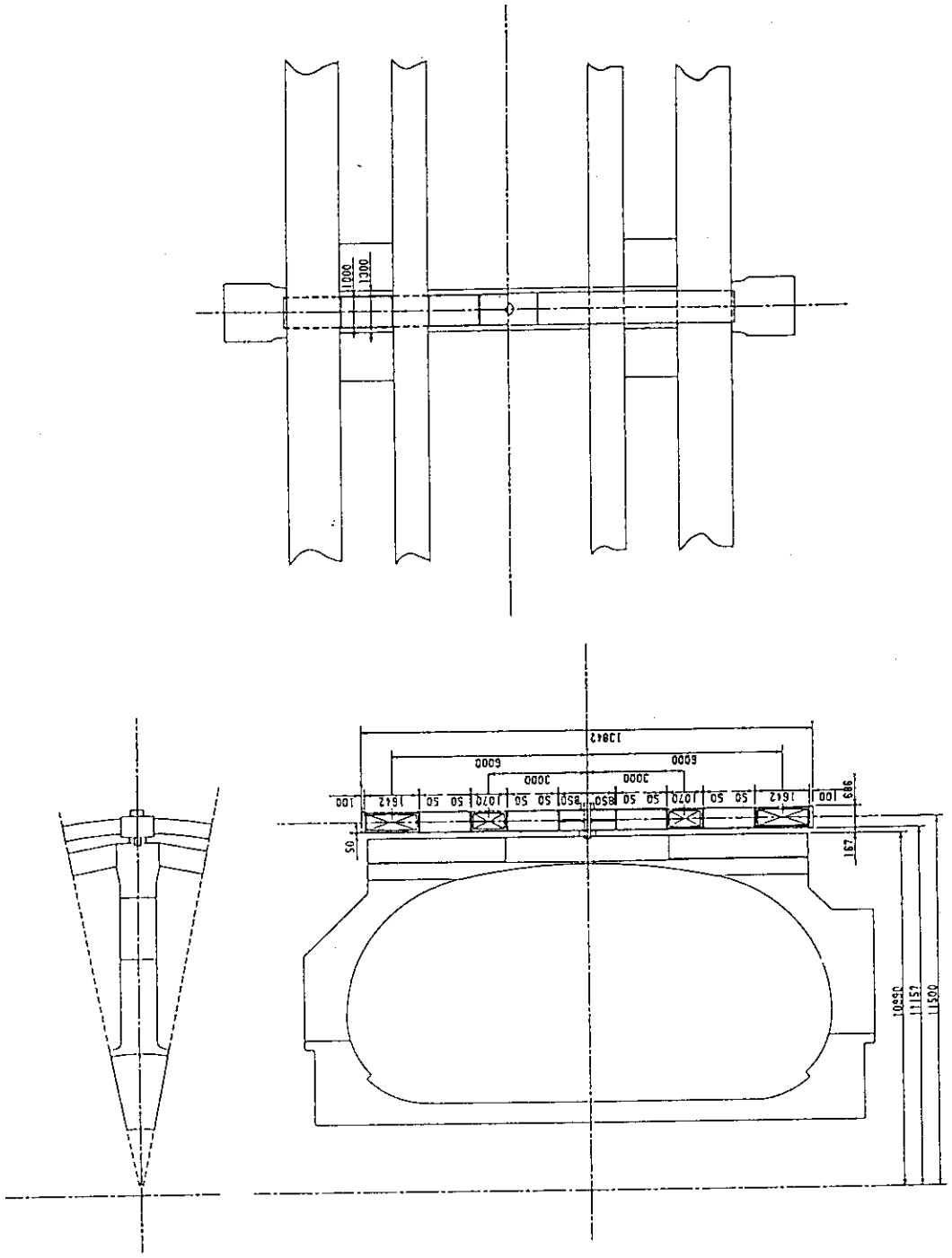

Fig.5.10 Support structure of the outer ring coils.

6. MECHANICAL DESIGN GUIDELINE

6.1 Scope

6.1.1 General

(1) This section describes a mechanical design guideline for superconducting coils for a tokamak fusion machine.

(2) The object of this section is to provide assistance in the materials selection, the design, the fabrication and the inspection of superconducting coils for a tokamak fusion machine.

(3) The basis of this guideline is a comparison between the design analysis and verification test results.

(4) This guideline is based on the 1986 ASME Boiler and Pressure Vessel Code.

6.1.2 Classification

(1) The following components, at temperatures ranging from 300 K to 4 K, are considered in this guideline.

(a) superconducting coils
(b) supports between coils
(c) weight supports
(d) pipes, valves and attachments
(e) nitrogen shield

(2) The following components are not considered to be within this guideline:

(a) vacuum tank
(b) electrical cable and attachments
(c) outside of the vacuum tank

6.1.3 Considerations

(1) The following items should be considered apart from this guideline.

(2) Superconducting coils are basically electric machines. Therefore, other electric rules have to be referenced.

(3) Each component in this guideline suffers from 14 MeV neutron bombardment from the plasma core, in spite of the fact

that every component is outside of the fusion core.

6.2 Materials

6.2.1 General

(1) The basis of this guideline is to determine the mechanical properties of the materials used in the superconducting coils this is needed because the mechanical data base for these cryogenic materials is in sufficient.

6.2.2 Metal

(1) The following mechanical data of each production batch should be measured at 4 K, 77 K and 300 K.

(a) yield strength (0.2% offset) : Sy
(b) ultimate strength : Su
(c) elongation : El
(d) fracture toughness : K1c
(e) crack growth rate : da/dn
(f) strain at beginning of serration : STs
(g) proportional limit strength : Spl
(0.01% offset)

(2) The following mechanical and electrical properties of each metal should be measured at 4 K, 77 K and 300K.

(h) Fatigue strength : Sn
(i) Young's modules : E
(j) Poisson's ratio
(k) Thermal contraction
(l) Resistivity
(m) Magnetic permeability
(n) corrosion resistance

(3) Experimental measurement methods are specified by another document.

(4) In case of pulsed coils, the strain rate during testing is determined from the actual magnet operation since mechanical properties depend on strain rates.

(5) For use of forced-flow-cooled Nb_3Sn conductors, test pieces of the conduit are heated to the same temperature as conductor samples.

(6) Allowable metals do not include the following:

(a) metals with an elongation of less than 5 %,

(b) ferrous metals,

(c) corroded metals.

6.2.3 Non-metal

(1) The following mechanical data of each production batch should be measured at 4 K, 77 K and 300 K [2].

(a) ultimate strength : Su

(b) elongation : EL

(c) fatigue : Sn

(d) Young's modulus : E

(e) Poisson's ratio

(f) thermal contraction

(g) resistivity

(h) out-gas from surface

(i) helium penetration rate

(2) Experimental measurement methods are specified by another document.

(3) In case of pulsed coils, the strain rate during testing is determined from the actual magnet operation since mechanical properties depend on the strain rates.

6.3 Design

6.3.1 General

(1) The design stress intensity value Sm is defined as follows:

(a) for the conduit of Nb_3Sn conductor:

Sm = S(2/3 ST.work)

ST.work = ST.crit - ST.bend

ST.crit is critical strain of Nb_3Sn

ST.bend is bending strain at winding

ST.work is working strain form the electro-magnetic force and thermal contraction.

(b) for the coil case, the supports and conduit of

Nb-Ti conducter:

$$Sm = \min\{ 2/3\ Sy,\ \underline{1/2}\ Su \}$$

(c) for a non-metal:

$$Sm = 1/6\ Su$$

(2) Material data for different operating temperatures:

(a) 4 K - 20 K : design by mechanical properties at 4 K,

(b) 20 K -130 K : design by mechanical properties at 77 K,

(c) 130 K - 300 K : design by mechanical properties at 300 K.

(3) Operating condition:

(a) normal condition : cool-down, warm-up, charging, nuclear heating,

(b) fault condition : quench

(c) failure condition : short circuit, melt down ground fault

6.3.2 Allowable stress

(1) The allowable stress of metals used below 20 K is determined by Table 6.1.

(2) The allowable stress of non-metals used below 20 K is determined by Table 6.2.

(3) The allowable stress from 20 K to 300 K is determined by the rule of ASME.

6.3.3 Design parameter evaluation

6.3.3.1 Rigidity of winding

(1) Winding rigidity in the three direction is measured by experiment because the calculated stress intensity of the conductor / conduit combination is strongly influenced by its rigidity.

(2) Experiments for evaluating winding rigidity are performed at 77 K to avoid the effect of thermal contraction.

6.3.3.2 Friction

(1) The friction factor of the slide mechanism that releases thermal stress during cool-down and warm-up is measured by experiment.

(2) Friction experiments are performed below 77 K and in vacuum environments.

6.3.3.3 Imperfect welding

(1) The joint efficiency of imperfect welding is examined experimentally.

(2) Samples of imperfect welding are to be larger than 50 mm thick.

6.3.4 Stress calculation

6.3.4.1 Calculation formula

(1) Calculation formulas given by the ASME BPVC code are available in this guideline.

6.3.4.2 Finite element method (FEM)

(1) Loads in the FEM result from electromagnetic forces, inner pressure and thermal contraction.

(2) The electromagnetic forces on the coils are confirmed by checking at different institutes.

(3) The geometric location of the nodes represents the actual structure. Fine divided mesh can be sufficient to evaluate the peak stress of structure.

(4) The rigidity of the element is obtained as in 6.3.3.1.

6.3.5 Fatigue Analysis

6.4. Fabrication

This section will be described later.

6.4.1 Conductor fabrication

6.4.2 Winding

6.4.3 Impregnation

6.4.4 Case forming

6.4.5 Welding

6.4.6 Coil assembly

6.4.7 Installation in the Tokamak
6.4.8 Final adjustment

6.5 **Inspection**

This section will be described later.

6.5.1 Welding inspection
6.5.2 Impregnation inspection
6.5.3 Final inspection of coils

(1) Pressure in the proof pressure test is 1.5 times the design pressure at the operating temperature.

(2) The gas of the proof pressure test is helium.

6.5.4 Inspection during installation
6.5.5 Final inspection on system.

6.6 **Safety device**

(1) In the case of the forced-flow-cooled conductor, the size of a safety device is determined by the conductor cross section.

(2) In the case of a pool boiling coil, size of a safety device is determined by the heat generation of the conductor during a quench.

(3) Two safety devices are required: one for operation from 300K to 20 K and one for operation from 20 K to 4 K since different design pressures in each temperature region might occur.

(4) The vacuum tank has a safety device to avoid a pressure rise inside the vacuum tank during a coil failure.

6.7 **Other consideration**

(1) The fracture toughness of a thin plate (about 2 mm) is defined by proper theory.

References

[1] ASME Section VIII Division 2 (1986) 483
[2] ASME Section X (1986) 106
[3] ASME Section XI (1986) 513

Table 6.1 The allowable stress of metals below 20 K

Stress Category	Conduit
NORMAL CONDITION	
Primary	1/2 Sm
Primary + Thermal	2/3 Sm
Peak	2/3 Sm
FAULT CONDITION (quench)	
Primary	3/4 Sm
Peak	Sm & Fatigue-Evaluation

Table 6.2 The allowable stress of non-metals below 20 K

Stress Category	
NORMAL CONDITION	
Primary	Sm
Primary + Thermal	2 Sm
FAULT CONDITION	
Primary	3 Sm

7. SUMMARY

After three years design activity, we understand the requirements from plasma physics, controls, and other units: vacuum vessel, shield, and diverters, and many ports for access. The magnet design unit allows the changing of the plasma shape and the reductions of the coil volume. We are still working on determining the requirements to develop the ITER coils.

We selected many technically advanced specifications for the superconducting strands and insulators because these components will be improved by the development during the log term R&D. There were many investigations from the demo poloidal coil program. Especially, the DPC-EX has excellent results for stability and AC loss. The Proto Toroidal Conductor developments has also given good information to help with the design the toroidal conductor. We believe that the most important information for the design is derived from experimental results, as it has always been in the history of the superconductivity. However, we cannot make real size model coils for the long term R&D because of the high cost and time limitatioms. Computer analysis also is important for the design the ITER magnet system in order to extrapolate the performances of test coils from model size to real size.

Finally, reliable management for design and R&D activities will become important to realize ITER magnet system. In area of the magnet development, the Large Coil Task program showed that international collaboration using hard wear can be successful.

ACKNOWLEDGEMENTS

The authors would like to thank Dr. S. Shimamoto and Dr. S. Mastuda for their strong support and kind encouragement of our design activities during the past three years. Also, the authors wish to thank the staff of the Superconducting Laboratory and the Fusion Experimental Reactor Design Team for their consultation. And authors would also like to thank Mr. T. Shimizu, Mr. Y. Nakane, Mr. H. Shimane, Mr. T. Nishino, and Mr. E. Yaguti from Kanazawa Computer Service Co Ltd for their computer analysis. Also thanks to Miss Y. Iida, Miss Y. Hasegawa, Mr. K.Hirano, and Miss H.Nagahori for the CAD operations, and Miss A. Miwa and Miss K.Idetsu of Gensiryoku Shiryo Service Co Ltd for the publishing.